RHODIUM ZEOLITES AS CATALYSTS FOR HYDRODESULFURIZATION REACTIONS

by

Kathryn Elizabeth Givens

Thesis submitted to the Faculty of the
Virginia Polytechnic Institute and State University
in partial fulfillment of the requirements for the degree of

MASTER OF SCIENCE

in

Chemistry

APPROVED:

J. G. Dillard, Chairman

B. E. Hanson

J. P. Wightman

April, 1982

Blacksburg, Virginia

To Howie

whose love and confidence made
these pages possible, and whose
absence provided a goal for which
to strive

ACKNOWLEDGEMENTS

Foremost, I would like to extend my deepest appreciation to my research advisor, Dr. John G. Dillard, for his assistance, guidance, faith, and most of all patience during the course of my graduate work. I would also like to thank him for the many truly enjoyable hours of competition endured on the tennis court. I also wish to thank the members of my graduate committee, Dr. Brian E. Hanson and Dr. James P. Wightman, for their interest and contributions to my work.

The services of the Virginia Polytechnic Institute and State University Glassblowing Laboratory, especially Mr. Andy Mollick, are greatly acknowledged. A special thanks is extended to Mr. Dave McCommon, Mr. Jim Hall, and Mr. Larry Jackson of the Virginia Polytechnic Institute and State University Chemistry Department Electronics Shop for all their extra effort to keep the laboratory equipment in working order. Acknowledgement is also extended to Dr. Harold McNair of the Virginia Polytechnic Institute and State University for the use of his gas chromatograph. The very capable services of my typists, Ms. Debbie Farmer and Ms. Donna Perdue were invaluable. I would like to thank the Department of the Interior and the Virginia State Coal and Energy Research for their financial support in this work.

Finally, I would like to express my most sincere gratitude to my parents Buck and Mimi Givens for their love and continuous encouragement throughout this endeavor. Without their help, none of this would have been possible. I also extend deep thanks to my brothers, Sam, John, and Charley for their invaluable advice and

support. Thanks also to my friends, especially Mr. Mike Ogden and Ms. Pat Sormani, for their help and for making my stay in Blacksburg a more enjoyable one. To Chuck and Sandi Johnson, I extend my love and a very special thanks for making these last nine months bearable.

TABLE OF CONTENTS

LIST OF FIGURES

LIST OF FIGURES (Con't)

page

LIST OF TABLES

LIST OF TABLES (Con't)

CHAPTER I

INTRODUCTION

The worldwide demand for petroleum fuels and petroleum products has drastically increased over the last few decades. With governments, industries, and individuals requiring more and more oil, and with the majority of the oil supply being tightly controlled by the OPEC nations, the price of petroleum has skyrocketed while the amount of natural reserves has greatly declined. It is these factors which have led to today's troubled energy situation. For instance, the price of gasoline alone rose 9.8% in 1981 (1), and has almost quadrupled in cost per gallon since 1970. It is no wonder that new sources of energy, new exploration projects and new refining techniques and procedures are under extensive investigation by scientists around the world. Until a new source of energy is developed and deemed both environmentally and economically sound, new techniques and methods of refining existing petroleum fuels must be developed.

Existing fuel stocks today contain a large percentage of sulfur, nitrogen and metals. Akhtar and coworkers (2) identified at least fourteen organic sulfur compounds in the liquid products from the hydrogenation of a Kentucky coal sample. Of the fourteen sulfur products identified, thirteen were thiophene derivatives. Environmental regulations requiring the removal of sulfur components in petroleum fuels necessitates the development of new refining procedures, or the upgrading of old ones to do a more efficient job.

Consequently, hydrodesulfurization reactions have become the topic for much research, and the need for an effective and economical catalyst for this reaction is paramount to the successful development of clean burning, low sulfur fuels.

The use of zeolites as catalysts has dominated the catalytic cracking process in petroleum refining since 1962. In the United States and Canada, all catalytic cracking of petroleum crudes has been accomplished with zeolites since 1976 (3). Petroleum cracking catalysts account for approximately 95% of the worldwide usage of zeolites (3). Faujasite zeolites are used as effective catalysts for cracking petroleum to produce gasoline range hydrocarbon products. Also, it has recently been shown that a new class of zeolite, ZSM5, demonstrates marked catalytic activity in converting methanol and other oxygen containing compounds to gasoline range hydrocarbons (4,5).

As previously mentioned, petroleum feedstocks can contain large amounts of sulfur. To produce gasoline and other useful fuel products, these sulfur components must be removed. Within the past few decades, many studies have been conducted on the hydrodesulfurization of thiophene and thiophene derivatives. It has been shown (6) that the sulfided form of the transition metals are effective catalysts for this reaction. In particular, the sulfided cobalt-molybdenum/alumina catalyst has been used with good success for desulfurization reactions. However, the mechanism of reaction and the exact role of the catalyst are still in question. It is known though, that a transition metal incorporated within a catalyst lends greater thermal

stability to the support and also provides an active site for the desulfurization and hydrogenation/dehydrogenation process.

Thus, since zeolites are useful for producing hydrocarbons in cracking reactions and deoxygenation reactions, the present study was initiated to investigate their catalytic activity for hydrodesulfurization reactions. Reactions with sulfide treated rhodium zeolites were studied to determine if the presence of rhodium leads to enhanced hydrocarbon yield. Rhodium was chosen as the metal of incorporation because second row transition metal sulfides are more effective in hydrodesulfurization reactions than first row metal sulfides.(6) Also, rhodium ions, particularly in low oxidation states, are able to interact with π donor molecules and soft donor atoms. This quality would be advantageous when working with thiophene. The hydrodesulfurization reactions were carried out as a function of gas flow rate, reaction temperature and method of catalyst conditioning.

The results obtained on the different rhodium zeolite catalysts are compared with results obtained on a commercial cobalt-molybdate catalyst. Surface properties of the catalysts are correlated with observed activity to determine optimum reaction conditions and the active surface species. Thiophene conversion results are used as the basis for determining whether the rhodium zeolites would make more effective catalysts for hydrodesulfurization than the widely used cobalt-molybdenum/alumina catalyst.

The compounds trichlororhodium(III)trihydrate, $RhCl_3 \cdot 3H_2O$, tetraacetodirhodium(II), $Rh_2(CO_2CH_3)_4$, and chlorotris(triphenyl-

phosphine)rhodium(I), $Rh(PPh_3)_3Cl$, were chosen for adsorption on the zeolites. This selection of compounds provides a means of comparing the adsorption and catalytic nature of each compound. The trichlororhodium(III)trihydrate compound was chosen as the model for a rhodium (III) ion. The tetraacetodirhodium(II) compound was selected to determine how the dimeric rhodium (II) ion would behave in adsorptive and catalytic studies. The chlorotris(triphenylphosphine)-rhodium(I) compound was used to provide the possibility of oxidative addition reactions between Rh(I) and thiophene during the course of hydrodesulfurization.

CHAPTER II

HISTORICAL

A. Hydrodesulfurization Reactions

Hydrodesulfurization is a very important process today due to the environmental and petroleum processing requirements placed on the refining of petroleum fuels. Refining requirements necessitate the efficient removal of sulfur from the thiophenes and condensed thiophenes in the petroleum feedstocks. Hydrodesulfurization is widely practiced in industry to produce a clean burning, low sulfur containing fuel. There is a definite need however, for extending this technology to other fuels, especially coal (7). Akhtar and coworkers (2) identified thiophene and many of its derivatives as major components in the hydrogenation products of a Kentucky coal sample. Therefore, the chemistry of the hydrodesulfurization reactions of these compounds, expected to be among the least reactive compounds in the fuel for this process, needs to be clearly understood. Many studies have been conducted to find a good catalyst to promote hydrodesulfurization reactions but the chemistry is poorly understood and questions regarding the role of the catalyst and the reaction mechanism still remain unanswered.

Hydrodesulfurization of thiophene has been studied as a model for the reactivity of condensed thiophenes. Owens and Amberg (8) investigated thiophene desulfurization over a cobalt molybdate catalyst using a microreactor technique. They found that the percent thiophene conversion to C_4 products increased with increasing

temperature, but that the percent unsaturation remained relatively constant. The product mixture over the cobalt-molybdate catalyst contained butane and butene, and no butadiene or hydrogen sulfide. They explained these occurrances by the ability of H_2S to totally adsorb on the catalyst surface, and that all the initial butadiene formed was immediately converted to butene. In the presence of enough H_2S to saturate the catalyst, it was found that butene hydrogenation was greatly decreased, but the conversion of butadiene to butene occurred too rapidly to be affected. The presence of H_2S, however, did not have a great effect on the rate of thiophene desulfurization. The authors suggest that H_2S competes for H_2 adsorption sites but not thiophene adsorption sites on the catalyst surface. They conclude that the first step in the desulfurization process of thiophene is C-S bond cleavage and not ring hydrogenation.

In a subsequent study, Owens and Amberg (9) investigated the hydrodesulfurization of thiophene over a chromia catalyst. As in their previous study (8), percent thiophene conversion increased with increasing temperature. The sulfided catalyst showed an increase in desulfurization activity over pure chromia, but a decrease in its hydrogenation ability. The authors suggest there are two different active sites for the desulfurization and hydrogenation processes. In contrast to the cobalt-molybdate results (8), H_2S had only a very slight effect upon butene hydrogenation over the chromia catalyst. Owens and Amberg found no evidence for the existence of any organosulfur compounds in the product mixture. Butane and butenes were the major components. They conclude that the desulfurization is

a stepwise reaction. The C-S bond is first cleaved to eliminate the sulfur, and desorption can occur to give either butadiene, butene or butane. However, if butadiene desorbs, it is immediately hydrogenated to butene. These results and conclusions support those put forth in their previous work (8).

Another report by Owens and Amberg (10) deals with the adsorption of thiophene and C_4 products over chromia. Based on data collected on the rapid desorption of thiophene and C_4 products, Owens and Amberg conclude that these two processes are unlikely to govern the rate of the reaction. They suggest that hydrogen chemisorption is the rate controlling step, as this process occurs at a very slow rate. The authors also found that the percent thiophene conversion was not dependent on the total amount of chemisorbed hydrogen, but rather on the partial pressure of H_2 in the gas phase. Thus, they conclude that hydrogen which is strongly chemisorbed to the catalyst surface is not reactive. The smaller amount of loosely held hydrogen, which is able to exist in an equilibrium state with the gas phase, is the reactive species. Hydrogen sulfide adsorption was also investigated and results were similar to those obtained on cobalt-molybdate (8). It seems that the H_2S poisons fast hydrogenation sites, leaving open only sites capable of desulfurization and slow hydrogenation. Owens and Amberg also performed experiments to determine the effect of reaction products occupying desulfurization sites. They found that the products did not inhibit the hydrodesulfurization reactions, and thus conclude that hydrocarbons are unable to compete successfully for the

desulfurization sites.

Kolboe and Amberg (11) found that the hydrodesulfurization reaction rate is dependent upon the amount of conversion obtained. To explain this dependence, Kolboe and Amberg propose that H_2S acts as an inhibitor in the desulfurization process, as found in previous studies (10). By working with very low conversion levels, the authors found that 1,3-butadiene was indeed present as a reaction product. They interpret this finding to mean that 1,3-butadiene is the first C_4-hydrocarbon formed from the desulfurization of thiophene. However, the butadiene product still undergoes rapid hydrogenation under conditions of higher conversion. Kolboe and Amberg conclude that a mixture of 1,3-butadiene, 1-butene, cis- and trans-2-butene, and n-butane comprise the initial reaction product.

In a later study of the desulfurization of thiophene, Kolboe (12) proposed that the reaction proceeds by dehydrosulfurization rather than hydrodesulfurization. He suggests that splitting off of a H_2S molecule occurs first in a reaction, analogous to the dehydration of an alcohol. Kolboe states that when the C-S bond is cleaved in an adsorbed species of the type $[R\text{-}CH_n\text{-}CH_n\text{-}S]_{ads}$, the product is $[R\text{-}(CH_{n-1})\text{-}CH_n]_{ads}$. Furthermore, he proposes that the hydrogen required for the C-S cleavage comes from thiophene and not from the catalyst. The dehydrosulfurization of adsorbed thiophene would thus lead to adsorbed 1-butene-3-yne-1-thiol. The splitting of the second C-S bond would result in a diacetylene species, which would then readsorb to the catalyst surface and undergo hydrogenation. This

process is schematically represented below.

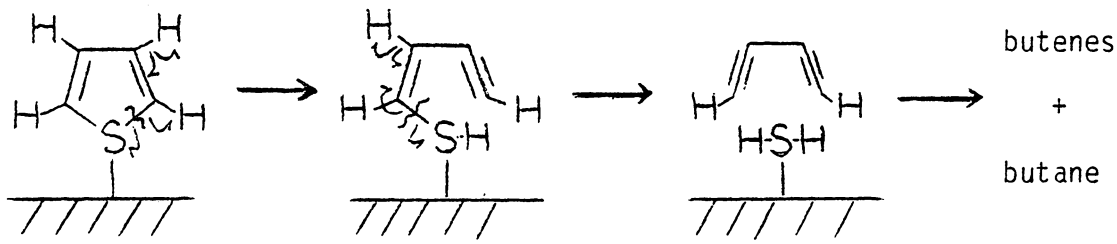

Kolboe's proposed mechanism is supported by his work on the rate of reaction and product distribution of the desulfurization of thiophene, tetrahydrothiophene, and butanethiol (12).

In a study of the adsorption of thiophene on cobalt molybdate and molybdenum disulfide, Nicholson (13-14) was able to identify the coordination of the sulfur species by infrared spectroscopy. Identification and semiquantitative analysis was principally based upon the carbon-hydrogen stretching vibrations between 3175 and 2900 cm^{-1}. Nicholson reasoned that thiophene could exist in a minimum of three forms on the surface:

1) one-point coordination: direct coordination of the sulfur atom to the surface

2) two-point coordination: two carbon atoms are united with the surface, a π complex

3) four-point coordination: four carbon atoms adsorbed to the surface in a flat form

The infrared bands corresponding to these forms occur at approximately 3086, 3005, and 2960 cm^{-1}, respectively.

On one sample of cobalt molybdenum, Mo/Co = 20, Nicholson found evidence for all three surface species, but with a higher concentration of the two point species. In cases where the catalyst

was supported on alumina, the amount of four-point species was greater than the two-point species. Nicholson also found that the presence of hydrogen and the temperature used in adsorption play an important role in the thiophene species found on the catalyst surface. On a catalyst surface saturated with H_2, the four-point species was observed along with hydrogenated species. In another study, Meites and Nicholson (15) report that thiophene adsorption at temperatures above 175°C on platinum(0) and rhodium(0) surfaces supported on Alon-C lead to the formation of the four-point species. On the basis of these works (13-15), Nicholson concludes that it is the four-point species that is the active intermediate.

In contrast to Nicholson's conclusion (13-15), Lipsch and Schuit (16) suggest that the active form is not the four-point species, but the one-point species. Since the vibrational band at 2960 cm^{-1} disappears upon reaction with hydrogen, Lipsch and Schuit conclude that the active intermediate is one where the sulfur atom is directly bonded to the surface. In studies of the desulfurization of thiophene at atmosphereic pressure on $CoO-MoO_3/Al_2O_3$, Lipsch and Schuit found that the catalyst was fully activated by reduction with hydrogen. Sulfidation of the catalyst with hydrogen sulfide did not increase its activity. The authors suggest that reduction of the catalyst leads to anion vacancies to which the thiophene molecule adsorbs in one-point coordination. Hydroxyl groups on the surface provide the hydrogen to rupture the carbon-sulfur bond, in accord with Owens and Amberg's (9) conclusion that C-S bond breakage occurs first. Lipsch and Schuit

propose that butadiene then desorbs from the surface, in agreement with Kolboe and Amberg (11). The original surface site is restored by reaction with hydrogen and desorption of H_2S. This process is depicted in the scheme below.

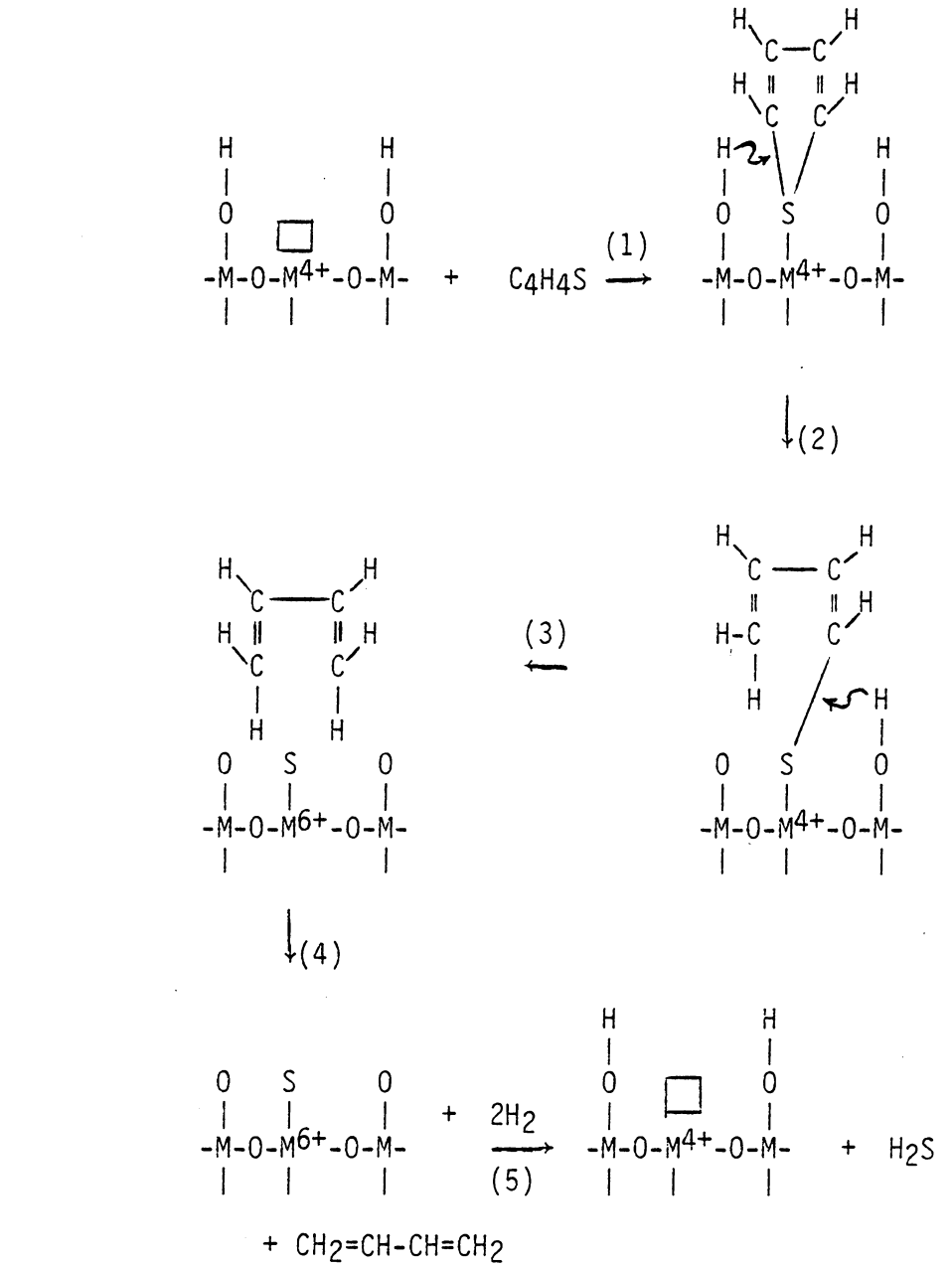

Lipsch and Schuit also found that at temperatures above 220°C, butene was hydrogenated by surface hydroxyl groups. Below 220°C, butene reacts directly with hydrogen from the gas phase.

Hargreaves and Ross (17) propose another mechanism for the desulfurization of thiophene. Working with reaction mixtures containing 1.33 Torr of sulfur or hydrocarbon compound, and 22 Torr of H_2 or He, the authors conclude that reaction occurs first by ring hydrogenation and then cleavage of the carbon-sulfur bond. Thiophene is hydrogenated to tetrahydrothiophene, and then dehydrosulfurization occurs. This results in the formation of 1,3-butadiene which then reacts further to give butene and butane. This proposal is in direct conflict with earlier studies by Owens and Amberg (8-10) where C-S bond cleavage occurred first. Hargreaves and Ross suggest that this contradiction is due to the higher pressures used in their experiments and also differences in catalysts. Owens and Amberg (8-10) used a chromia catalyst which was activated in H_2 by heating to 400°C for a few hours. Hargreaves and Ross used cobalt-molybdate catalysts which had been sulfided with H_2S at 300°C for 17 hours. These differences in catalysts, preparations and pressures could explain the differences in results obtained.

Investigations such as these on the desulfurization of thiophene have been carried out as model studies for the reaction of heavier sulfur compounds. Condensed thiophenes such as benzothiophene and dibenzothiophene make up a large percentage of sulfur compounds of the middle distillates in petroleum. Thus, investigations have been

performed on these compounds to determine their hydrodesulfurization reactivity. But, as has been demonstrated (18-24), there exists a definite change in the reactivity in going from thiophene to benzothiophenes.

Kilanowski and coworkers (18) found in their low pressure studies of the reactivity of benzothiophenes and dibenzothiophenes that a simple sulfur extrusion pathway was followed. Major products from these two compounds were biphenyl and corresponding methyl-substituted biphenyls. These results contradict those of Givens and Venuto (19) who observed alkyl migrations and dealkylation in their low pressure studies. Kilanowski et al. explain this discrepancy as differences in catalyst preparation and temperatures used in the experiments. Kilanowski et al. observed virtually no dependence of reactivity upon the number of rings in the reactant, in contrast to results of others (20). Frye and Mosby (20) observed that the reactivity at high pressures decreased as the number of rings increased. To explain this difference, Kilanowski et al. suggest that the structure-reactivity pattern for hydrodesulfurization depends upon the pressures used in the study. Kilanowski et al. also observed that benzothiophene and dibenzothiophene reactivity at 450°C over a cobalt-molybdate catalyst were nearly the same. However, with the addition of methyl substituents in the 2-or 8-positions to dibenzothiophene, an increase in the reactivity was observed. This increase in reactivity can be explained by a combination of induction effects and hyperconjugation of the methyls in a para position relative to the α-carbons. This

positioning leads to enrichment of the electron density around the α-carbons, increasing the reactivity (18, 21, 22). Methyl substituents in the 4-or 6-position, however, lead to a decrease in reactivity. This effect is explained by steric hindrance of the methyl groups. The methyl hydrogens are in a position to shield the lone pair electrons on the sulfur atom and to prevent bonding to the catalyst surface (18, 21, 22).

In a similar study at 300°C, 100 atm, and using a sulfided Co-Mo/Al_2O_3 catalyst, Houalla et al. (23) found that 4,6-dimethyldibenzothiophene is approximately 10 times less reactive than dibenzothiophene, but only approximately 2 times less reactive than 4-methyldibenzothiophene. This finding is in accord with the results of Kilanowski et al. (18). If reaction is by the one-point mechanism, Kwart et al. (21) suggested that expected steric hindrance should lead to reactivity differences of several orders of magnitude between these two compounds. Similarly, Givens and Venuto (19) observed that 3-methylbenzothiophene was slightly less reactive than 2-methylbenzothiophene, which should be more sterically hindered. Furthermore, Kwart et al. (21) point out that if hydrodesulfurization of dibenzothiophene proceeds by the one-point Kolboe mechanism (12), a highly unstable benzyne intermediate would result, a process he considers highly unlikely. Measurements of the bond order, free valence and charge density of thiophene show that the C_1-C_2 bond of the thiophene molecule has the highest electron availability. Also, the lone electron pairs on sulfur are greatly involved with resonance

of the thiophene nucleus, thus leaving little residual electron availability on the sulfur atom (21). All of these determinations led Kwart et al. (21) to propose that thiophene bonding to the catalyst occurs through the C_1-C_2 bond, as a π complex, and not through direct coordination with the sulfur atom (8-12, 16, 17).

The multipoint mechanism (21) involves the C_1-C_2 bond of thiophene coordinating to a surface anion vacancy with the adjacent sulfur atom interacting with a sulfur atom on the catalyst surface. When the π complex is formed, electron density on the thiophene ring is redistributed, resulting in an electron deficient sulfur atom. This deficiency promotes sulfur bonding with a surface sulfur atom (see below). Hydrogenation of one carbon atom results in cleavage of

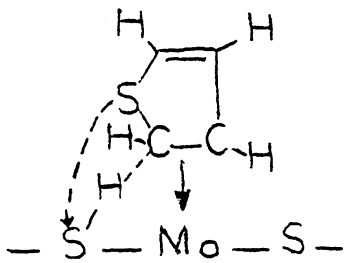

Kwart et al. suggested surface structure

the C-S bond as shown here.

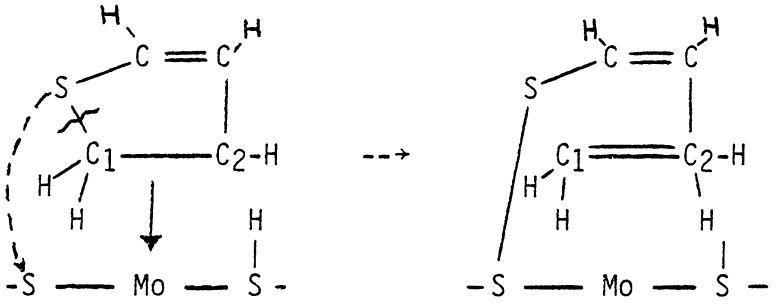

Adsorption of the olefinic portions of this structure to the catalyst results in cleavage of the second C-S bond. The final result is that butadiene is liberated, which either desorbs as such, or is further hydrogenated to give butenes and butane.

The Kwart et al. mechanism (21) readily accounts for the observed reactivity between methyl substituted dibenzothiophenes. A 4-methyl substituted dibenzothiophene causes a steric hinderance inhibiting planar adsorption of the active centers on the ring to those on the catalyst. The hydrogens of the methyl group "sweep out a sphere of revolution above and below" the plane of the ring (21), thus interferring with the coordination ability of the thiophene to the catalyst. However, since dibenzothiophene is planar, a second methyl group at the 6-position would not create any greater steric hinderance to adsorption.

In another study of the hydrodesulfurization of sulfur heterocyclic compounds at high pressure, Singhal et al. (24) found evidence of coordination of the thiophene compounds through the sulfur atom and also as a π complex. Singhal and coworkers propose that the reaction pathway is structure dependent. They state that if electron density is localized on the sulfur atom, direct coordination of the sulfur to an active surface site can occur. However, if the electron density is delocalized over a π system, coordination will occur to give a π complex.

As can be seen from this brief literature review, the mechanism for desulfurization of thiophene and its derivatives has not yet been

clarified. However, conflicting results and postulates could be due to the variety of reaction conditions and catalyst preparations used in these studies.

To better understand the hydrodesulfurization process, many studies have been carried out to determine the properties of the catalyst and its structure in both the calcined and active state (25-32). Since the majority of current hydrodesulfurization work has been with cobalt-molybdate catalysts, this next section will deal with the surface characteristics of this particular catalyst.

B. Catalyst Surfaces

Chin and Hercules (25) investigated the surface properties of a series of cobalt impregnated alumina catalysts. By use of x-ray photoelectron spectroscopy, ion scattering spectroscopy and secondary ion mass spectrometry, they determined that catalyst surface characteristics are affected by both metal content and calcination temperature. Chin and Hercules observed that low cobalt loadings (<10%) and high calcination temperatures (600°C) led to cobalt primarily occupying tetrahedrally coordinated lattice positions. Greater metal loadings and lower calcination temperatures led to the cobalt occupation of octahedral lattice sites and the eventual build up of a Co_3O_4 surface layer. The authors conclude that the ability of the catalyst to undergo reduction is directly related to the metal-support interaction. They found that as the metal-support interaction increased, i.e. more chemically inert tetrahedral cobalt present, catalyst reduction ability decreased.

In a study by Breysee, Bennett, and Chadwick (26), the surface composition of a Co-Mo/graphite catalyst was investigated by means of XPS and Mossbauer spectroscopy. Since the XPS Mo 3d spectrum of the sulfided catalyst appeared identical to that of a molybdenum sulfide (MoS_2) reference sample, the authors concluded that complete sulfidation of the molybdenum had occurred to give MoS_2 on the surface. The cobalt XPS spectra from the Co-Mo/graphite catalyst was similar to that of Co/graphite and yielded a binding energy for the Co $2p_{3/2}$ photoelectron peak of 778.7 eV. No strong satellite peaks were observed, and the difference in energy between the $2p_{3/2}$ and $2p_{1/2}$ was 15.1 eV for both the Co-Mo/graphite and Co/graphite samples. The authors measured the S 2p/Co $2p_{3/2}$ intensity ratio as 0.3 and state that it compared favorably with the 0.23 value for Co_9S_8. Thus, they conclude that cobalt exists as Co_9S_8 on the catalyst surface. As further proof of their conclusion, the Mossbauer spectrum obtained from the Co-Mo/graphite catalyst was identified as Co_9S_8.

Delannay and coworkers (27) used ion scattering spectrometry to study the surface structure of the oxidized Co-Mo/Al_2O_3 catalyst. In the initial ISS spectra, the authors observed high molybdenum signals and hardly any cobalt. However, as the analysis progressed, the molybdenum signal decreased exponentially as the cobalt signal steadily increased. Delannay et al. interpreted these findings to mean that the surface structure of the catalyst consists of a deposited cobalt oxide layer, over which lies a separate molybdenum oxide layer.

By use of extended x-ray absorption fine structure (XAFS), Clausen et al. (33) were able to obtain structural information on both the calcined and active cobalt-molybdate catalysts. They found that molybdenum is present in a highly disordered state in the calcined samples. However, after sulfiding the catalysts, an ordering takes place. Clausen et al. conclude that the molybdenum in the sulfided catalysts exists in a MoS_2-like structure. Furthermore, these structures are ordered in very small domains. Clausen et al. also reason that for either the sulfided or the calcined catalysts, the molybdenum atoms are not greatly affected by the presence of cobalt.

The literature review in this section has been just a small representation of the advances which have been made in the area of the hydrodesulfurization process for sulfur heterocyclics. However, to fully comprehend the mechanism involved and the role of the catalyst, more research needs to be undertaken. As has been stated earlier, most of the investigative work has been carried out with cobalt-molybdate catalysts. There is the distinct possibility that hydrodesulfurization could be maximized with another class of catalysts. It has been shown (34, 6) that metal sulfides are effective catalysts for reactions such as hydrogenation, disproportionation, dehydrogenation, isomerization and hydrodesulfurization. Zeolites are good catalysts for many reactions, including the conversion of oxygen containing compounds to hydrocarbons (35-39). A brief review of the role of metal sulfides and zeolites as catalysts will be covered in the next few sections.

C. Metal Sulfides.

A study by Fukuda and coworkers (34) was carried out on the activity of first row transition metal sulfides for the reaction H_2S + CO = H_2 + COS. Fukuda et al. observed a twin-peak effect, with two activity maxima occurring for Cr_2S_3 and Co_9S_8. This activity pattern is similar to results obtained by Dowden et al. (40) for the activity of 3d metal oxides, and also for metal sulfide activity in the hydrogenolysis of carbon disulfide (41). However, no explaination was given for the results.

Pecoraro and Chianelli (6) have investigated the role of transition metal sulfides as catalysts for the hydrodesulfurization of dibenzothiophene. Transition metals from the first, second, and third row were studied. Hydrodesulfurization reactions of dibenzothiophene (DBT) at 400°C over all the metal sulfide catalysts result in biphenyl as the reaction product. With RuS_2, however, some cyclohexylbenzene was formed. Pecoraro and Chianelli (6) observed that maximum activity was obtained with second and third row transition metal sulfides on a per gram basis. Of the second row, RuS_2 achieved maximum conversion of approximately $3x10^{19}$ molecules DBT converted/gm·sec. Osmium sulfide resulted in maximum conversion among third row elements, about $8x10^{18}$ molecules DBT/gm·sec. The order of activity observed at 400°C (6) in decreasing order is:

Second Row $RuS_2 > Rh_2S_3 > PdS > MoS_2 > NbS_2 > ZnS$

Third Row $Os°+S > Ir°+S > ReS_2 > PtS > WS_2 > TaS_2$

At 350°C, RuS_2 is still most active, but a switch occurs in that MoS_2

is more active than PdS. At this temperature maximum conversion in the third row is reached with ReS_2. In agreement with Fukuda et al. (34) the authors (6) observed two activity maxima for the sulfides of the first row transition metals. The two maxima were reached with Cr_2S_3 and Co_9S_8, about $4x10^{16}$ and $1x10^{16}$ molecules DBT/gm·sec, respectively.

Pecoraro and Chianelli (6) found that because of differences in structure and geometry, hydrodesulfurization activities of the transition metal sulfides do not, in general, correlate well with B.E.T. surface areas. Thus, they assert that normalizing the hydrodesulfurization activity to a per gram, or per metal basis, yields the most reliable activity for the metal sulfides. Based on experimental data, the authors conclude that the most active catalysts are those with the highest percentage d character available. Pecoraro and Chianelli also found that the most active metal sulfides were those that had intermediate heats of formation, ΔH_f. The most active members of the second and third row metal sulfides, RuS_2 and OsS_2, had ΔH_f values between 30 and 55 kcal/mole. Pecoraro and Chianelli propose that the metal-sulfur bond must not be too strong or too weak to obtain the maximum desulfurization rate. This proposal is consistent with the idea of vacancies on the catalyst surface being the active site in hydrodesulfurization (16). Reactants would adsorb to the vacancy, then react and desorb so as not to poison the catalyst.

The use of zeolites as catalysts for hydrodesulfurization of

sulfur containing compounds is also a distinct possibility. Zeolites are active catalysts for other processes such as disproportionation of toluene and conversion of methanol into hydrocarbons. Before looking into zeolite catalysis, however, it is necessary first to be familiar with the structures and physical properties of zeolites.

D. Structures of Zeolites.

Zeolites have been defined by Breck (42) as "an aluminosilicate with a framework structure enclosing cavities occupied by large ions and water molecules, both of which have considerable freedom of movement, permitting ion exchange and reversible dehydration." Zeolites compromise the largest group of the tecktosilicates, which also contain the feldspars and feldpathoids. There are over 35 naturally occurring zeolites and approximately 100 different zeolite structures have been synthesized. The different zeolite structures lead to alterations in physical and chemical properties.

Differences in the structures of zeolites arise in the way in which the fundamental building units are linked together. The basic structural unit of all zeolites is the $(Si, Al)O_4$ tetrahedron. The silicon, or aluminum, atom is situated in the center position and is tetrahedrally coordinated to four oxygen atoms. When an aluminum atom substitutes for a silicon atom, a net negative charge on the tetrahedron is created, which must be neutralized by a counterion. In naturally occurring zeolites, this counter ion is predominantly an alkali metal or an alkaline earth metal, but a variety of ions are used in synthetic zeolites.

Structural classifications of zeolites have been proposed by Meir (43). The classifications are based on framework topology, grouping together those zeolites with a common array of $(Si, Al)O_4$ tetrahedra. Meir calls these arrays secondary building units (SBU). Thus, zeolites with common SBU arrays, such as double six rings or double four rings, are classified in the same scheme.

Structure of Zeolite 13X

Zeolite X, a synthetic aluminosilicate, is closely related to the naturally occurring, but rare, mineral faujasite. Thus, they are grouped in the same classification scheme. This structural group is often referred to as the "sodalite group", as its structure is also very similar to that of the feldspar sodalite. Consequently, these names are often used interchangeably.

A typical cell composition for the hydrated zeolite X is $Na_{86}[(AlO_2)_{86}(SiO_2)_{106}]\cdot 276\ H_2O$ with $1 \leq Si/Al \leq 1.5$. Zeolite Y, another faujasite, has a cell composition of $Na_{57}[(AlO_2)_{57}(SiO_2)_{135}]\cdot 276\ H_2O$ with $1.5 \leq Si/Al \leq 3.0$. The unit cell of zeolite X is cubic and contains 192 $(Si, Al)O_4$ tetrahedra. It has a cell dimension of 25Å and the largest known void volume of any zeolite, approximately 50 vol % of the dehydrated crystal. The $(Si, Al)O_4$ tetrahedra are arranged in the corners of a truncated octahedron as shown in Figure 1. This octahedron is a common feature of the sodalite group, and it contains eight hexagonal faces, six square faces, 24 vertices, and 36 edges. The truncated octahedra are connected to each other at four of the

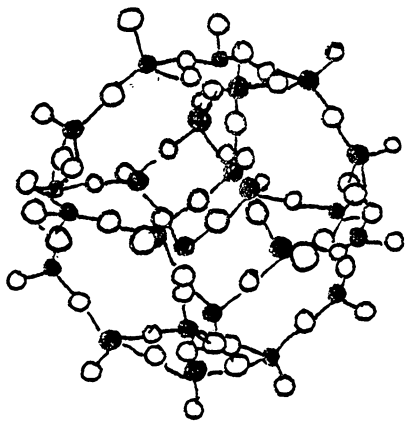

○ = oxygen atom

● = silicon, aluminum atom

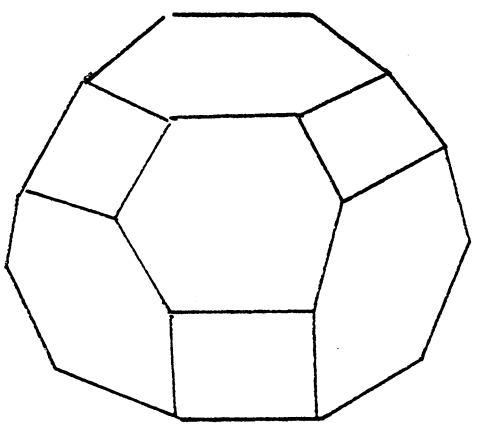

Figure 1. 13X Truncated Octahedra

hexagonal faces through its SBU's of double six rings, or hexagonal prisms. The end result is a tetrahedral arrangement of truncated octahedra. A diagram illustrating the structure and the large α-cage, or supercage, is shown in Figure 2. This supercage has a free diameter of 13Å, whence the zeolite gets its name. The supercage cavity entrance is a 12-membered ring approximately 8Å in diameter. The cavity inside the truncated octahedron is known as the β-cage and has a diameter of 6.6Å. The diameter of the interconnecting hexagonal prisms is about 2.4Å.

Structure of ZSM5

In contrast to the cage structure of 13X, a new class of synthetic zeolites, ZSM5, has recently been developed (44) which has a unique channel structure. The channel structure results in a difference in sorptive, shape selective, and catalytic properties of ZSM5.

ZSM5 crystallizes in the orthorhombic system and has a high silicon to aluminum ratio, $10 \leq Si/Al \leq 60$. The Na^+-saturated form of ZSM5 has a typical unit cell composition of $Na_nAl_nSi_{96-n}\cdot O_{192}\cdot \sim 16H_2O$, where $n<27$ and usually about 3 depending on the method of synthesis. The primary building unit of ZSM5 is the $(Si, Al)O_4$ tetrahedron. The structure of ZSM5 is based on a unique configuration of linked tetrahedra in a series of eight five-membered rings, as shown in Figure 3. These linked tetrahedral units are joined together by their edges which results in long chains. These chains are further connected to form infinite sheet structures and eventually a three

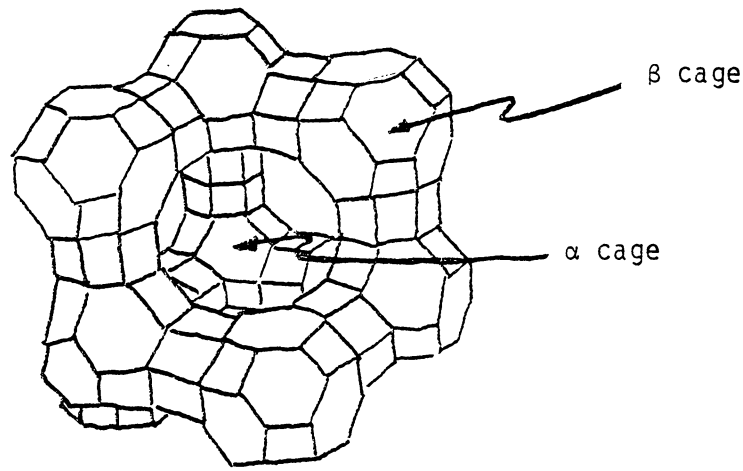

Figure 2. Structure of 13X

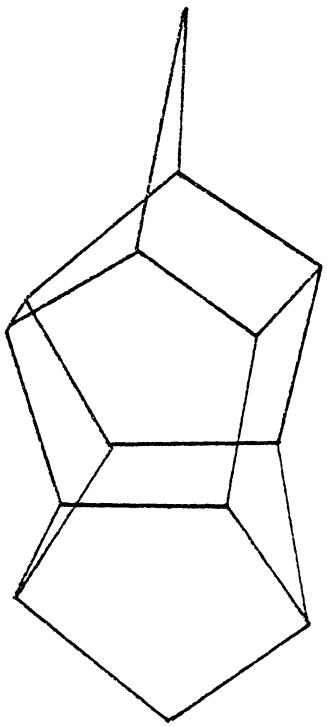

Figure 3. Building Unit of ZSM5

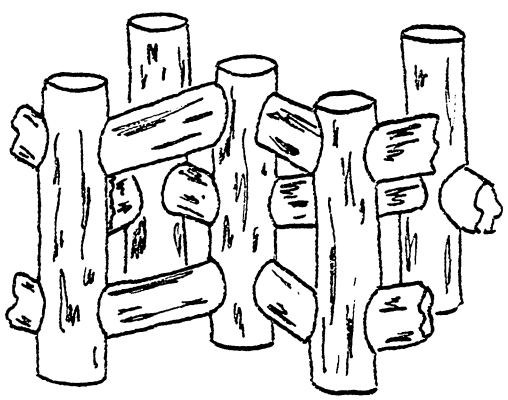

Figure 4. Channel Structure of ZSM5

dimensional network. The distinct channel pattern running through ZSM5, (Figure 4), consists of two intersecting but independent channels. One channel, shown running horizontally, has a nearly circular shape and traces out a sinusoidal path through the zeolite. Openings to this channel are approximately 5.4 x 5.6Å. The second channel, running vertically and extending throughout the entire structure, is linear and elliptical in shape. The openings to this channel are governed by 10-membered rings and are about 5.1 x 5.8Å in diameter.

E. Zeolite Catalysis

Because of these unique structures, zeolites have often been used in shape selective reactions with great success. Derouane and Gabelica (45) recently reported on a special quality of ZSM5, that of "molecular traffic control". This effect occurs when reactants enter the catalyst through one channel system, and products diffuse out by the other channel. This "traffic control" accounts for the lack of counterdiffusion effects in reactions over ZSM5 which can limit catalytic conversion. Derouane and Gabelica found that isoaliphatics, methyl-aliphatics, and monocyclic aromatics would diffuse into ZSM5 by the nearly circular, sinusoidal channels. These compounds would react at channel intersections, at the location of active sites and form bulkier molecules. Derouane and Gabelica observed that the larger products then diffused out of the ZSM5 structure through the elliptical channels. Thus, the authors assert a traffic control is imposed,

whereby reactants are supplied and products cleared away from the active sites, without interference from each other.

Kaeding and coworkers (46,47) have conducted studies of the shape selective properties of ZSM5 in the alkylation and disproportionation reactions of toluene. Para-xylene was found to be the major product of both reactions. Since the para isomer has the smallest dimension of the substituted xylenes, it was proposed that the restrictive size of the ZSM5 channels prohibits a more complete formation of the ortho- and meta-xylenes. Therefore, para-xylene is able to diffuse out of the channels at a much faster rate. The ortho- and meta-isomers formed could further isomerize to para, thus increasing the yield.

Derouane and Vedrine (48) have made recent studies on the shape selective role of ZSM5 in the conversion of alcohols to hydrocarbons. Their findings indicate that the aromatic hydrocarbon products are formed at the channel intersections (approximately 9Å diameter) and are then able to diffuse to the external surface of the zeolite through the elliptical channels. The authors suggest that the strong acid catalytic sites must be located at these channel intersections. Derouane and Vedrine therefore conclude that the shape selective qualities of ZSM5 consist of two different effects: 1) steric restrictions associated with the active sites which govern product formation, and 2) the different channel systems preferentially utilized by the reactants and products. This conclusion supports the idea of molecular traffic control (45).

ZSM5 has also been used as a catalyst for the conversion of methanol and other oxygen compounds to hydrocarbons of the gasoline boiling range. Many studies have been conducted to determine the mechanism of this conversion reaction (35-39).

In one such study, Chang and Silvestri (37) report their findings on the conversion of oxygen compounds to hydrocarbon products. Using ZSM5 as the catalyst, methanol, t-butanol and 1-heptanol react to give essentially no hydrocarbons above C_{11}. The authors suggest that the product distribution is based on the shape selective qualities of ZSM5. The dimensions and shapes of the zeolite channel limit the product chain length, and also contribute to the hydrocarbon isomer distribution. Those isomers with lower diffusivity through the channels are consequently not formed. In a reaction with methanethiol, Chang and Silvestri observed conversion was more difficult than that of the alcohols. A temperature 100°C higher than ones used for alcohols had to be employed in order to obtain conversion to hydrocarbons.

To explain their observed results, Chang and Silvestri propose a mechanism involving formation of a carbene species as the first step. Methanol loses a molecule of water to produce [$:CH_2$] which can then dimerize and produce ethylene, or interact with another molecule of methanol by an insertion reaction. Chang and Silvestri consider this latter reaction more probable and occurring as shown:

$$[:CH_2] + CH_3\text{-}OR \longrightarrow CH_3CH_2\text{-}OR$$

$$CH_3CH_2\text{-}OR \xrightarrow{-HOR} C_2H_4$$

Brooks (49) has studied thiophene hydrodesulfurization using transition metal zeolites as catalysts. The two zeolites used were a synthetic mordenite and a synthetic faujasite Y in the sodium, ammonium and transition metal forms, with and without nickel. By comparison of initial reaction rates, Brooks found that both the transition metal and the zeolite contribute to hydrodesulfurization. Zeolite Y, both with and without metal loading, was superior in activity to mordenite and a commercial $Ni\text{-}MoO_3\text{-}Al_2O_3$ catalyst, when referred to a weight basis. Brooks proposes that since the adsorption coefficients for the thiophene pulses were much larger for zeolite Y, a reflection of its greater surface area, that this could be a contributing factor to the greater activity. Maximum activity for the mordenite zeolite was achieved with nickel, copper and rhodium loadings. Brooks concludes that the hydrodesulfurization of these zeolites is attributable to 1) enhanced adsorption of the reactant thiophene on the high specific surface area zeolites, 2) hydrocracking due to the high acidity of the zeolite, and 3) an enhancement of hydrogenolysis reactivity over the metal.

F. Rhodium Catalysts

The ability of transition metals to act as homogeneous catalysts for many reactions has been known for a long time. But the use of

transition metals in supports such as alumina or zeolites as heterogeneous catalysts has only recently come under study. Supported transition metal catalysts are becoming more prevalent in today's catalytic processes.

Christensen and Scurrell (50) recently reported on the selectivity of a heterogeneous rhodium catalyst for the carbonylation of alcohols. The reaction selectivity of methanol, ethanol and 2-propanol was investigated using an aqueous rhodium trichloride exchanged 13X zeolite as the catalyst. The selectivity for the carbonylation of methanol to methyl acetate was >90% between 160 and 240°C. The selectivity for carbonylation of 2-propanol was essentially 0%, as the product from the reaction was exclusively propene between the temperatures 160 and 200°C. The selectivity for ethanol carbonylation was approximately 50%, depending upon the reaction temperature. Thus, Christensen and Scurrell conclude that the rhodium-zeolite catalyst provides high activity and selectivity for the carbonylation of methanol, but is greatly decreased for ethanol and 2-propanol. The authors made no mention of the role of the zeolite support, the catalytic role of rhodium, or the actual rhodium species present on the catalyst.

In later studies, Scurrell and coworkers (51-53) investigated various rhodium catalysts to better understand their role in carbonylation reactions. Studies were carried out on $RhCl_3$-X, $Rh(NH_3)_5Cl$-X, $RhCl_3/SiO_2$, $RhCl_3/MgO$, $RhCl_3/SnO_2$, and $Rh(NH_3)_5Cl$/mordenite. Highest activity was reported for the systems having

zeolites as supports. Scurrell and Howe (52) report that greater dispersion of rhodium in the zeolite framework was achieved using $[Rh(NH_3)_5Cl]Cl_2$ rather than $RhCl_3$. They also report the active species present in all preparations of Rh-zeolites as the Rh(III) ion, indicated by the binding energy of the Rh $3d_{5/2}$ photoelectron peak at 310.2 eV. The authors suggest that the effect of the zeolite is to bond the rhodium in such a way that the ligands are easily removed forming active centers. The active centers then coordinate to CO and CH_3I molecules to initiate reactions. It is also proposed that strong electrostatic fields within the zeolite lattice facilitate the formation of active centers and/or increase the rate determining step of the carbonylation reaction.

Brinen and Melera (53) conducted XPS studies on three rhodium/charcoal hydrogenation catalysts to determine the chemistry of the catalyst surface. The broadness of the Rh $3d_{3/2}$ and $3d_{5/2}$ photoelectron peaks for each catalyst indicate a mixture of oxidation states on the surface. For the three hydrogenation catalysts, the Rh $3d_{5/2}$ photoelectron peak occurred at about 308.4 eV. By comparison to the Rh $3d_{5/2}$ binding energy of rhodium sesquioxide at 308.4 eV, Brinen and Melera conclude that some of the rhodium present on the hydrogenation catalyst is an oxide species. However, in each case a second $3d_{5/2}$ peak occurred at approximately 307.1 eV suggesting metallic rhodium. From the intensities of the $3d_{3/2}$ and $3d_{5/2}$ photoelectron peaks, the low activity catalyst has a higher metal to oxide ratio than the higher activity catalysts. Brinen and Melera

thus conclude there exists a direct correlation between hydrogenation activity and the oxide to metal ratio on the surface of the catalyst. They further state that the desirable catalytic properties may be attributable to the oxide species.

Kuznicki and Eyring (54) have investigated rhodium(III)-exchanged zeolites by means of XPS. They exchanged aqueous $RhBr_3$ with zeolite A and zeolite Y. The initial color of the rhodium exchange solutions was reddish brown. After the 72 hour exchange period the solutions had been extensively decolorized. This observation led Kuznicki and Eyring to reason that complete rhodium exchange had occurred with the zeolites. XPS revealed that the rhodium was present in both zeolites as Rh(III). The binding energies of the Rh $3d_{3/2}$ and Rh $3d_{5/2}$ photoelectron peaks were 313.6 eV and 309.5 eV, respectively. After heat activation at 300°C and $2x10^{-3}$ Torr for two hours, zeolite Y had turned black, while zeolite A retained its initial light brown color. XPS measurements determined that the rhodium in zeolite A was still present as Rh(III). The XPS rhodium spectrum for Rh(III)-Y, however, indicated a mixture of oxidation states. Kuznicki and Eyring attribute the 3d peaks at 313.6 and 309.5 eV to the original Rh(III) species, and the two new 3d peaks at 311.9 and 307.1 eV to rhodium(0). Noting that zeolite A has previously demonstrated a lack of catalytic activity and zeolite Y has proven active for a variety of reactions, the authors suggest that metallic rhodium is the true catalytic agent in so-called Rh(III)-zeolite catalysts.

This literature review was meant to give a brief introduction into the realm of zeolites, transition metal sulfides, and hydrodesulfurization reactions. It is by no means all encompassing, since research involved in these subjects has been carried out for decades. However, it is evident from the works presented that theories regarding the mechanism of hydrodesulfurization reactions are still incomplete and the selection of catalysts is not clearly established. Since hydrodesulfurization is such an economically important process, investigative studies will continue until the key to understanding this process is found.

CHAPTER III

EXPERIMENTAL

This section will describe the experimental aspects of the research. A description of materials used, adsorption studies, preparation of catalysts, syntheses performed, equipment used and catalytic reactions carried out will be presented.

A. 13X

The 13X zeolite, $Na_{86}[(AlO_2)_{86}(SiO_2)_{106}]\cdot 276\ H_2O$, used in the adsorption and catalytic studies was purchased from the Linde Division of Union Carbide Corporation. It was received in a Na^+-saturated form. All experiments were carried out on the as-received form. X-ray diffraction data, given in Table 1, confirmed that the sample was 13X.

B. ZSM5

A complimentary 10g sample of ZSM5 zeolite was supplied by Dr. C. S. Cheng of Mobil Research and Development Company. The Mobil ZSM5 was an NH_4^+-saturated powder and was used in the adsorption studies. X-ray diffraction confirmed its identification as shown in Table 2.

C. Preparation of ZSM5

In order to have a larger quantity of ZSM5 zeolite, a sample was synthesized according to the method of Argauer and Landolt (44). The Mobil ZSM5 was then used as reference material.

The synthesis of ZSM5 required tetrapropylammonium hydroxide, (TPAOH), which was prepared according to the reaction:

Table 1

X-ray Diffraction Lines for 13X

d ± 0.1Å	intensity	d - literature*	intensity*
15.5	vs	14.5	vs
3.9	vs	3.8	s
2.9	s	2.9	s
5.9	s	5.7	s

vs = very strong
s = strong

* reference to D. W. Breck (55).

Table 2

X-ray Diffraction Lines for Mobil ZSM5

d ± 0.1Å	intensity	d - literature*	intensity*
11.9	vs	11.4	vs
3.9	vs	3.8	vs
10.5	vs	10.2	s
3.8	s	3.7	vs

vs = very strong
s = strong

* reference to D. W. Breck (55).

H_2O + 2 TPABr + Ag_2O ⟶ 2 AgBr + 2 TPAOH. To prepare the silver(I) oxide, approximately 36g of $Ag(NO_3)_{(s)}$ was added to 7.0 g of $NaOH_{(s)}$ in approximately 100 mL CO_2-free water. The CO_2-free water was prepared by bubbling nitrogen gas through doubly distilled water. Upon addition of the $AgNO_3$, a black precipitate formed immediately. The precipitate was collected by filtration, and dried on a vacuum line at approximately 10^{-5} Torr and 25°C for 24 hours. The precipitate was presumed to be Ag_2O. Tetrapropylammonium hydroxide was prepared by mixing 34.99 g of tetrapropylammonium bromide (Fisher Scientific Co.) with 15.49 g of Ag_2O and 100 mL distilled H_2O. This mixture was allowed to stir under flowing nitrogen until the black color of Ag_2O was no longer visible. The resulting solution, tetrapropylammonium hydroxide was filtered using a Buchner funnel.

Fifteen mL of 1.34 N TPAOH was added to 3.11 g SiO_2. The mixture was heated to approximately 100°C until partial dissolution of SiO_2 occurred. To this solution was then added a mixture of 0.20g $Na_2Al_2O_4 \cdot 3H_2O$ in 5 mL of distilled H_2O. This was allowed to stir for a further 10 minutes and was then placed in a thick walled pyrex tube. The tube was sealed and put in an oven at 165°C for 6 days. The resulting white solid was collected by centrifugation, washed with 1 L H_2O and calcined at 500°C for 12 hours in order to remove the amine. Three grams of ZSM5 were recovered. By comparison of X-ray diffraction, infrared spectroscopy and X-ray photoelectron spectroscopy data collected on the synthesized sample with that of Mobil ZSM5, it was confirmed that the two zeolites were structurally

identical. This data is presented in Tables 3, 4, and 5. The synthesized sample will be designated as ZSM5-G2, and Mobil ZSM5 as ZSM5(M).

D. Co-Mo/Al_2O_3

The oxide form of a cobalt-molybdate commercial catalyst was purchased from Alfa Products. Catalytic reactions were run on the Co-Mo/Al_2O_3 catalyst in order to compare the conversion results with those obtained on the rhodium zeolites.

E. Rhodium Compounds

Complimentary samples of trichlororhodium(III)trihydrate $RhCl_3 \cdot 3H_2O$, and chlorotris(triphenylphosphine)rhodium(I), $Rh(PPh_3)_3Cl$, were supplied by Engelhard Industries. Tetraacetodirhodium(II) $Rh_2(CO_2CH_3)_4$, was prepared according to Rempel (56). A 5.00 g sample of $RhCl_3 \cdot 3H_2O$ was combined with 10.01 g of $NaCO_2CH_3$, approximately 100 mL glacial acetic acid, and approximately 100 mL absolute ethanol in a round bottom flask. The solution was refluxed under flowing N_2 for one hour. The initial reddish brown solution changed to a black-green color after about 15 minutes of refluxing. After 30 minutes, the contents of the flask had turned dark green. After the 1 hour reflux the solution was cooled to room temperature. The resulting aqua-blue crystals were then collected by filtration through a Buchner funnel and dissolved in approximately 600 mL boiling methanol. The hot methanol solution was filtered to collect any impurities. The dark blue-green solution was then concentrated to about 400 mL and refrigerated overnight. The dark green crystals were

Table 3

X-ray Diffraction Lines for Mobil ZSM5 and ZSM5-G2

ZSM5-G2		Mobil ZSM5	
d ± 0.1Å	intensity	d ± 0.1Å	intensity
11.9	vs	11.9	vs
3.9	s	3.9	vs
10.7	s	10.5	s
3.8	s	3.8	vs

vs = very strong

s = strong

Table 4

Infrared Bands for 13X, ZSM5(M), ZSM5-G2

13X (cm^{-1})	ZSM5(M) (cm^{-1})	ZSM5-G2 (cm^{-1})	
1006	1098	1092	T-O stretch
738	790	788	external T-O stretch
656	612	627	internal T-O stretch
558	548	549	ring stretch
457	446	445	T-O bend
352	379	350	pore-opening bend

T = tetrahedral atom (Si, Al)

Table 5

XPS Results for 13X, ZSM5(M), ZSM5-G2

	Binding Energy (eV)				Atomic Ratio	
Zeolite	Si 2p	Al 2p	Na 1s	N 1s	Si/Al	Na(Si + Al)
13X	101.7 (±0.2)	73.8 (±0.3)	1071.9 (±0.2)	---	1.3	0.55
ZSM5(M)	103.4 (±0.3)	73.9 (±0.2)	---	401.8 (±0.3)	26.9	---
ZSM5-G2	103.4 (±0.2)	74.3 (±0.2)	1072.1 (±0.3)	---	31.6	0.020

collected by filtration and the solution was concentrated to approximately 200 mL. After concentration, the solution was cooled in an ice bath in order to draw any remaining crystals out of solution. The solution was filtered and approximately 0.1 g of emerald green crystals were obtained. The filtrate was again concentrated to 100 mL, and the cooling procedure repeated. However, no more crystals were obtained. The total quantity of $Rh_2(CO_2CH_3)_4 \cdot 2CH_3OH$ obtained from the synthesis was 2.64 g, a product yield of 54.8% based on the original amount of $RhCl_3 \cdot 3H_2O$. The acetate crystals were dried on a vacuum line at approximately 10^{-5} Torr and 45°C for 18 hours. A C, H, and N analysis of the rhodium dimer, $Rh_2(CO_2CH_3)_4$, performed by Mr. Geno Iannacconne of the V.P.I. & S.U. Chemistry Department revealed:

Found:	C - 21.63%	H - 2.54%
Calculated:	C - 21.73%	H - 2.71%

F. Adsorption of Rhodium onto Zeolites

The rhodium(III) complex, $RhCl_3 \cdot 3H_2O$, was adsorbed onto 13X, ZSM5(M), and ZSM5-G2, by the method of ion exchange. A sample of 0.235 g $RhCl_3 \cdot 3H_2O$ was dissolved in 15 mL of 6M NH_4OH to insure that the rhodium remained in solution as the ammine complex and was not precipitated as the hydroxide. To this solution was added 2.0 g of 13X, ZSM5(M) or ZSM5-G2 which was then allowed to stir for three days. The initial $RhCl_3$-13X solution was orange-yellow and after three days turned a creamy yellow color. The pH of the $RhCl_3$-13X solution, measured with an Orion Research Model 701 digital pH meter with a Sensorex S200C pH electrode, was 11.65 and remained constant during the

three day period. The initial color of the $RhCl_3$-ZSM5(M) was brown-orange and the pH was 10.94. After three days, the color of the $RhCl_3$-ZSM5(M) solution was creamy yellow and the pH was 10.81. The $RhCl_3$-ZSM5-G2 solution was initially orange-brown and had a pH of 12.22. After the adsorption period, the solution was a light yellow color and the pH had remained relatively constant at 12.20. The solutions were centrifuged, the rhodium-zeolite removed and washed three times with a total of 1 L H_2O and then dried overnight in air at 80°C.

The Rh(I) complex, $Rh(PPh_3)_3Cl$, was adsorbed on 13X in the same manner as $RhCl_3 \cdot 3H_2O$. A 0.450 g sample of $Rh(PPh_3)_3Cl$ was dissolved in 15 mL of 6M NH_4OH. To this solution was added 2.0 g 13X. The solution was allowed to stir for three days. The pH stayed constant at 12.76 and the color of the exchange solution changed from a red-purple to a light orange. Washing and drying of the Rh(I)-13X was carried out as in the Rh(III)-13X preparation.

The Rh(II) complex, $Rh_2(CO_2CH_3)_4$ was adsorbed on 13X from a methanol solution. Methanol was used because the solubility of $Rh_2(CO_2CH_3)_4$ is greater in alcohol than in water. A 0.111 g sample of $Rh_2(CO_2CH_3)_4 \cdot 2CH_3OH$ was dissolved in 25 mL CH_3OH. Two grams of 13X were added. There was no apparent color change of the solution during the three day exchange period.

G. X-Ray Diffraction

A Norelco X-ray diffractometer employing nickel filtered Cu K_α

radiation was used. The x-ray generator was operated at 40 kV and 20mA. A Digital Equipment Corporation PDP11 computer was used in conjunction with the diffractometer. Zeolite samples were mounted randomly on quartz slides by making a suspension of the sample in water, pipetting a few drops onto the slide, and allowing the water to evaporate. The d spacings of the zeolites were calculated by use of the Bragg equation, $n\lambda = 2d\sin\Theta$, and are given along with relative intensities in Tables 1, 2, and 3.

H. Infrared Spectroscopy

A Perkin Elmer 283B spectrophotometer was used to collect infrared data. Samples were ground to a fine grain size using an agate mortar and pestle and/or a Wig-L-Bug. The samples were combined with dry IR grade KBr and a pellet was hand pressed. All samples were run as KBr pellets in the range 4000 cm^{-1} to 200 cm^{-1}. Positions of the most intense vibrational bands for the three zeolites are given in Table 4.

I. X-ray Photoelectron Spectroscopy

X-ray photoelectron spectroscopy (XPS or ESCA) was used as a means of characterizing the zeolite surface both before and after catalytic reactions. A Dupont 650 spectrometer was used to collect the data. Most samples were mounted in a thin and evenly distributed layer on a brass probe with Scotch brand double stick tape. Some samples were prepared using a water dispersion which was placed on the brass probe and the water was allowed to evaporate in air. A magnesium anode, $h\nu$ = 1253.6 eV was used as the x-ray source. Spectra were calibrated by

reference to the binding energy of the C 1s photoelectron peak at 284.6 ± 0.1 eV. This value was previously determined by reference to the binding energy of the Au $4f_{7/2}$ peak at 83.4 eV. It was found that rhodium compounds on the zeolites undergo photoreduction while under x-ray bombardment in the spectrometer. As evidenced from the decreased binding energy and broader peak shape of the Rh $3d_{3/2}$ and Rh $3d_{5/2}$ photoelectron peak, Rh(III) undergoes a process to give reduced rhodium. This process is complete after only about two hours in the spectrometer. Thus, all rhodium spectra to be discussed are those which were obtained as an initial scan before significant photoreduction had occurred. To achieve reproducibility of XPS results, at least four different measurements were made on the zeolites, Co-Mo/Al_2O_3, rhodium compounds and rhodium treated zeolites. In most cases, two measurements were made on the sulfided catalysts. However, only one measurement was taken on the catalyst after the hydrodesulfurization reactions had occurred. Atomic ratios of elements on the surface of the sample were obtained by triangulating the photoelectron peak, correcting for the cross section and ratioing the peak areas. A Digital Equipment Corporation PDP 8/I computer interfaced to the spectrometer allowed transfer of data, via the MADCAP program, to storage on paper tapes. Manipulation of the data, i.e. curve resolution, was performed using the GASCAP program, an extension of MADCAP. Curve resolution was achieved by inputing three parameters per peak: 1) peak position, 2) peak width and 3) peak height.

J. Electrophoresis

Electrophoretic mobility studies were made using a Rank Brothers Mark II Particle Microelectrophoresis instrument. Two platinum blacked platinum electrodes were placed in either side of a quartz flat cell holding the suspension of interest. The interelectrode distance or cell constant, (c), was determined by measuring the resistance of a 0.1M KCl solution and employing equation (1):

$$c = RKA \tag{1}$$

where R = electrical resistance of KCl solution, R = 5430 ohms, K = electrical conductivity of KCl solution, K = 1.289×10^{-2} $ohm^{-1}cm^{-1}$ and A = cross sectional area of cell at the plane of viewing. The cell constant for the flat cell was 8.18 cm.

Electrophoretic solutions were made with approximately 0.1 g of the zeolite in 500 mL of 10^{-2}M $NaClO_4$, or 10^{-3}M $NaClO_4$, in 500 mL volumetric flasks. These solutions were allowed to stir for two hours and were then placed in polyethylene bottles. The pH of the solutions was measured and adjusted to a range of 2.0 to 8.0 pH units with 0.07 M NaOH and 0.07 M HNO_3. The pH measurements were taken both before and after electrophoretic measurements. The mobility measurements were made using a constant applied voltage of 60V. Ten measurements were made (five in each direction) at both the front and back viewing plane. The average of the results was taken and the mobility ($\overline{\mu}$) of the zeolite particles was calculated from equation (2):

$$\overline{\mu} = \frac{\ell/t}{E/D} \qquad (2)$$

ℓ = particles moving distance

t = average time of movement

E = electrode potential

D = cell constant

The error for each mobility measurement is ± 0.5 μ·cm/V·s.

K. Catalytic Reactions

The thiophene hydrodesulfurization reactions were carried out in a pulse microreactor/gas chromatograph system. A GOW-MAC Series 550 gas chromatograph was used. The reaction components were detected using a thermal conductivity detector. Chromatographs were recorded on a Hitachi QPD53 chart recorder. The microreactor consisted of a 1 mm inside diameter stainless steel tube mounted upstream from the analytical column and directly behind the injection port. With this positioning, it was possible to make the 0.5 μL thiophene injections directly into the reaction cell. The injections were made with a liquid syringe at atmospheric pressure. A five milligram sample of catalyst (Rh-zeolite or Co-Mo/Al_2O_3) was loaded in the reactor and was sandwiched by quartz wool plugs. The thiophene hydrodesulfurization reactions were carried out as a function of gas flow rate (30, 40, 60, 80 mL/min) and reaction temperature (250, 350, 400, 450, 600°C). At least three reaction runs were performed at each temperature and flow rate.

In initial reactions, the stainless steel microreactor was heated

using a Briskeat heating tape wrapped around the tube. A chromel-alumel thermocouple, calibrated at 149, 204, 260 and 302°C with Omega melting point standards, was used to monitor the temperature of the reactor. An aluminum box packed with quartz wool was positioned around the microreactor for insulation. This arrangement provided a method of heating the reactor cell and column oven separately. The Briskeat heating tape did not prove to be an effective heating element for the reactor as it would frequently short out. Therefore, a heating system for the microreactor consisting of a 4.5 cm long, 2 cm diameter quartz tube wrapped with 1 1/2 feet of Nichrome wire was used. A ceramic sealer was used to hold the wire in place and as an insulator. The Nichrome wire was heated with a Variac, which controlled the amount of current passing through the wire. This heating system provided a stable and reproducible means of heating the microreactor, and was used throughout the remaining experimental work. A Weston voltmeter was used for temperature read-out. A diagram of the apparatus is shown in Figure 5.

Since hydrogen must be present in the system for the hydrodesulfurization reactions, hydrogen was used as the carrier gas for the experiments. The hydrogen was purified before use in the reactor/gas chromatograph system by means of a molecular sieve trap for removal of water and hydrocarbons, and an oxygen trap. The hydrogen flowed from the gas cylinder, through the purification traps, and through an Airco Model 751 flow meter into the chromatograph.

As has been demonstrated in previous works (6), the sulfided form

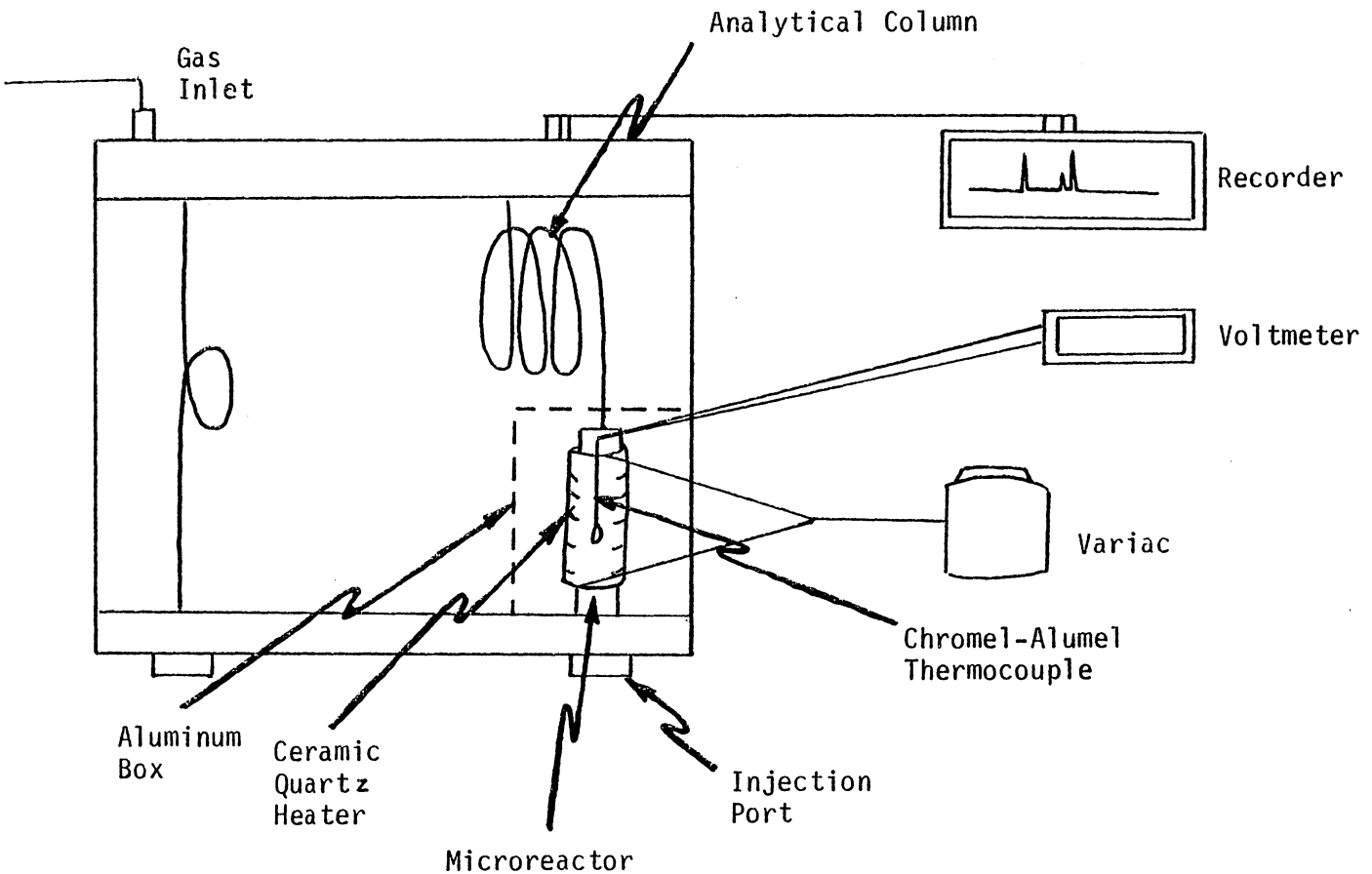

Figure 5. Top View Microreactor/Gas Chromatograph System (not to scale)

of the transition metal is the active species for hydrodesulfurization reactions. It was reasoned that the most active catalyst would contain the greatest quantity of surface sulfur. Thus, two methods were investigated to determine what conditions produced the most sulfur on the catalyst surface. The first method involved making 0.5 μL injections of thiophene (Aldrich 99+% purity) into the system until the peak shapes and the ratio of peak heights of products to unreacted thiophene was reproducible to within 0.5 percent. The conditioning process was usually complete after about ten injections. Initially, the sulfiding procedure was carried out on the catalyst after it had been previously reduced in flowing H_2 at 600°C for two hours. However, XPS results on the catalyst sulfided in this way showed no sulfur on the surface, thus, this sulfidation method was abandoned. By making the thiophene injections into the catalyst system without prior reduction and at a temperature of 100°C, XPS results showed that sulfur was present as sulfide on the surface of the catalyst in a S/Rh ratio of 0.25.

The second method of sulfiding was to contact the catalyst with a flowing stream of a 10 vol % H_2S/90 vol % H_2 gas mixture for two hours at the temperatures 22, 150, 250, 350, 400 and 400°C. XPS results indicated a maximum sulfur to rhodium ratio was achieved at a temperature of 250°C.

L. Standard Reactions

To determine the retention times in the chromatographic system for thiophene and the expected products butane, butene, butadiene, and

hydrogen sulfide, blank runs were made. The microreactor containing only quartz wool was mounted in the system and 0.5 μL injections of the compounds of interest were made at different temperatures and flow rates. The retention times were measured from the point of injection to the middle of each peak. Mixtures of thiophene and each of the expected products produced baseline separation of the peaks. However, mixtures of butane, butene, butadiene and hydrogen sulfide could not be resolved using a four foot long, 1/4 inch diameter stainless steel column. The packing used was Supelco 3% SP-2250 on 100/120 mesh Supelcoport, a slightly polar substance. Also, product peaks resulting from the hydrodesulfurization reactions could not be resolved. Even decreasing column temperature to 35°C did not result in peak resolution.

To achieve better separation of the components, an eight foot long, 1/8 inch diameter column was employed. This change did improve separation slightly, enabling distinction of butane and the olefins by the presence of a shoulder on the hydrocarbon peak. However, no mixtures of the expected products produced reliable separation and baseline separation could not be achieved. Thus, in order to determine the individual compounds and the percentage of each in the hydrodesulfurization products, mass spectrometry was used.

M. Mass Spectrometry

A UTI model 100C quadrupole mass spectrometer was used as a means of identifying the hydrodesulfurization reaction products and their

relative concentrations. A Honeywell 1706 visicorder was used to record spectra. Filament emission was 80 mA in all experiments, the electron energy was 70 eV, and instrument sensitivity was either 10^{-9} or 10^{-10} amps. Standard spectra of butane, cis-2-butene, and 1,3-butadiene were collected and used as references for the product analyses. The precision of the intensity measurements (±5%) made it impossible to distinguish between 1-butene and cis-and trans-2-butene.

In order to collect and transfer the HDS products from the gas chromatograph system to the mass spectrometer system, a liquid nitrogen trap device was employed. A coiled glass tube fitted with vacuum stopcocks, shown in Figure 6, was used to trap the products for mass spectrometry analysis. By means of Swagelok fittings, the glass trap was attached to the gas outlet line of the chromatograph. A bypass line was also attached to the system so that the eluting thiophene would not be trapped. When the products began to elute from the analytical column, they were collected by passing the effluent gas stream through the trap which was submerged in liquid N_2. After the products had been collected, the back vacuum stopcock was closed while simultaneously opening the bypass stopcock. This procedure prevented any trapping of air. The front stopcock was then closed so that the eluting unreacted thiophene was not collected. This procedure was repeated for five times before analysis by mass spectrometry.

Product components were identified based upon the mass spectral patterns. Molecular ion peaks, m/z 54, 56, 58 were used to indicate

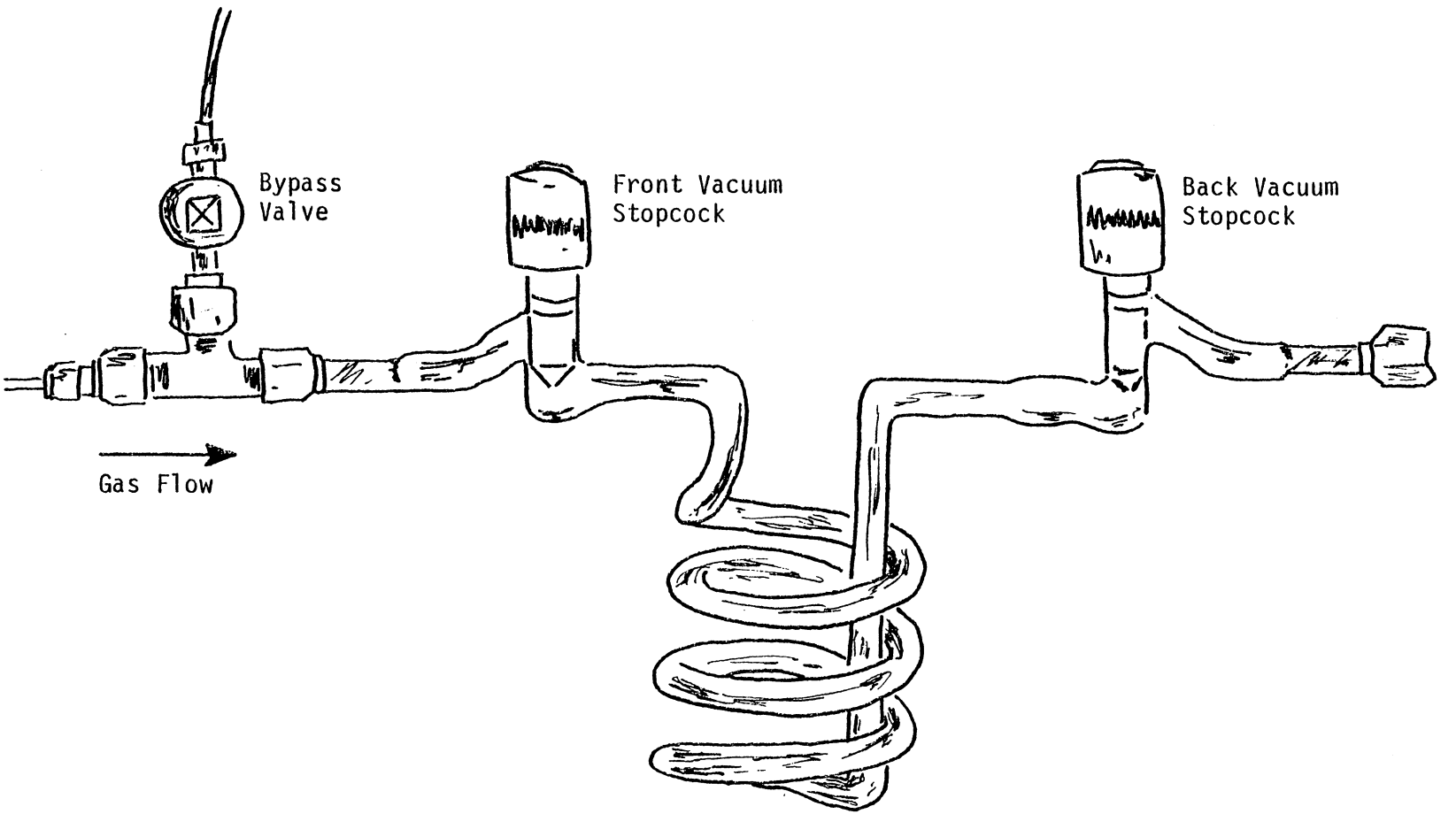

Figure 6. Glass Product Trap

the presence of butadiene, butene, and butane, respectively. The relative abundance of each mass peak in the standard spectrum was determined relative to its base peak. Base peaks were m/z 39, 41, and 43 for 1,3-butadiene, butene, and butane, respectively. These relative abundances were used in the product spectra to determine the contribution of each component to the total spectrum. Relative concentrations of the individual products were calculated using the intensity (peak height) of the base peak of each component, the intensity of the same peak in the standard spectrum, and the total ion pressure of the standard spectrum, as in equation (3).

$$\frac{\text{m/z peak height product}}{x} = \frac{\text{m/z peak height standard}}{\text{total ion pressure standard}} \qquad (3)$$

x = partial pressure of product

The ratio of the product partial pressures of the components is a measure of the relative concentrations in the total mixture.

CHAPTER IV

RESULTS AND DISCUSSION

A. Characterization of Zeolites and Co-Mo/Al_2O_3

The zeolites were characterized by means of x-ray diffraction (XRD), infrared spectroscopy (IR), microelectrophoresis, and x-ray photoelectron spectroscopy (XPS), The cobalt molybdate sample was characterized by XPS. The IR and XRD results were previously discussed in the experimental section.

Microelectrophoresis

The mobility of 13X, ZSM5(M), and ZSM5-G2 in 10^{-2}M $NaClO_4$ was determined as a function of pH to compare the electrophoretic properties of the zeolites. The point of zero charge (PZC) is defined as that pH where the net charge on the surface of the particle is zero. This value is taken as the pH of zero mobility. The PZC was 6.3, 2.6, and 2.4 pH units for 13X, ZSM5(M), and ZSM5-G2, respectively. Adsorption of $RhCl_3 \cdot 3H_2O$ in 6 M NH_4OH on the zeolites was carried out at pH values above the PZC, to facilitate adsorption of the positively charged metal complex on a negatively charged zeolite surface. The lower PZC for ZSM5(M) and ZSM5-G2 compared to 13X, reflects the greater acidic nature of these two zeolites. Mobility measurements for the zeolites are shown in Figures 7-9.

X-ray Photoelectron Spectroscopy

X-ray photoelectron spectroscopy (XPS) was used to characterize the surface of the zeolites and the cobalt-molybdate catalyst. XPS is an instrumental technique used to determine binding energies according

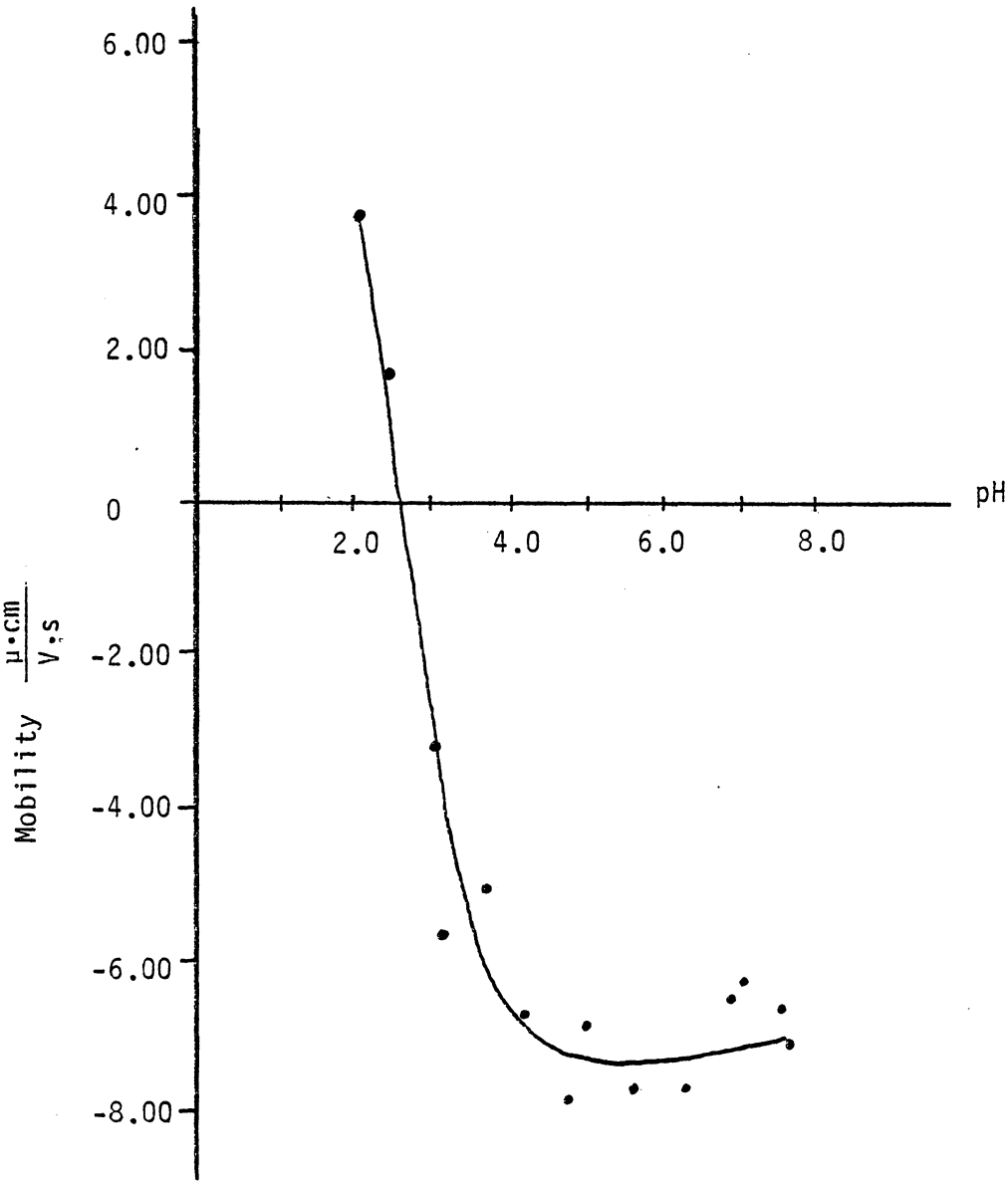

Figure 7. Electrophoretic Mobility of Na-ZSM5 in .01M $NaClO_4$

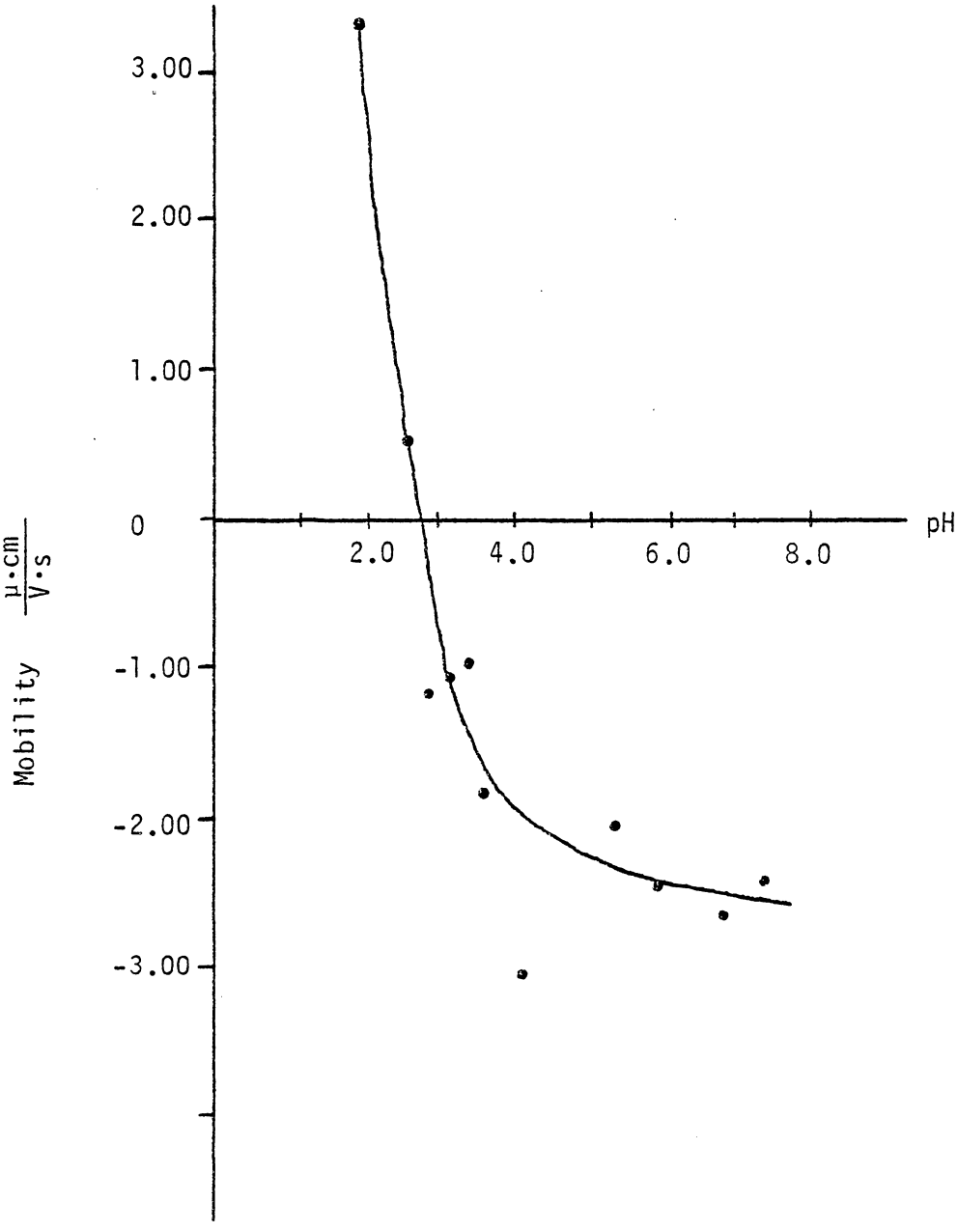

Figure 8. Electrophoretic Mobility of Na-ZSM5-G2 in .01M $NaClO_4$

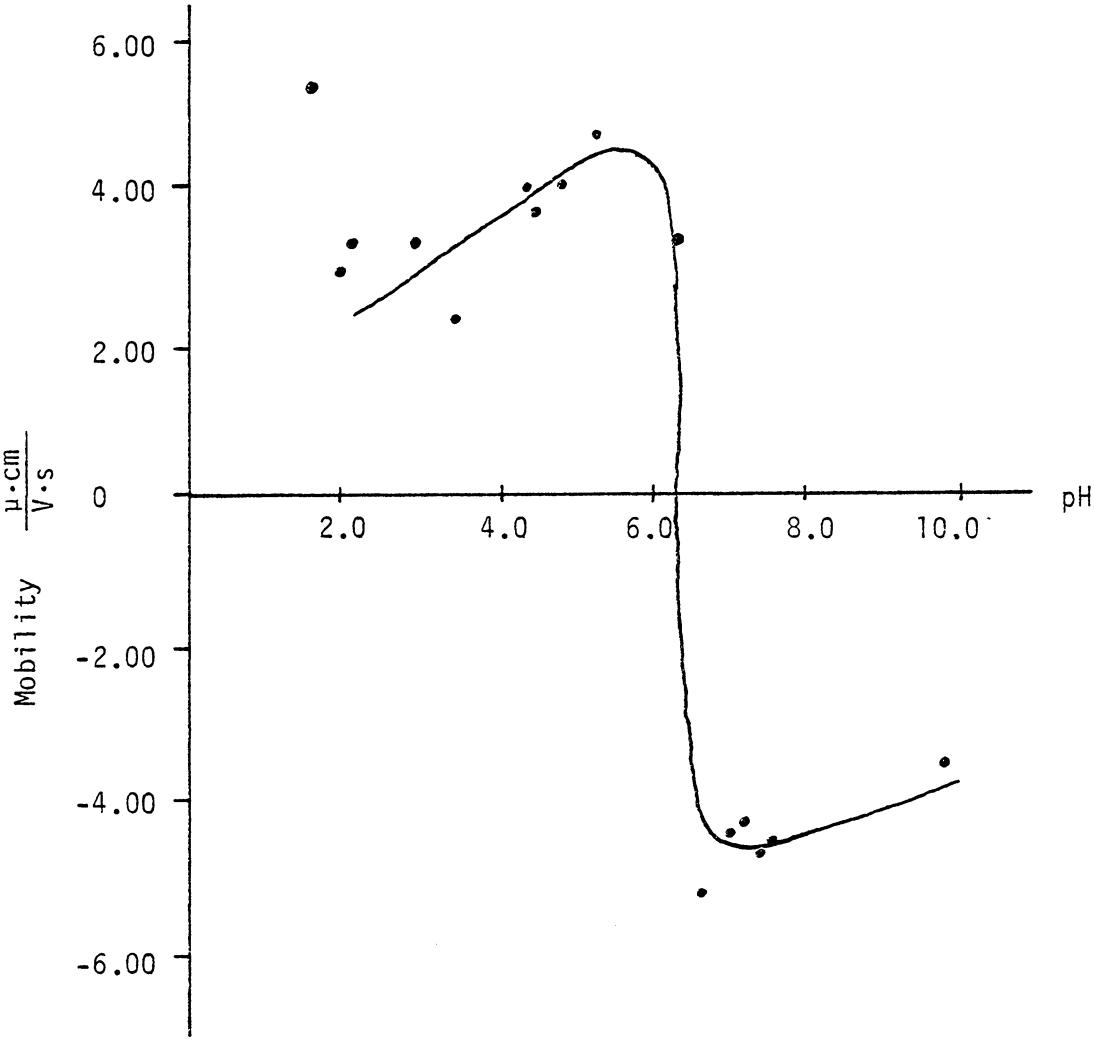

Figure 9. Electrophoretic Mobility of Na-13X in .01M $NaClO_4$

to the equation $h\nu = KE + BE + \phi$, where $h\nu$=energy of the photon, KE=kinetic energy of ejected electron, BE=binding energy of ejected electron, and ϕ=spectrometer work function. From the binding energies, the chemical oxidation state and chemical environment of elements on the sample surface may be inferred. XPS also enables a determination of the atomic ratios of the surface elements. Shown previously in Table 5 are the binding energies and atomic ratios for zeolites 13X, ZSM5(M) and ZSM5-G2. The difference of 1.7 eV for the Si 2p binding energy of ZSM5 samples and 13X is due to the vast difference in the silicon to aluminum atomic ratio of the two zeolites. The electron density around silicon in 13X is greater than in ZSM5 due to more substitution of Al^{3+} for Si^{4+} in 13X. This substitution of Al^{3+} for Si^{4+} results in a greater negative charge in the zeolite and thus, the energy required to remove one of the Si 2p electrons in 13X is less. The ZSM5(M) sample was an ammonium saturated form of the zeolite and thus nitrogen appears in the XPS spectrum at a binding energy characteristic of quaternary amines. Zeolites 13X and ZSM5-G2 were Na^{+}-saturated samples. The slight increase in the Si/Al atomic ratio for the synthesized ZSM5-G2 sample compared to ZSM5(M) is due to the method of preparation.

XPS data for the cobalt-molybdenum/alumina catalyst is given in Table 6. Binding energies for cobalt are not reported due to interference from oxygen Auger peaks.

B. Rhodium Adsorption on Zeolites

The adsorption of the rhodium compounds on the zeolites was

Table 6

XPS Data for Co-Mo/Al_2O_3

Binding Energy (eV)				Atomic Ratio
Mo $3d_{3/2}$ (±0.1)	Mo $3d_{5/2}$ (±0.2)	Al 2p (±0.3)	O 1s (±0.3)	Mo/Al
234.9	232.2	74.3	531.4	0.11

carried out as reported in the experimental section. Decolorization of the Rh(I) and Rh(III) zeolite exchange solutions after 72 hours provided visual evidence that rhodium adsorption had occurred. XPS results for the starting rhodium compounds are given in Table 7. The observed binding energies for the Rh $3d_{5/2}$ photoelectron peak for the Rh(I) and Rh(II) compound are in agreement with literature values (57,58). XPS results for the rhodium compounds absorbed on 13X are given in Table 8. The Rh $3d_{3/2}$ and $3d_{5/2}$ binding energies for $RhCl_3$-13X are in good agreement with results obtained by Kuznicki and Eyring (54). Since the binding energies of the Rh $3d_{3/2}$ and $3d_{5/2}$ photopeaks are the same for $RhCl_3 \cdot 3H_2O$ and for $RhCl_3$-13X, it is concluded that rhodium exists as Rh(III) on the zeolite surface. A decrease in the Na/(Si+Al) atomic ratio for 13X from an initial value of 0.55 to 0.29, and a Rh/(Si+Al) atomic ratio of 0.18 indicate that sodium ions were replaced by the incoming rhodium(III) ions on a nonequivalent basis.

XPS results on the $Rh_2(CO_2CH_3)_4$-13X system reveal a decrease in the Rh $3d_{3/2}$ and $3d_{5/2}$ binding energy after adsorption. A decrease of 0.7 eV (±0.2) suggests that reduction of the rhodium(II) species has occurred to give a different rhodium species or a mixture of oxidation states on the surface. The XPS spectra are shown in Figure 10. A mixture of oxidation states is also suggested by the broadness of the photoelectron peaks. The peak width at half maximum (PWHM) of the Rh $3d_{5/2}$ peak increased from 2.1 eV for the pure $Rh_2(CO_2CH_3)_4$, to an average value of 2.9 eV for $Rh_2(CO_2CH_3)_4$-13X. The intense peak at

Table 7

XPS Results for Rhodium Compounds

Compound	Binding Energy (eV) Rh $3d_{3/2}$	Rh $3d_{5/2}$	Rh $3d_{5/2}$*	Cl 2p	P 2s
$RhCl_3 \cdot 3H_2O$	314.3(±0.1)	309.6(±0.1)	310.2	198.5(±0.2)	---
$Rh_2[CO_2CH_3]_4$	313.4(±0.2)	308.6(±0.2)	308.8	----	---
$(PPh_3)_3ClRh$	314.1(±0.2)	309.4(±0.2)	309.0	198.6(±0.1)	189.2(±0.4)

*Literature values (51, 57, 58)

Table 8

XPS Results for Rhodium Exchanged 13X

Zeolite	Binding Energies (eV)							Atomic Ratio	
	Rh $3d_{3/2}$	Rh $3d_{5/2}$	Cl 2p	Na 1s	P 2s	Si 2p	Al 2p	Rh/(Si+Al)	Na/(Si+Al)
$RhCl_3$-13X	314.2(±0.1) *313.6	309.5(±0.2) *309.5	198.4(±0.2)	1071.7(±0.2)	--	101.7(±0.2)	73.7 (±0.1)	0.18	0.29
$Rh_2[CO_2CH_3]_4$-13X	312.7(±0.3)	307.8(±0.5)	---	1072.(±0.1)	--	101.8(±0.1)	73.8(±0.2)	0.031	0.50
$(PPh_3)_3ClRh$-13X	314.0(±0.1)	309.4(±0.1)	198.2(±0.1)	1071.7(±0.2)	189.3(±0.2)	101.6(±0.1)	73.7(±0.2)	0.18	0.12

*Values from Kuznicki and Eyring (54).

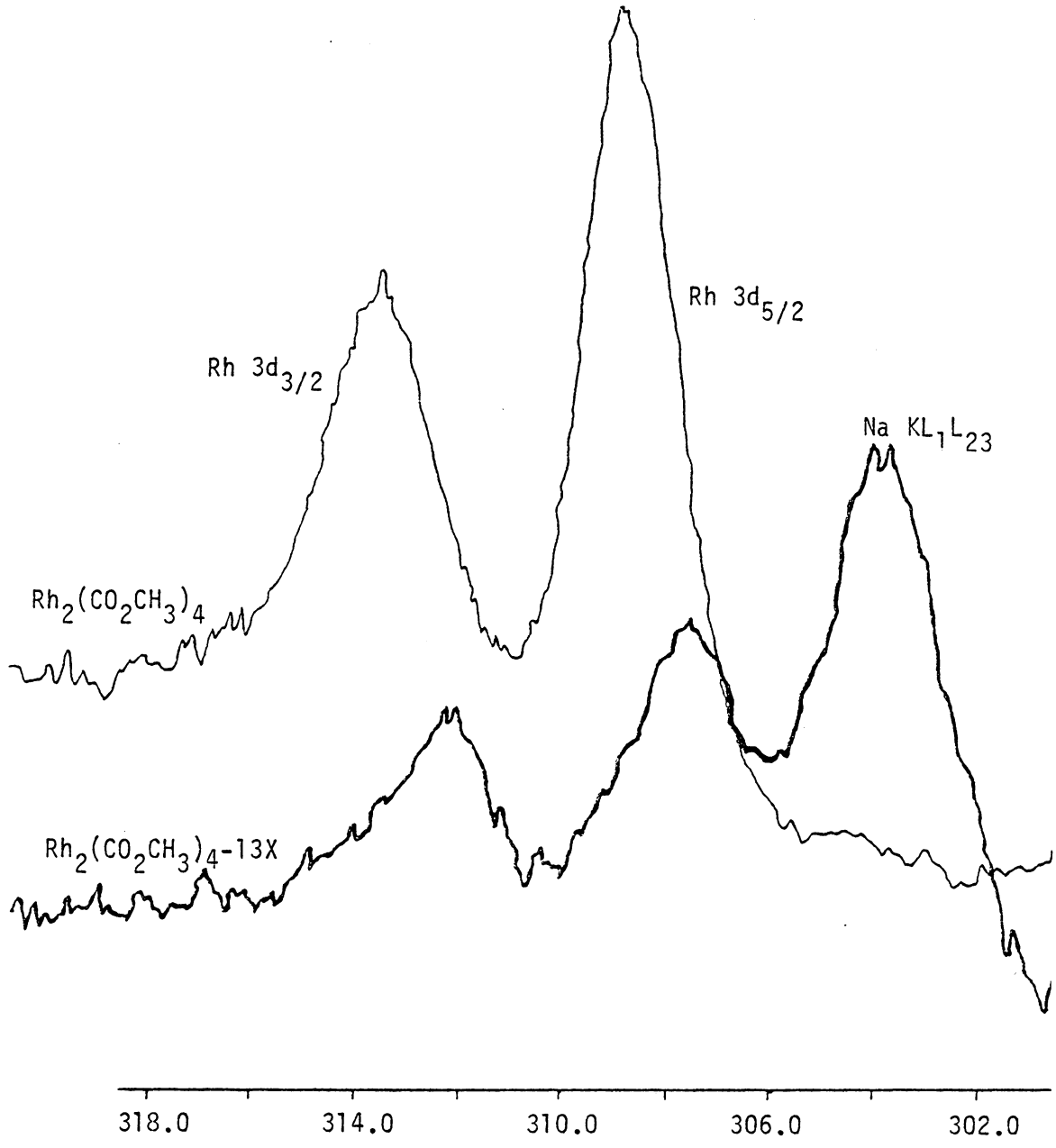

Figure 10. XPS Spectra - $Rh_2(CO_2CH_3)_4$ and $Rh_2(CO_2CH_3)_4$-13X

303.9 eV is due to the KL_1L_{23} Auger of sodium. However, as evidenced by the Rh/(Si+Al) intensity ratio for $Rh_2(CO_2CH_3)_4$-13X, only a small amount of rhodium was adsorbed on the zeolite surface. Rhodium is present in such a limited quantity that the Na/(Si+Al) ratio has not been affected. A plausible explanation for this result is that the bulkiness and relatively large size, approximately 12x12Å (59), of the rhodium acetate dimer inhibits its passage through the openings (~9Å) to the 13X cage thus preventing adsorption within the zeolite cage.

The binding energies for the Rh $3d_{3/2}$ and $3d_{5/2}$ photoelectron peaks for $Rh(PPh_3)_3Cl$ and for $Rh(PPh_3)_3Cl$-13X are equal. However, due to the similarity in binding energies with Rh(III), it is impossible to tell whether the Rh(I) adsorbed to the 13X surface as Rh(I). It is possible that upon adsorption the rhodium was oxidized to Rh(III) in the 6M NH_4OH solution where the Rh(I) adsorption was carried out. The color of the $Rh(PPh_3)_3Cl$-13X zeolite was light brown while the $RhCl_3$-13X zeolite had a yellow tint. The color difference might lend support to the presence of the Rh(I) species, but this evidence is not conclusive. The near equality of the Rh/(Si+Al) ratio for both $RhCl_3$-13X and $Rh(PPh_3)_3Cl$-13X, indicates that the same amount of rhodium was adsorbed in both cases. Phosphorus and chlorine are detected on the zeolite surface, but it is not known whether these ligands are still associated with the rhodium ion or have dissociated and readsorbed.

Table 9 gives XPS data collected on $RhCl_3$-ZSM5(M) and $RhCl_3$-ZSM5-G2. The equivalent binding energies of the Rh $3d_{3/2}$ and Rh

Table 9

XPS Results for $RhCl_3$-ZSM5(M), $RhCl_3$-ZSM5-G2

	Binding Energy (eV)						Atomic Ratio
Sample	Rh $3d_{5/2}$	Cl 2p	Na 1s	N 1s	Si 2p	Al 2p	Rh/(Si+Al)
$RhCl_3$	309.6(±0.1)	198.5(±0.2)	--	--	--	--	-
$RhCl_3$-ZSM5(M)	309.8(±0.6)	198.5(±0.1)	--	399.7(±0.3)	103.0(±0.3)	73.9(±0.3)	0.17
$RhCl_3$-ZSM5-G2	309.8(±0.1)	198.3(±0.3)	1071.6(±0.3)	--	102.8(±0.1)	74.3(±0.4)	0.11

$3d_{5/2}$ photopeaks in the zeolite samples and in $RhCl_3 \cdot 3H_2O$ indicate that rhodium exists on the zeolite surface in the +3 oxidation state. From the Rh/(Si+Al) atomic ratio, it is evident that the amount of rhodium adsorbed varied in the manner 13X ~ZSM5(M)>ZSM5-G2.

In summary, the adsorption of Rh(II) onto 13X resulted in a very minimal amount of adsorbed rhodium. The binding energies of the Rh $3d_{3/2}$ and $3d_{5/2}$ levels for $Rh(PPh_3)_3Cl$ make it impossible to distinguish between this Rh(I) compound and $RhCl_3$ by XPS. Therefore, since a significant amount of rhodium from $RhCl_3$ was adsorbed on 13X, (Rh/(Si+Al)=0.18), and ZSM5(M), (Rh/(Si+Al) = 0.17), and on ZSM5-G2 (Rh/(Si+Al)=0.11) all subsequent catalytic studies were carried out with $RhCl_3$-zeolites.

The Rh(I) and Rh(II) compounds used in this study undergo photoreduction under x-ray bombardment (10 kV to generate x-rays) in the XPS spectrometer. The pure compound $RhCl_3$, however, shows no evidence for photoreduction after more than one hour under x-ray bombardment. The binding energy of the Rh $3d_{5/2}$ peak stays constant at 309.4 eV (±.1) and the PWHM is 1.8 eV (±.1) throughout all runs. A spectrum of $RhCl_3$ after approximately 1 1/2 hours in the spectrometer is shown in Figure 11 and is no different from one obtained in the first scan at time zero.

The Rh photopeak of the pure Rh(II) compound becomes broader under x-ray bombardment after about an one hour. The binding energy of the Rh $3d_{5/2}$ peak stays constant at 308.6 eV. However, after approximately 45 minutes of x-ray bombardment in the spectrometer, the Rh $3d_{5/2}$

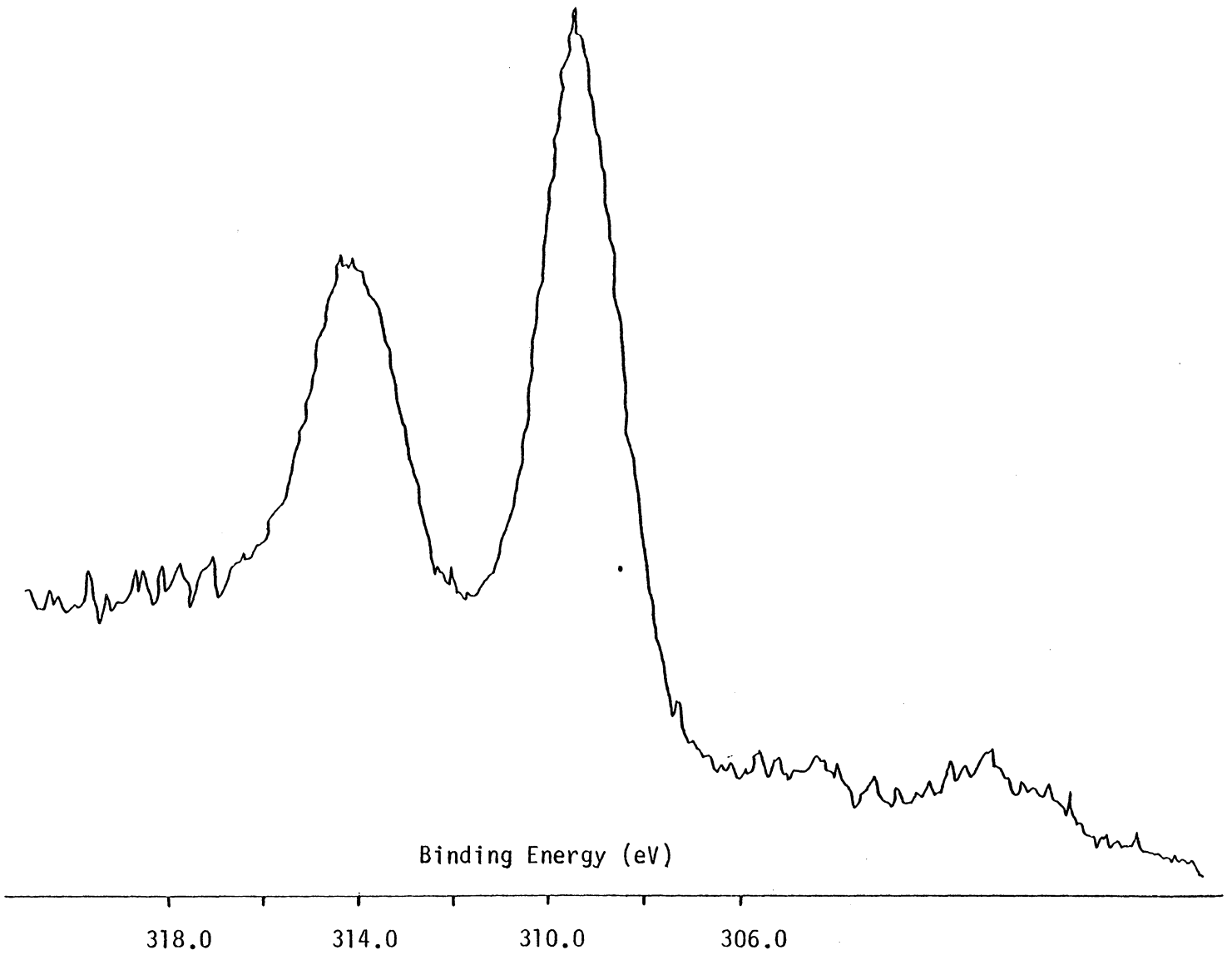

Figure 11. XPS Spectrum of $RhCl_3$ after 1 1/2 hrs. in Spectrometer

PWHM increased from an initial value of 2.1 eV (±.1) to 2.4 (±.1) eV. This broadening is suggestive of the onset of reduction of Rh(II).

Shown in Figure 12 are the Rh $3d_{3/2}$ and Rh $3d_{5/2}$ peaks for a $Rh(PPh_3)_3Cl$ sample 1) within the first few minutes of introduction into the spectrometer, and 2) after about 30 minutes in the spectrometer. After one half an hour, the Rh $3d_{3/2}$ and Rh $3d_{5/2}$ binding energies decreased by approximately 0.4 eV and the PWHM of the $3d_{5/2}$ photopeak increased by 0.6 eV. After about 1 hour in the spectrometer, the $3d_{5/2}$ binding energy decreased to 308.8 eV. These results are suggestive of a fairly rapid reduction of Rh(I).

For the rhodium-zeolite samples, this photoreduction process is enhanced. In contrast to previous behavior, the Rh photopeaks for $RhCl_3$ on both 13X and ZSM5(M) change after about 1 1/2 hours in the spectrometer. The binding energy for the Rh $3d_{5/2}$ peak changes from 309.6 to 307.5 eV over 1 1/2 hours and suggests x-ray induced reduction of Rh(III). Figure 13 shows a spectrum of a Rh(III) zeolite after ~ 2 hours. The two Rh $3d_{5/2}$ photopeaks in Figure 13 occur at 309.3 and 307.5 eV corresponding, respectively, to rhodium(III) and a reduced rhodium species. From the intensities of the peaks, it is concluded that the rhodium on both the 13X and ZSM5(M) zeolite surface exists predominantly as the reduced species.

Rhodium tetraacetate adsorbed on 13X is photoreduced at a much faster rate, and more completely than when in pure form. An initial XPS scan recorded the Rh $3d_{5/2}$ peak at a binding energy of 308.3 eV and a PWHM of 2.7 eV. As noted previously, some reduction of

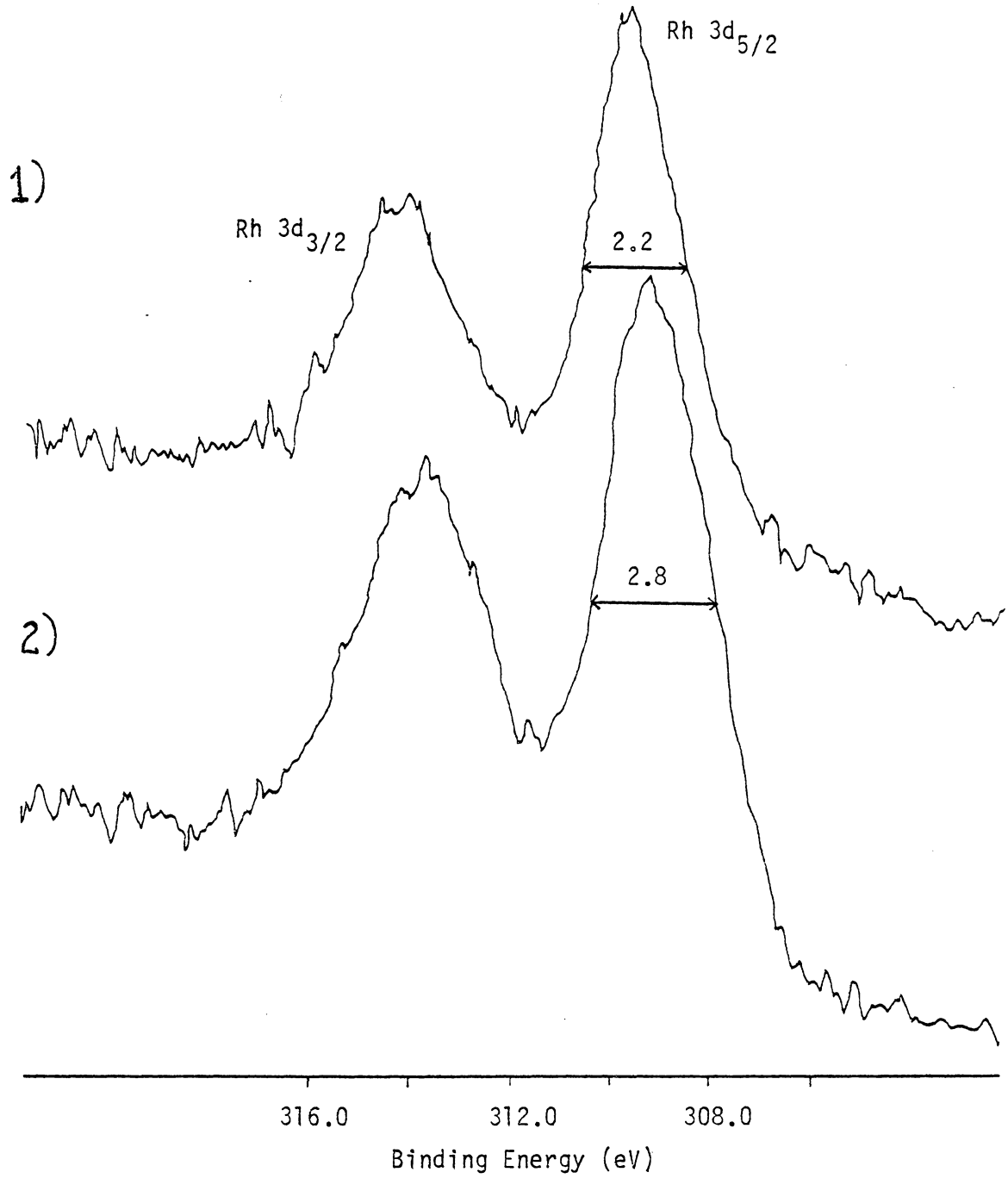

Figure 12. XPS Spectra for $Rh(PPh_3)_3Cl$

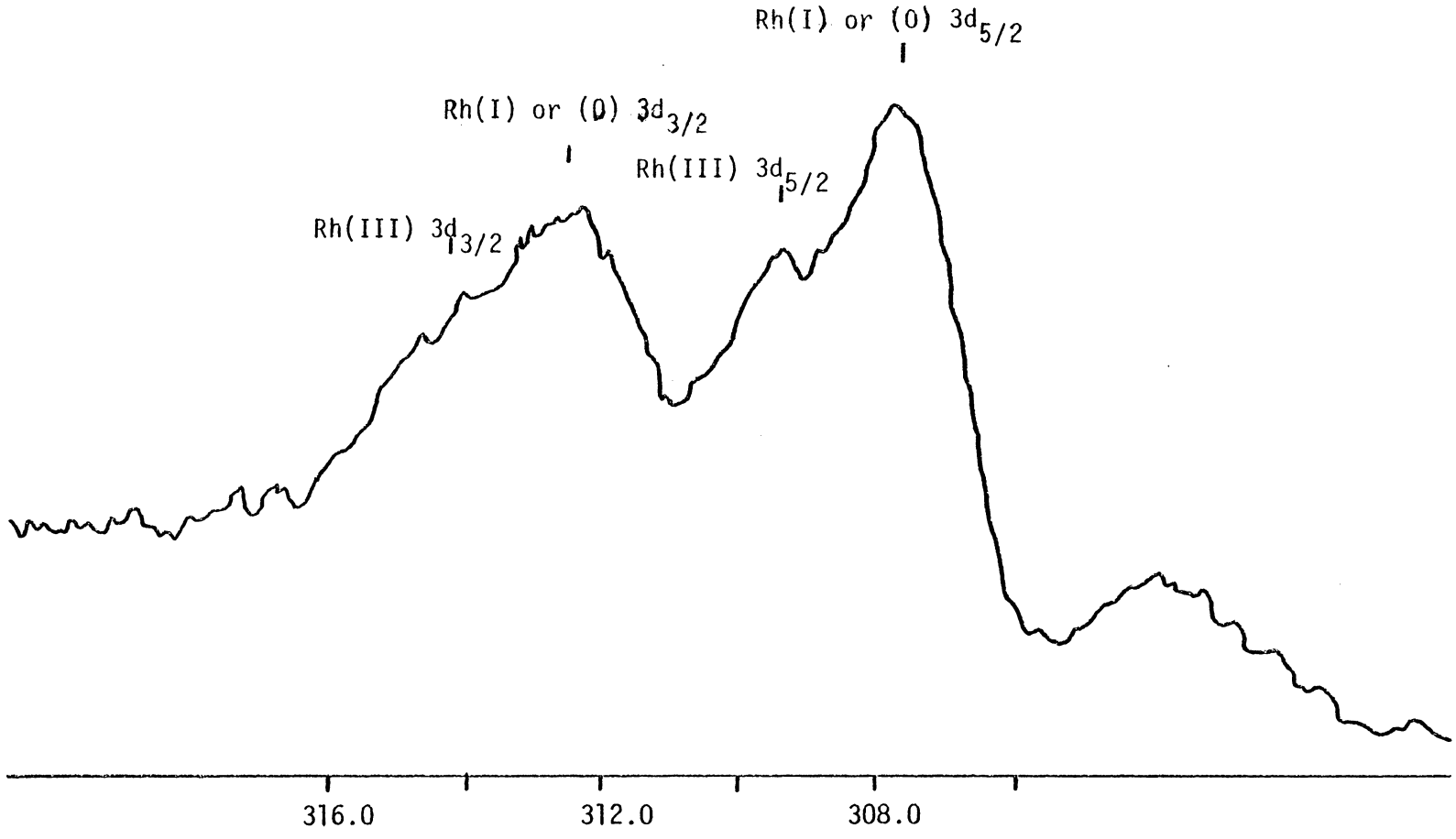

Figure 13. XPS Spectrum for $RhCl_3$-13X
After ∿ 2 hrs. in Spectrometer

Rh(II) apparently occurs during the adsorption process. After approximately 1 1/2 hours, the binding energy for Rh $3d_{5/2}$ decreased, to 307.4 eV, suggesting a reduced rhodium species.

The x-ray induced reduction of the $Rh(PPh_3)_3Cl$-13X system is similar to that for pure $Rh(PPh_3)_3Cl$. The Rh $3d_{5/2}$ photopeak initially occurs at a binding energy of 309.3 eV with a PWHM of about 2.2 eV. After about 45 minutes of x-ray bombardment, the binding energy is 308.4 eV and the peak width has broadened to 3.1 eV, indicating a mixture of oxidation states. After approximately 2 hours, the binding energy has decreased to 307.7 eV and the PWHM is 2.8 eV indicating further reduction of rhodium.

C. Catalyst Characterization - Before Reactions

Recognizing the literature reports (6) that sulfided transition metal catalysts are the active form for hydrodesulfurization, the Rh-zeolites and Co-Mo/Al_2O_3 catalysts used in this study were sulfided in two ways. The first method to be discussed is that of sulfidation of the catalyst by thiophene injections.

As a first means of thiophene sulfidation, the $RhCl_3$-ZSM5(M) catalyst was reduced in flowing H_2 at 600°C for 2 hours. XPS results on this sample give a binding energy for the Rh $3d_{5/2}$ photoelectron peak of 307.5 eV (±0.2). This binding energy value suggests that the conditioning procedure has resulted in a reduced rhodium species on the catalyst surface. Ten 0.5 μL injections of thiophene were then made into the catalyst system which was held at 600°C. XPS analysis on this sample gave a Rh $3d_{5/2}$ binding energy of 307.4 eV. The severe

reducing conditions employed and the Rh binding energy suggest the presence of Rh(0). After the repeated thiophene injections, no sulfur was detected on the zeolite surface by XPS. The lack of sulfur suggests that when rhodium(0) is present on the zeolite surface, it is unable to react with sulfur and form a rhodium sulfide species. Another possibility is that sulfur is present on the zeolite in a small amount below the detectable limits of the spectrometer. This limit is estimated from the S/(Si+Al) ratio from other measurements to be approximately <0.01 atomic units. Thus, since it has been shown (6) that sulfur must be present to activate the transition metal catalyst for hydrodesulfurization, this method of thiophene sulfidation was abandoned.

The next method of thiophene sulfidation was to sulfide the catalyst prior to reduction of rhodium. This method was carried out on all three $RhCl_3$-zeolites. Ten thiophene injections (0.5 μL) were made into the reactor system which was held at approximately 100°C. XPS measurements were then made on the sulfided Rh-zeolites. In cases where sulfidation resulted in a reduction of rhodium on the zeolite, it was not always possible to determine the exact oxidation state. Literature values for the binding energies of the 3d level for Rh(0) and Rh(I) overlap and can vary by much as 2 eV depending upon ligand effects. Nefedov et al. (60) have conducted an XPS study on donor-acceptor ligand effects on the binding energy of transition metals. They found that the binding energy of a metal ion is determined by its oxidation state and by the ligands surrounding it. The authors state that the binding energy for the $3d_{5/2}$ or $4f_{7/2}$ level

of a transition metal increases by approximately 1 eV with each unit increase in oxidation number. They also found that the binding energy of the $3d_{5/2}$ level for Rh(III) can vary as much as 1.5 eV depending upon the ligands in coordination. The ability of ligands to draw electron density off the metal affects its binding energy. A strong electron withdrawing ligand like NO_3^- creates a more positive environment around the metal and thus, increases its binding energy. Similarily, a ligand such as PPh_3 can donate electrons to the metal and thus, decrease its binding energy. This effect is visualized in the Rh $3d_{5/2}$ binding energy for $K_3[Rh(NO_3)_6]$ of 311.3 eV and for $Rh(PPh_3)_3Cl_3$ of 309.9 eV.

Table 10 gives a comparison of literature binding energies for the $3d_{5/2}$ level for Rh(0) and Rh(I) and shows this variation and the overlap of results. The reported binding energies for $Rh(PPh_3)_3Cl$ have a range of 1.7 eV. The Rh 3d binding energies for Rh(0) are in the same region as Rh(I) and vary as much as 0.5 eV. Thus, the distinction between Rh(I) and Rh(0) cannot be made on XPS binding energy results alone.

Table 11 gives the XPS results for the $RhCl_3$-zeolites sulfided with thiophene at 100°C. As evidenced from the Rh 3d binding energies for the $RhCl_3$-ZSM5(M) and $RhCl_3$-ZSM5-G2 zeolites, the sulfiding conditions are sufficient to cause reduction of Rh(III) to either Rh(I) or Rh(0). The existence of only one oxidation state is suggested from the Rh $3d_{5/2}$ PWHM of 1.8 eV. However, this is not the case with thiophene-sulfided $RhCl_3$-13X. In the XPS rhodium spectrum

Table 10

Literature Values for the Rh $3d_{5/2}$ Binding Energy of Various Rh(I) Compounds and Rh(0)

	Binding Energy (eV)	
	Rh(I)	Rh(0)
$Rh(CO)_2NO$	307.7 (61)*	307.1 (61)
$[Rh(CO)_2Cl]_2$	307.8 (62)	307.7 (54)
$RhH(PPh_3)(CO)$	309.5 (63)	307.2 (66)
$Rh(PPh_3)_3Cl$	308.2 (62)	307.4 (67)
	307.2 (64)	307.4 (this work)
	307.2 (60)	
	309.0 (57)	
	307.3 (65)	
	309.4 (this work)	

*Numbers in parentheses are references

Table 11

XPS Results for $RhCl_3$-ZSM5(M), $RhCl_3$-ZSM5-G2, $RhCl_3$-13X Sulfided with Thiophene at 100°C

	Binding Energy (eV)			Atomic Ratios			
Sample	Rh $3d_{3/2}$ (±0.2 eV)	Rh $3d_{5/2}$ (±0.2 eV)	S 2p (±0.2 eV)	S/Rh	S/(Si+Al)	Rh/(Si+Al)	Na/(Si+Al)
$RhCl_3$-ZSM5(M)	312.6	307.7	163.1	0.13	0.017	0.13	--
$RhCl_3$-ZSM5-G2	312.4	307.4	163.1	0.22	0.018	0.081	0.010
$RhCl_3$-13X	314.2 {311.7	309.4 {307.2	162.5	0.63	0.10	0.16	0.10

(Figure 14), there are four photoelectron peaks in the rhodium 3d region. The two peaks at 314.2 and 309.4 eV correspond respectively to the $3d_{3/2}$ and $3d_{5/2}$ of the original Rh(III) species. The peaks at 311.7 and 307.2 eV correspond to reduced rhodium. Thus, unlike $RhCl_3$-ZSM5(M) and $RhCl_3$-ZSM5-G2, this behavior suggests that 13X is able to slow down the reduction process of Rh(III) under the experimental conditions. The similarities in the S/(Si+Al) ratio for the $RhCl_3$-ZSM5(M) and $RhCl_3$-ZSM5-G2 zeolites indicate that the same amount of sulfur is present on the surface of each zeolite. The S 2p binding energy of 163.1 eV is intermediate between that of thiophene, 164.0 eV (66), and Na_2S, 162.0 (66). The PWHM of a single chemical sulfur photopeak is 2.2 eV. The PWHM of the S 2p photopeak on the zeolites is 2.5 eV. These results suggest that the sulfur may exist on the catalyst surface as both adsorbed thiophene and Na_2S. Since the possibility exists that Rh(I) is on the surface, sulfur could also be in the form Rh_2S. From the S/(Si+Al) ratio for $RhCl_3$-13X, however, a larger amount of sulfur is present on this zeolite. From the binding energy of the S 2p level, 162.5 eV, it appears that the sulfur is in the form of Rh_2S_3. The measured binding energy for S 2p of Rh_2S_3 is 162.3 eV. This occurrance also explains the Rh(III) photopeaks observed in Figure 14.

The second procedure for sulfiding the catalyst was with a 10 vol% H_2S/90 vol% H_2 gas mixture. Sulfiding was carried out at 22, 150, 250, 350 and 400°C in order to determine which temperature resulted in the maximum amount of sulfur on the catalyst surface. It is assumed

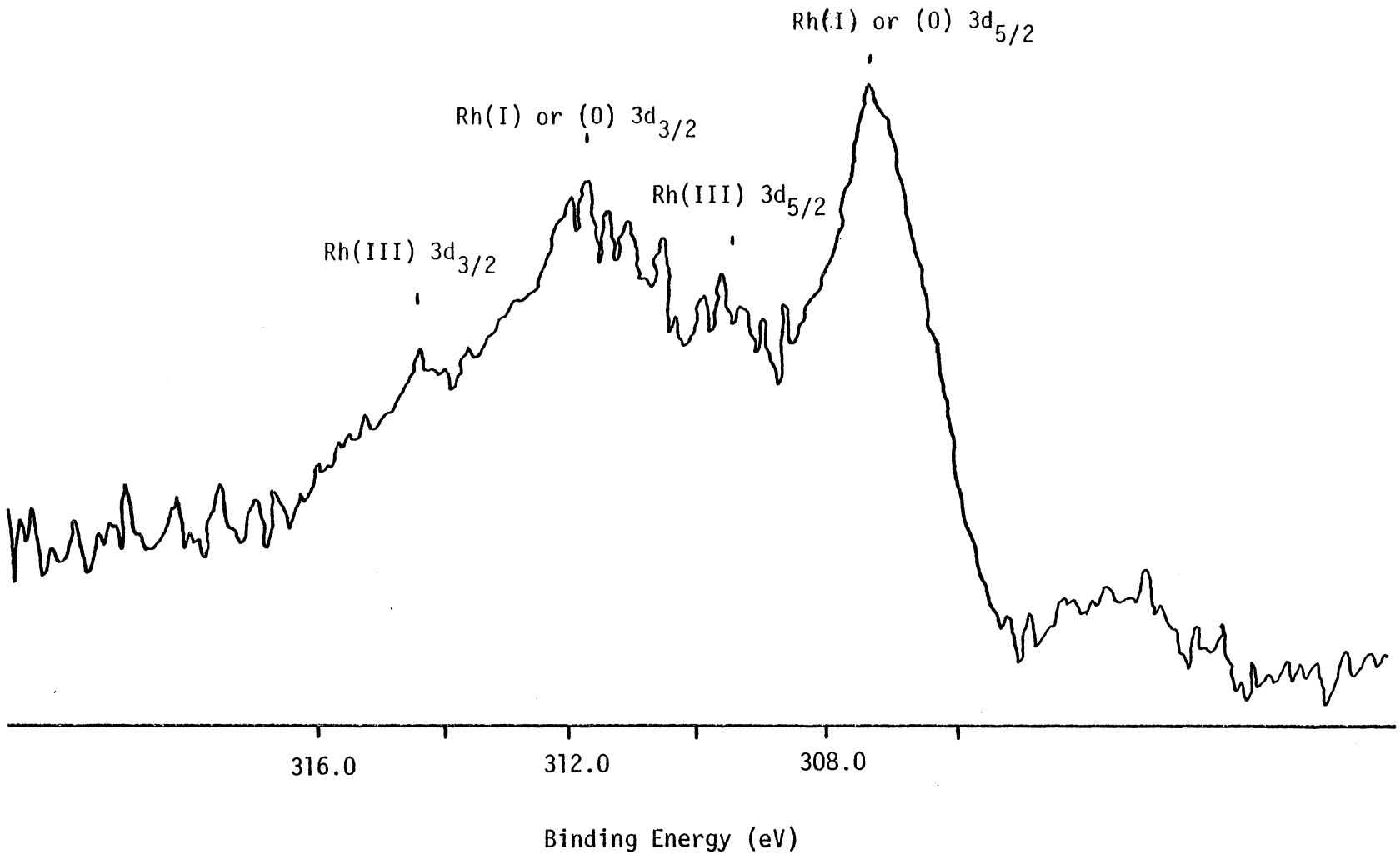

Figure 14. XPS Spectrum for Thiophene Sulfided $RhCl_3$-13X

that since the sulfided form of a transition metal catalyst is the active species for hydrodesulfurization, maximum sulfur will result in maximum activity. XPS results are given in Table 12 for $RhCl_3$-ZSM5-G2 sulfided at these different temperatures. The maximum sulfur on the surface of $RhCl_3$-ZSM5-G2, S/(Si+Al) = 0.25, is obtained at a temperature of 250°C. The binding energies of the Rh $3d_{3/2}$ and Rh $3d_{5/2}$ photoelectron peaks for the zeolite prepared at this temperature give evidence that reduction of rhodium has occurred to give a mixture of oxidation states. An increase in the Rh $3d_{5/2}$ peak width from an inital Rh(III) value of 1.8 eV to a value of 2.0 eV also indicates a mixture of oxidation states, presumably Rh(III) and Rh(I). The XPS results for the sample sulfided at 400°C show that the ratio S/(Si+Al) = 0.09, and that rhodium is present in a reduced form, either Rh(I) or Rh(0). Figure 15 shows the S 2p photoelectron peak of $RhCl_3$-ZSM5-G2 sulfided with H_2S at 250 and 400°C. The Rh-zeolites sulfided at 250 and 400°C differ in the amount of sulfur present and the oxidation state of rhodium on the catalyst surface. Thus, these two temperature conditions were chosen for comparison in further studies.

The $RhCl_3$-13X and Co-Mo/Al_2O_3 catalysts were sulfided at 250 and 400°C with a 10 vol% H_2S/90 vol% H_2 gas mixture for 2 hours. Table 13 gives XPS results collected on $RhCl_3$-13X after the sulfidation procedure. For $RhCl_3$-13X sulfided at 250°C, the Rh $3d_{5/2}$ binding energy of 307.5 eV suggests a reduced rhodium species, either Rh(0) or Rh(I). The PWHM of the $3d_{5/2}$ photopeak of 1.8 eV is indicative of only one oxidation state. The S 2p binding energy of 162.2 eV

Table 12

XPS Results for $RhCl_3$-ZSM5-G2
10 vol% H_2S/90 vol% H_2 for 2 hours

Binding Energies (eV)

Temperature (°C)	Rh $3d_{3/2}$ (±0.1)	Rh $3d_{5/2}$ (±0.2)	S 2p (±0.1)	Na 1s (±0.2)
22	313.8	309.2	162.4	1071.6
150	313.0	308.4	162.3	1071.4
250	312.8	308.2	162.2	1072.2
350	312.3	307.7	162.3	1072.1
400	312.2	307.6	162.2	---

Atomic Ratios

Temperature (°C)	S/Rh	S/(Si+Al)	Rh/(Si+Al)	Na/(Si+Al)
22	0.36	0.04	0.11	0.08
150	2.30	0.23	0.10	0.02
250	2.50	0.25	0.10	0.03
350	0.90	0.09	0.10	0.01
400	1.01	0.09	0.089	----

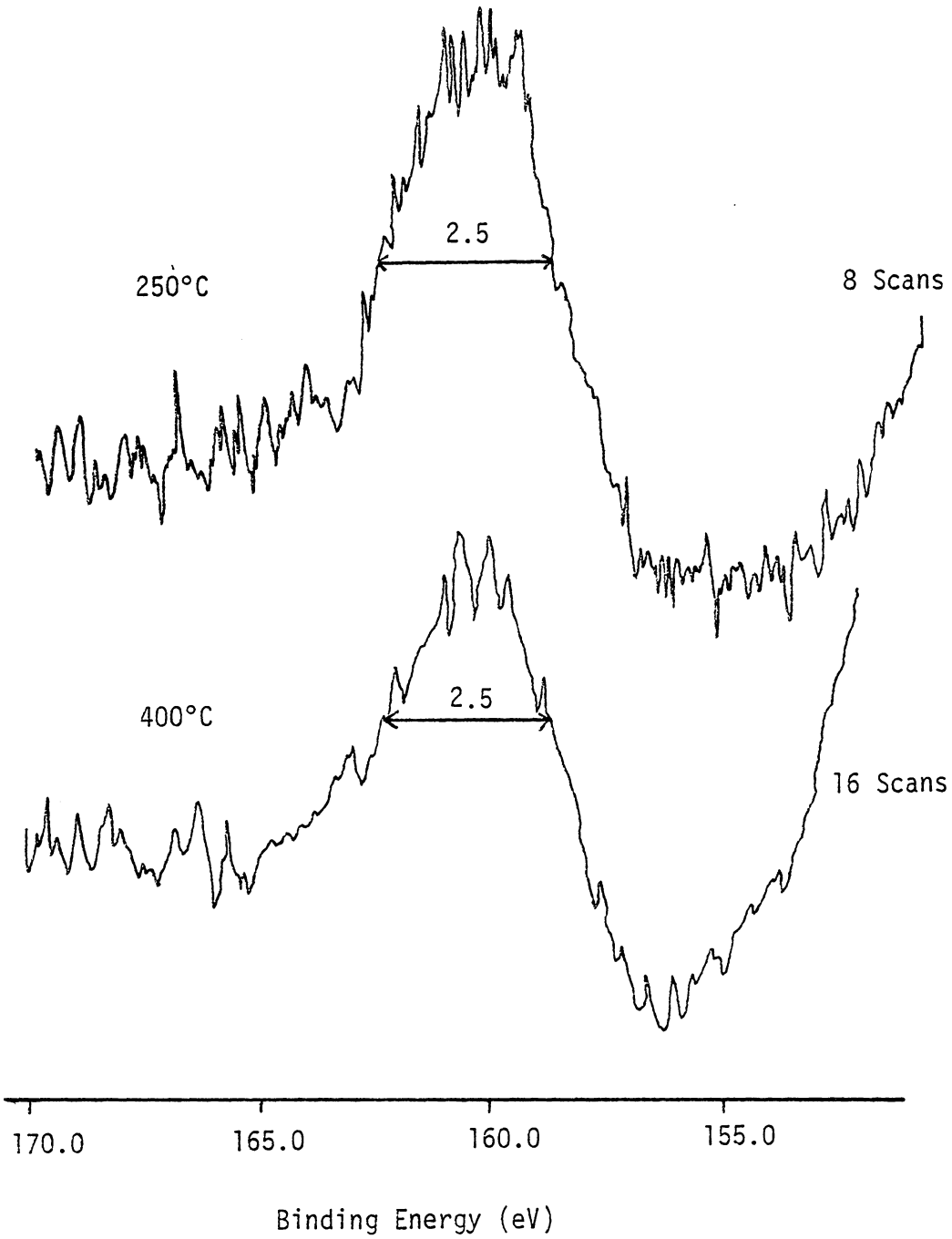

Figure 15. XPS Spectra of S 2p for $RhCl_3$-ZSM5-G2 Sulfided with H_2S at 250°C and 400°C

Table 13

XPS Results for $RhCl_3$-13X
10 vol% H_2S/90 vol% H_2
2 hrs.

	$RhCl_3$-13X Sulfided at 250° BE(eV)	$RhCl_3$-13X Sulfided at 400° BE(eV)
Rh $3d_{5/2}$	307.5	308.0
S 2p	162.0	162.4
Na 1s	1072.2	1072.1
S/Rh	1.67	2.06
S/(Si+Al)	0.25	0.33
Rh/(Si+Al)	0.15	0.16
Na/(Si+Al)	0.11	0.066

suggests that sulfur is present as either Na_2S (162.0 eV) or Rh_2S_3 (162.3 eV). However, since no Rh(III) photopeak was observed, the existence of Rh_2S_3 is unlikely. As the binding energy of the Rh 3d level suggests, sulfur might be in the form Rh_2S. For the $RhCl_3$-13X sample sulfided at 400°C, the Rh $3d_{5/2}$ binding energy occurs at 308.0 eV with a PWHM of 1.8 eV. By comparison with literature values (Table 10), the Rh binding energy is suggestive of a Rh(I) species. The narrow peak width furthermore indicates the presence of only oxidation state of rhodium.

The XPS spectra for the sulfided and non-sulfided Co-Mo/Al_2O_3 catalyst are given in Figure 16. The top spectrum shows the Mo $3d_{3/2}$ and $3d_{5/2}$ photoelectron peaks of the sample before sulfiding (MoO_3). The bottom spectrum was obtained after the catalyst had been sulfided with H_2S at 250°C for 2 hours. The XPS results for the sulfided sample are given in Table 14. As shown in Figure 16, the appearance of a third photoelectron peak indicates that the sulfiding procedure has resulted in a mixture of molybdenum oxidation states on the catalyst surface. The peak at 235.1 eV corresponds to the Mo $3d_{3/2}$ peak of the original MoO_3, some of which is still present. Sulfur is present on the catalyst as a sulfide species as indicated from the binding energy of the S 2p peak. Thus, the new peak at 228.7 eV must correspond to the Mo $3d_{5/2}$ peak of MoS_2, and the peak at 232.1 eV a combination of MoO_3 $3d_{5/2}$ and MoS_2 $3d_{3/2}$. Literature values are included for comparison in Table 14. The reduction of Mo(VI) to Mo(IV) is also observed at the H_2S-sulfiding temperature of 400°C.

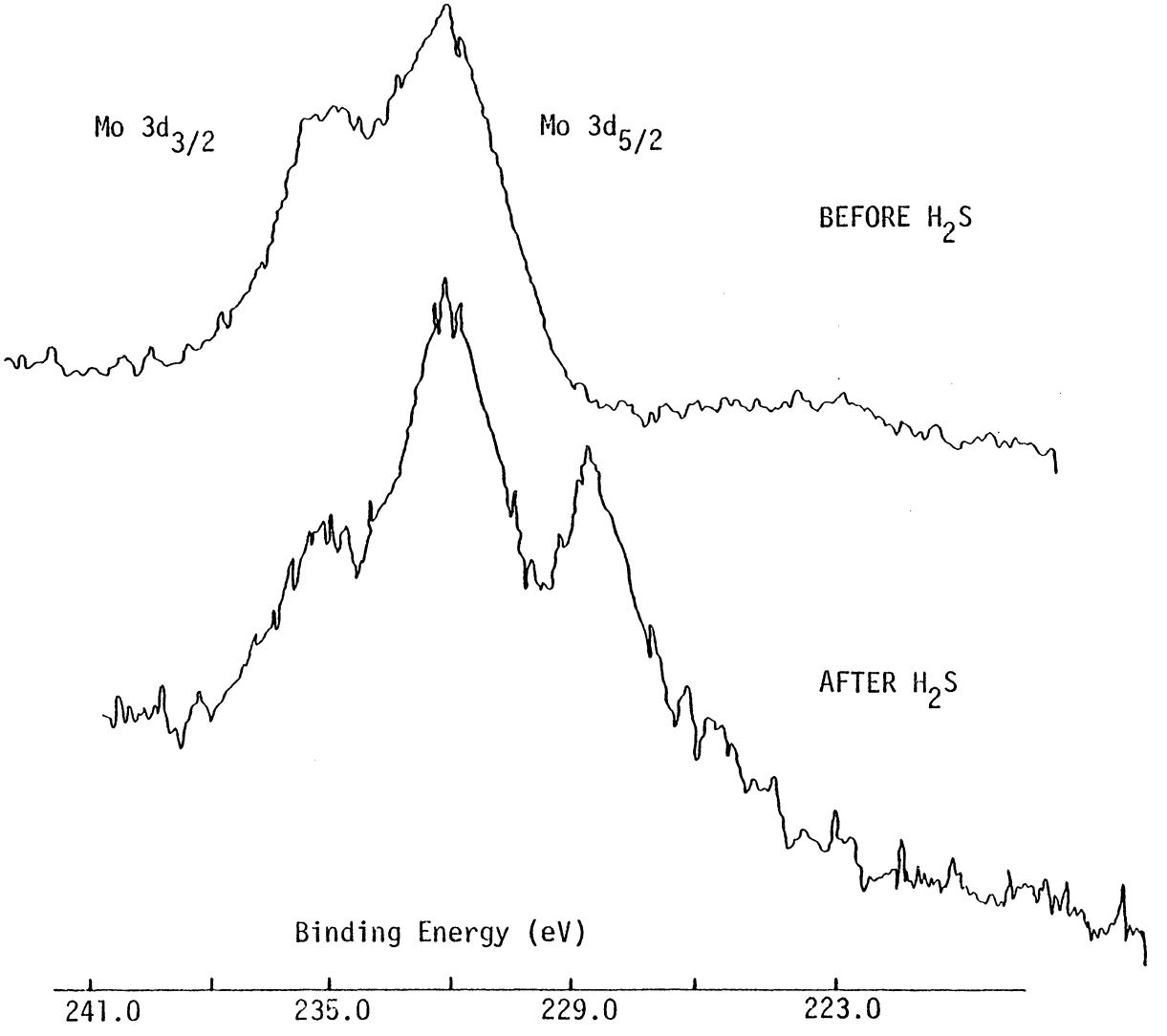

Figure 16. XPS Spectra for Co-Mo/Al_2O_3 Before and After H_2S at 250°C

Table 14

XPS Results for Co-Mo/Al_2O_3
10 vol% H_2S/90 vol% H_2
2 hours

	Binding Energy (eV)		
	Sulfided at 250°C	Sulfided at 400°C	Literature Values*
MoO_3, Mo $3d_{3/2}$	235.1	235.5	235.5
MoS_2, Mo $3d_{3/2}$ + MoO_3, Mo $3d_{5/2}$	232.1	232.4	232.1
MoS_2, Mo $3d_{5/2}$	228.7	228.8	228.9
S 2p	162.1	162.5	
	Atomic Ratios		
Mo/Al	0.043	0.037	
S/Al	0.10	0.10	

*Patterson et al. (68)

D. Percent Thiophene Conversion

In order to determine if the pure zeolite possessed any catalytic activity for the desulfurization of thiophene, conversion reactions were carried out on Na-13X and Na-ZSM5-G2. Reaction runs were also performed with the stainless steel reactor containing only quartz wool. The reactions were run at each of the temperatures 350, 400, 450, and 600°C. Thiophene conversion was not observed on either zeolite or in the blank reactor cell at any of the temperatures employed. The limit of detection of C_4 products was 0.10% thiophene conversion. Thus, any desulfurization activity over the Rh-zeolites was due to the presence of the rhodium or to a combination effect of both rhodium and the zeolite support.

Thiophene hydrodesulfurization reactions over the sulfided $RhCl_3$-ZSM5-G2 catalyst were studied as a function of reactor temperature and gas flow rate. Thiophene conversion was measured by ratioing the height of the C_4-product peak to that of unreacted thiophene. Figure 17 shows typical gas chromatograph peaks for the hydrodesulfurization reactions. Studies were made on the thiophene-sulfided catalyst and the H_2S-sulfided (250 and 400°C) catalyst. Results of thiophene conversion for the different catalysts are given in Table 15. Figure 18 shows results for a typical reaction run for thiophene hydrodesulfurization over the $RhCl_3$-ZSM5-G2 catalyst sulfided with H_2S at 250°C. Precision bars are included which show the deviation from the mean for each data point. Each point represents a minimum of two conversion runs. The data points for the

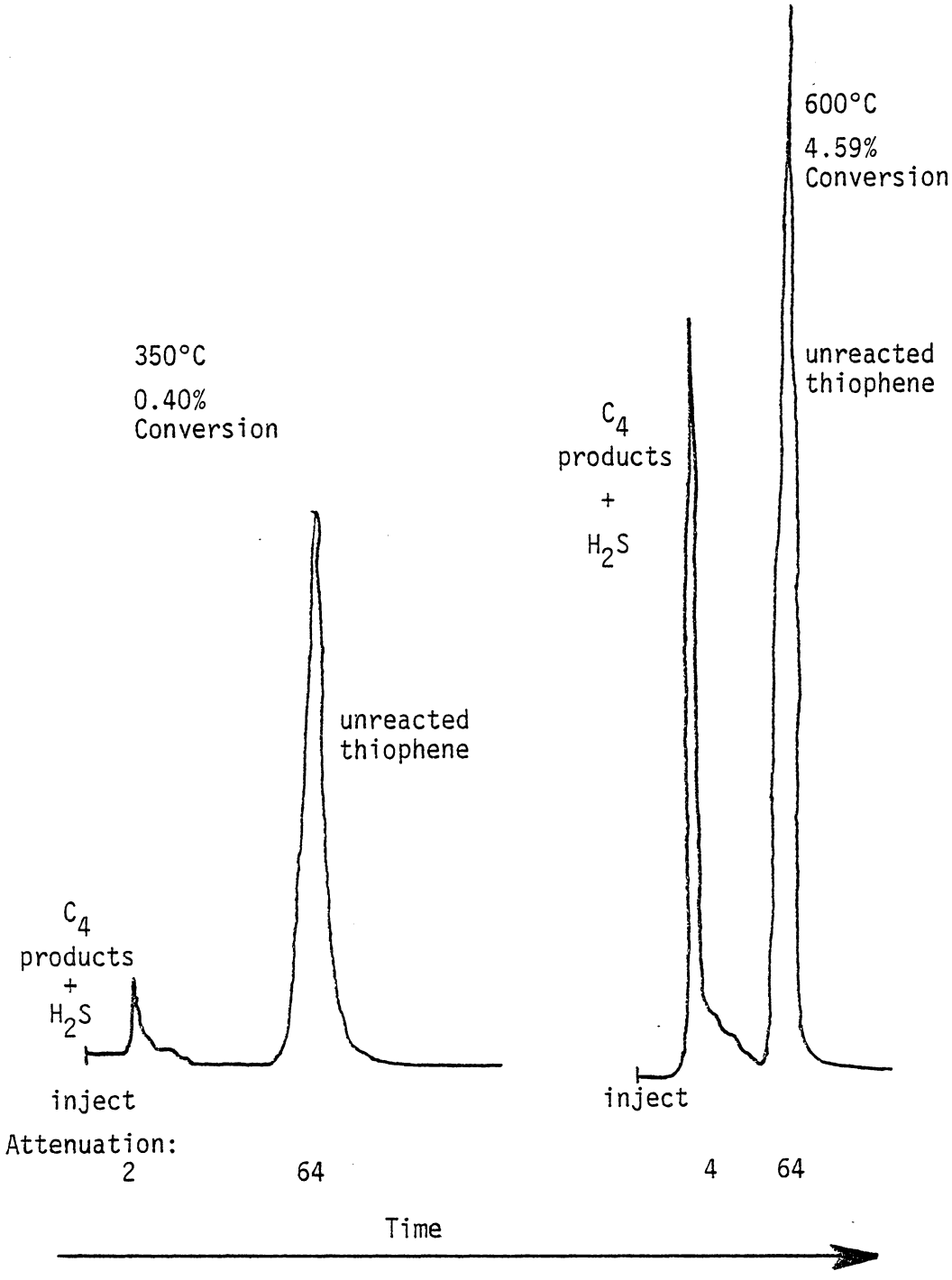

Figure 17. G. C. Peaks for Hydrodesulfurization Reactions
$RhCl_3$-ZSM5-G2; .5 µL thiophene; H_2S, 250°C; 40 mL/min.

Table 15

Percent Thiophene Conversion over $RhCl_3$-ZSM5-G2
Under Different Sulfiding Conditions

Reactor Temp(°C)	Flow Rate(mL/min)	Thiophene @ 100°C	H_2S @ 250°C*	H_2S @ 400°C
350	80	0.36	0.26	0.25
	60	0.41	0.24	0.30
	40	0.50	0.34	0.37
	30	0.56	0.19	0.40
400	80	0.46	0.23	0.30
	60	0.51	0.28	0.38
	40	0.70	0.31	0.41
	30	0.81	0.40	0.46
450	80	0.58	0.37	0.42
	60	0.61	0.43	0.52
	40	0.72	0.50	0.57
	30	0.74	0.51	0.81
600	80	2.62	1.46	1.77
	60	2.48	1.50	1.91
	40	2.44	1.68	1.87
	30	2.50	1.89	1.93

*Shown in Figure 18

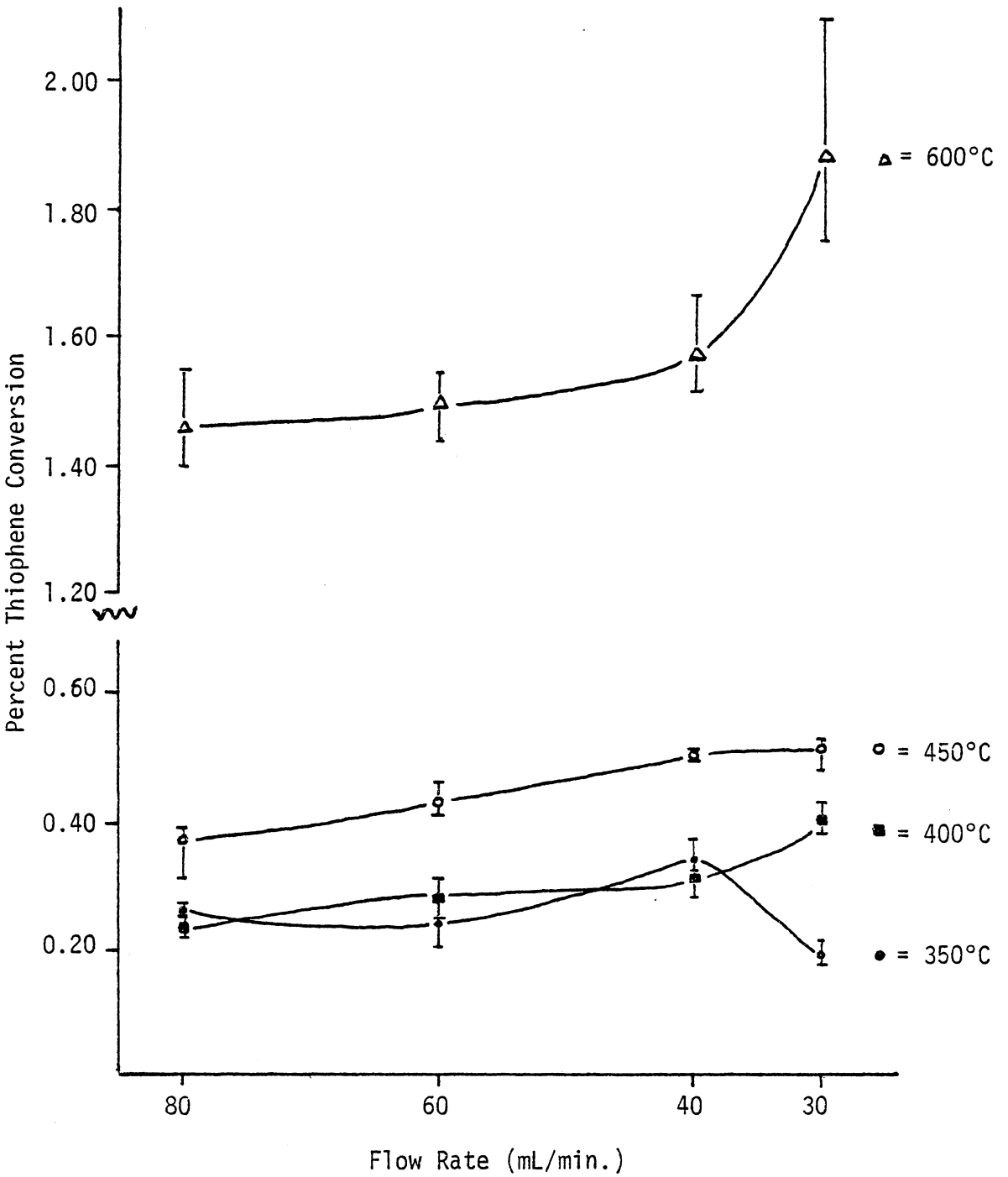

Figure 18. Percent Thiophene Conversion over $RhCl_3$-ZSM5-G2 (H_2S, 250°C)

350 and 400°C runs indicate that percent conversions are essentially the same for the reactions run with flow rates 80, 60 and 40 mL/min. Two trends can be observed from the graph. First, percent thiophene conversion increases with increasing temperature. This finding is in agreement with Owens and Amberg's (8) results. In general, percent thiophene conversion also increases with a decrease in carrier gas flow rate. This can be explained by the fact that a decrease in flow rate means that the thiophene experiences a longer contact time over the catalyst, allowing reaction to occur to a greater extent. Results obtained on $RhCl_3$-ZSM5-G2 sulfided with H_2S at 400°C, and with thiophene at 100°C also exhibited these trends. Maximum thiophene conversion occurred at a flow rate of 30 mL/min and a temperature of 600°C.

Thiophene conversion studies were conducted on both the H_2S- and thiophene-sulfided $RhCl_3$-13X catalyst, and on H_2S-sulfided Co-Mo/Al_2O_3 as a function of temperature and at a flow rate of 40 mL/min. Thiophene conversion results for these catalysts are given in Table 16. Each value represents the average of at least three reactions. Figures 19-21 show these results in graphical form. Reactions were run at the temperatures 350, 400, 450, and 600°C (±3°C) but are plotted so as to allow distinction between the error bars. Examination of Figure 19 indicates that all three catalysts show similar activities for catalysts sulfided with H_2S at 250°C. At a reaction temperature of 600°C, the Co-Mo/Al_2O_3 catalyst exhibits maximum conversion ability at a mean conversion value of 5.57%. Under these sulfiding conditions, $RhCl_3$-13X shows the least activity for

Table 16

Percent Thiophene Conversion Over Catalysts*

Reactor Temperature	$RhCl_3$-ZSM5-G2			$RhCl_3$-13X			Co-Mo/Al_2O_3	
	TH[1]	250°C[2]	400°C[3]	TH	250°C	400°C	250°C	400°C
350°C	0.34	0.44	0.49	0.76	0.48	0.34	0.52	0.40
400°C	0.60	0.49	0.57	2.01	0.43	0.91	0.63	0.31
450°C	0.96	1.09	0.70	4.23	0.72	1.76	1.09	0.60
600°C	3.13	4.73	3.32	13.42	3.81	4.28	5.57	2.82

*40 mL/min flow rate

[1]Sulfided with thiophene at approximately 100°C

[2-3]Temperature of sulfidation with 10 vol% H_2S/90% vol% H_2

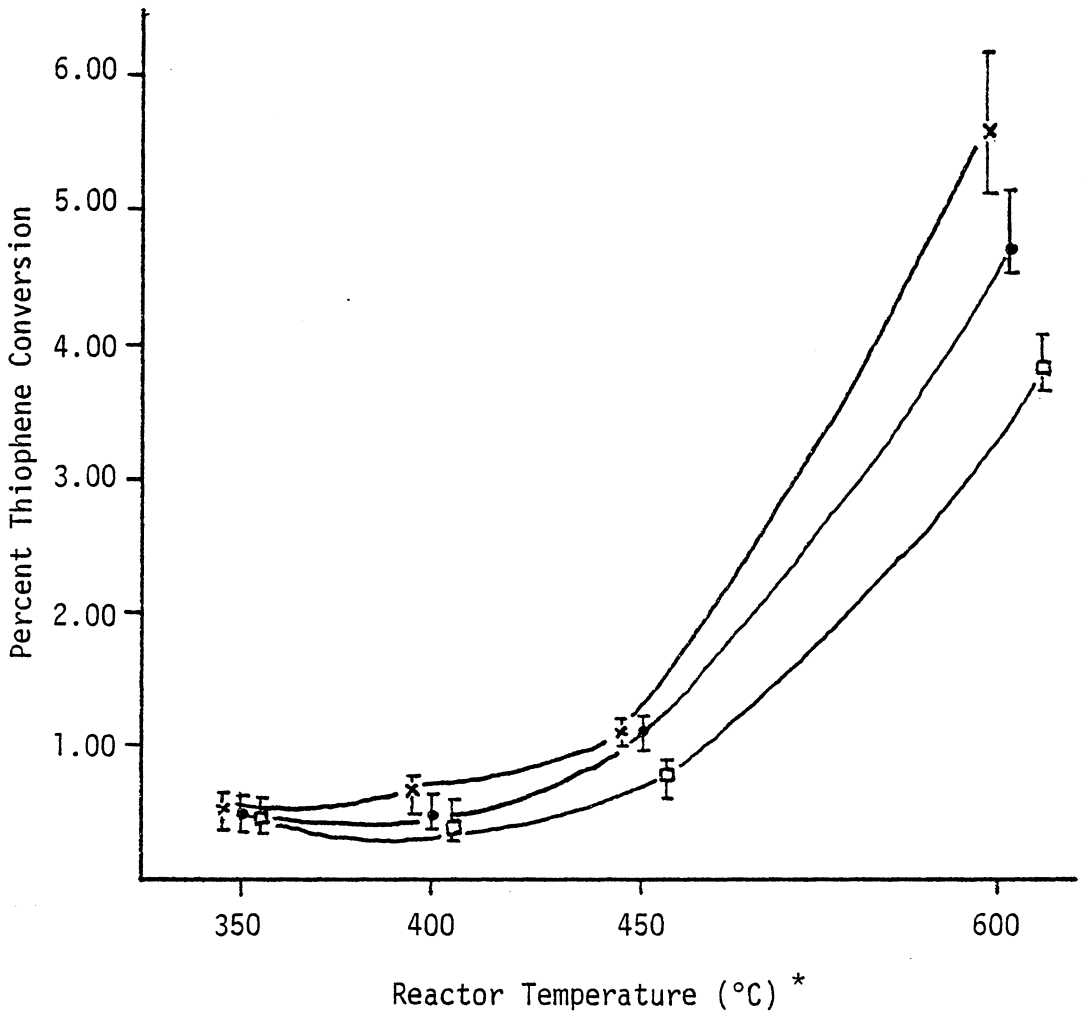

X = $Co\text{-}Mo/Al_2O_3$

● = $RhCl_3$-ZSM5-G2

□ = $RhCl_3$-13X

Flow Rate = 40 mL/min.

*Data points at T° ± 3°C; Points plotted to allow distinction of error bars.

Figure 19. Percent Thiophene Conversion over Catalysts Sulfided with H_2S at 250°C

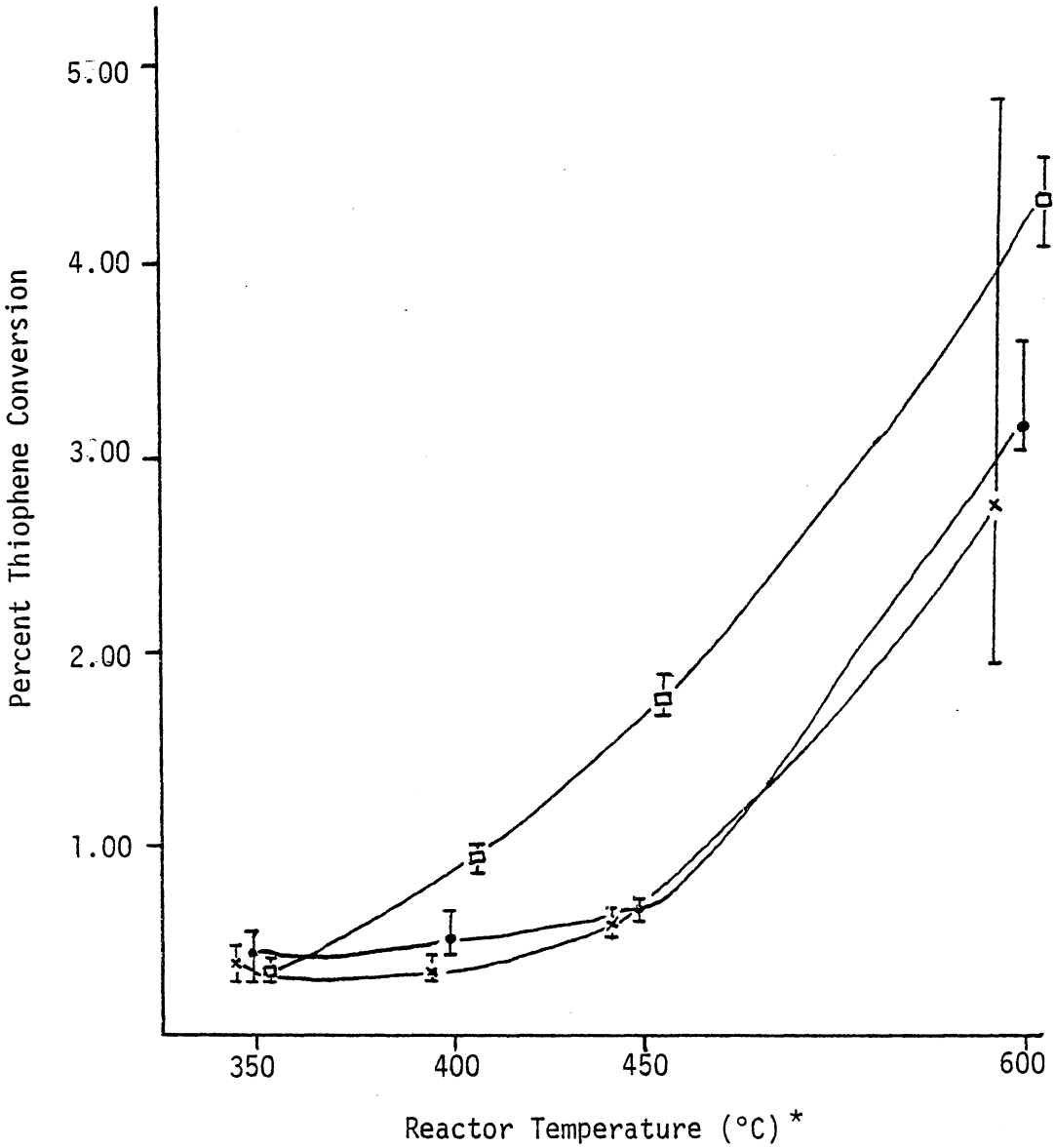

× = $Co\text{-}Mo/Al_2O_3$

● = $RhCl_3$-ZSM5-G2

□ = $RhCl_3$-13X

Flow Rate = 40mL/min.

* Data points at T° ± 3°C; Points plotted to allow distinction of error bars.

Figure 20. Percent Thiophene Conversion over Catalysts Sulfided with H_2S at 400°C

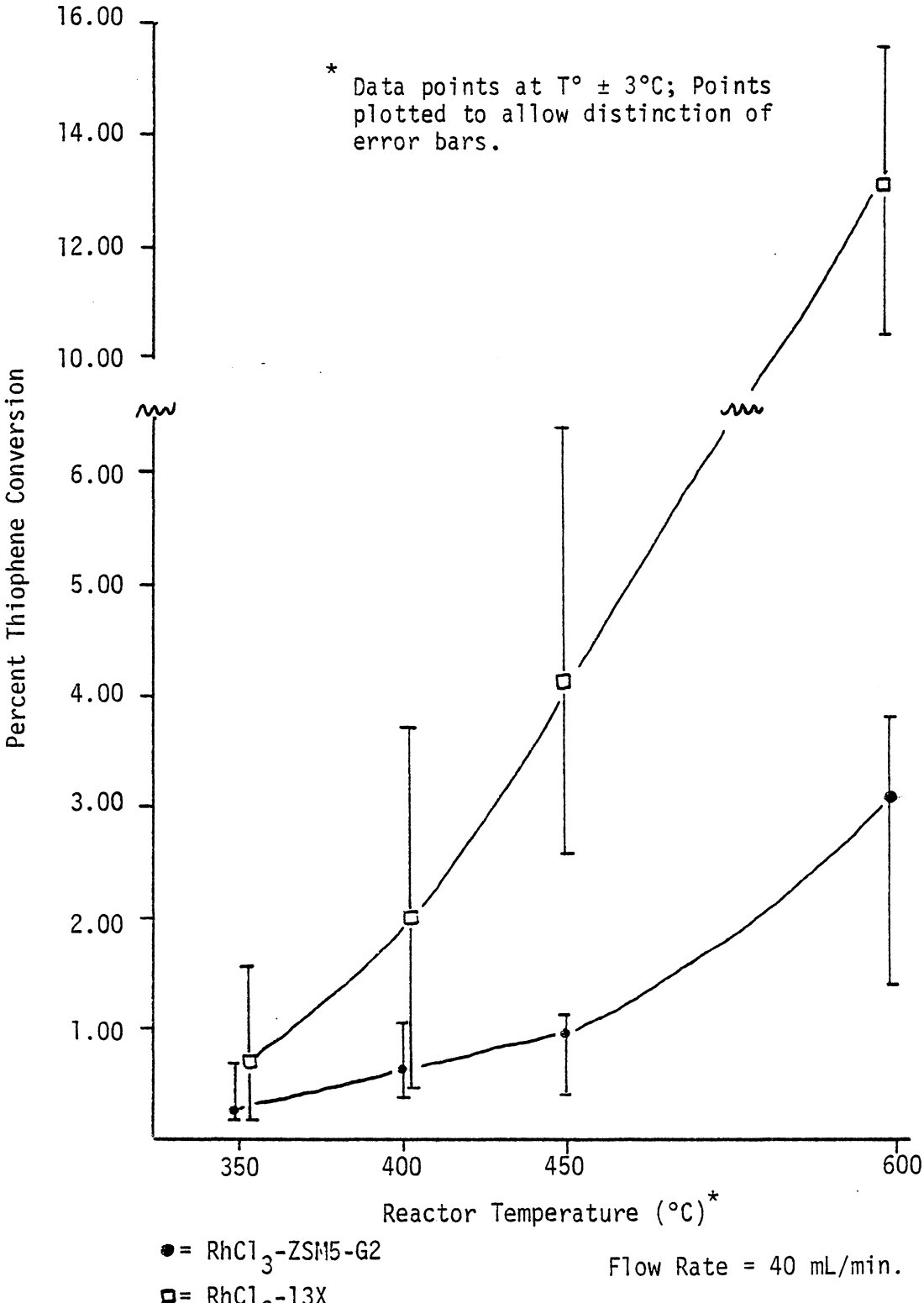

Figure 21. Percent Thiophene Conversion over Catalysts Thiophene Sulfided at 100°C

hydrodesulfurization of thiophene.

The opposite trend is found for the catalyst sulfided with H_2S at 400°C. Figure 20 shows that $RhCl_3$-13X has considerably higher conversion at the temperatures 400, 450, and 600°C than either Co-Mo/Al_2O_3 or $RhCl_3$-ZSM5-G2. Under these conditions, Co-Mo/Al_2O_3 has the lowest mean conversion value of 2.82%. Thus, it is concluded that under conditions of H_2S sulfidation at 400°C, $RhCl_3$-13X is the most active catalyst for the desulfurization of thiophene.

For the thiophene-sulfided catalysts (Figure 21), the results indicate that $RhCl_3$-13X has the superior conversion activity. However, as can be seen from the range of the mean deviation for each data point, the results lack good precision. Multiple reaction runs were made on these catalyst systems in order to improve reproducibility but to no avail. The average 600°C thiophene conversion result over thiophene sulfided $RhCl_3$-13X is 13.42%. Since this result is almost three times that of any other catalytic system, a more extensive study of the catalyst surface characteristics during the course of the reactions was carried out. This study will be discussed in more depth in a later section.

From thiophene conversion results presented here, it is concluded that Co-Mo/Al_2O_3 is the most active catalyst when pre-sulfided with H_2S at 250°C. However, $RhCl_3$-13X possesses superior hydrodesulfurization catalytic activity for thiophene-sulfided (100°C) and H_2S-sulfided (400°C) samples. This is not to say, however, that $RhCl_3$-13X is the "best" catalyst for thiophene hydrodesulfurization.

These results hold only for these specific conditions. Also, 13X has a low tolerance to poisoning or coke deposition compared to ZSM5 (69). Coke deposition can greatly affect activity and catalyst lifetime. In this study, no experiments were performed to determine the time the catalyst maintains its activity. Considerations of this sort must be recognized in determining a "best" catalyst for a particular process.

E. Product Distribution

Product distribution over each catalyst at different reaction conditions was determined by mass spectrometry. The possible products of the hydrodesulfurization reaction were unreacted thiophene, tetrahydrothiophene, 1,3-butadiene, 1-butene, cis- and trans-2-butene, butane and hydrogen sulfide. The mass spectra of the three butenes are indistinguishable except for the relative intensities of their mass peaks. For the butenes, the difference in the relative intensity of peaks in the lower mass to charge range is only about 7%. These three products could not be distinguished with the mass spectrometer used because of background contamination from air and other impurities. In all experiments, the only products identified were butane, butene, and hydrogen sulfide. For calculation of product distribution, it was assumed that the hydrodesulfurization and hydrogenation reactions proceeded according to the stoichiometric equation:

$$C_4H_4S + \text{excess } H_2 \longrightarrow H_2S + [C_4H_6 + C_4H_8 + C_4H_{10}]$$

Thus, H_2S made up 50% of the reaction products. Molecular ion and base peaks for 1,3-butadiene, cis-2-butene, n-butane and hydrogen sulfide

are given in Table 17.

Product distribution results of thiophene desulfurization over the three catalysts are presented in Table 18. Results are given for each sulfiding procedure employed. Graphical representations of these results are shown in Figures 22-24. The butene/butane ratio increases with increasing temperature for Co-Mo/Al_2O_3 and $RhCl_3$-ZSM5-G2 sulfided at 250°C with H_2S. The same trend is observed for all three catalysts when sulfiding is performed with H_2S at 400°C. A possible explanation for the increasing butene/butane ratio is that the rate of desulfurization of thiophene is greater than the rate of butene hydrogenation. Thus, at higher temperatures, butene is being formed at a faster rate than it can be hydrogenated to butane. Since no 1,3-butadiene was observed in any of the reaction products, it is concluded that if 1,3-butadiene is formed initially from the desulfurization of thiophene, it is immediately hydrogenated to butene. This proposal is in agreement with Owens and Amberg's (8-10) theory. Another possible explanation is that simultaneous hydrogenation and desulfurization occur resulting in direct desorption of butene from the catalyst. However, no experiments were carried out to determine the actual mechanism involved. A decrease in the butene/butane product ratio at the lower temperatures is observed over $RhCl_3$-13X sulfided at 250°C (Figure 22). This behavior indicates that the reaction goes more toward completion under these conditions.

Table 17

Molecular Ion and Base Peaks for Reaction Products

	Molecular Ion Peak (m/z)	Base Peak (m/z)
1,3-butadiene	54	39
cis-2-butene	56	41
n-butane	58	43
hydrogen sulfide	34	32

Table 18

Product Distribution

Butene/Butane

Reactor Temperature (°C)	$RhCl_3$-ZSM5-G2 H_2S,250°	H_2S,400°	* TH,100°	$RhCl_3$-13X H_2S,250°	H_2S,400°	* TH,100°	Co-Mo/Al_2O_3 H_2S,250°	H_2S,400°
350	1.02	0.92	1.08	2.42	0.64	2.22	0.81	0.22
400	1.91	1.60	1.59	1.80	2.06	2.97	1.72	1.65
450	2.26	1.64	2.05	1.66.	3.31	3.55	2.50	2.08
600	3.48	3.17	2.44	3.44	3.90	2.81	6.80	4.07

* TH = Thiophene

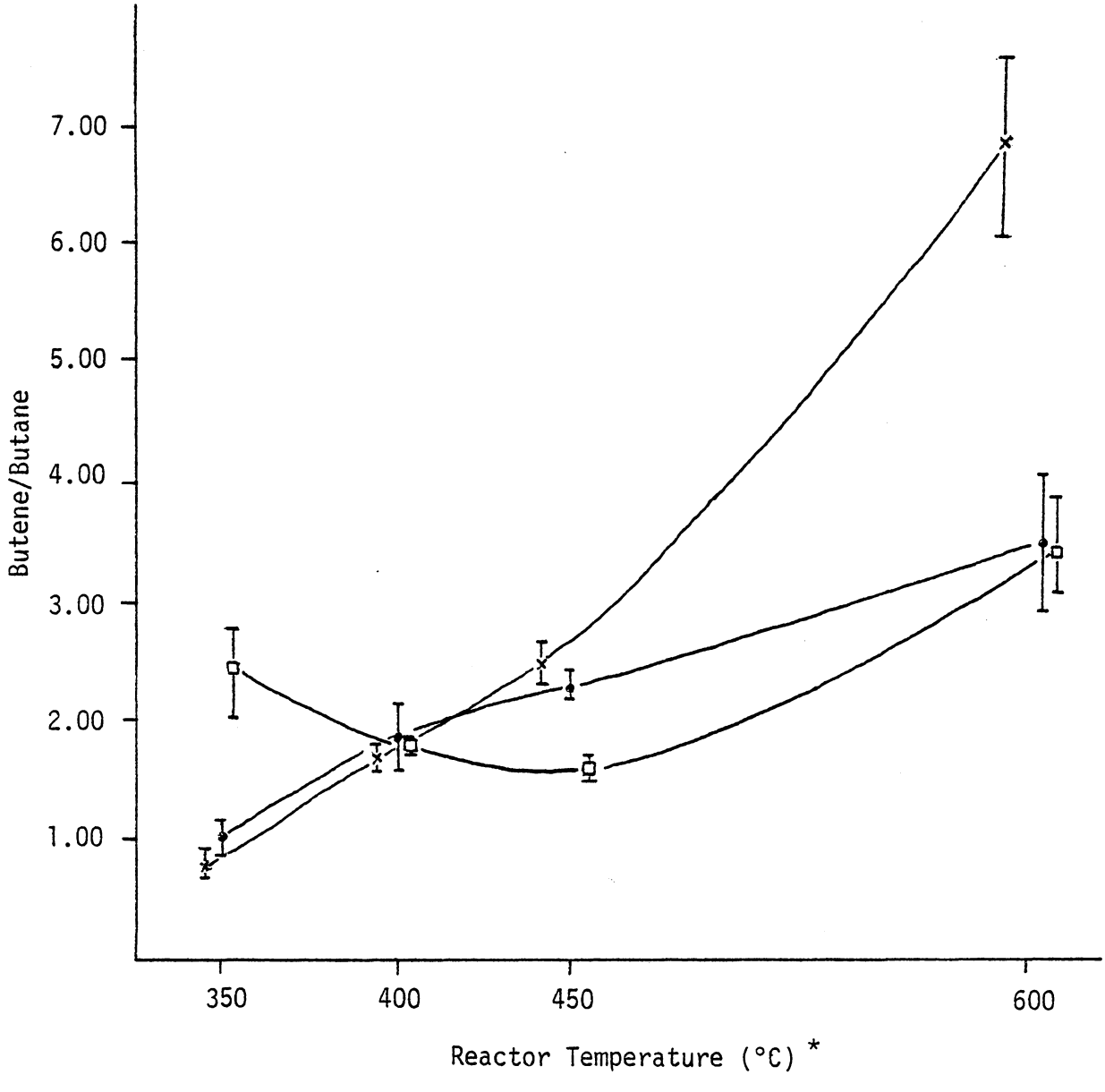

× = Co-Mo/Al_2O_3

● = $RhCl_3$-ZSM5-G2

□ = $RhCl_3$-13X

Flow Rate = 40 mL/min.

* Data points at T° ± 3°C; Points plotted to allow distinction of error bars.

Figure 22. Product Distribution
250°C, 10% H_2S - Sulfiding Conditions

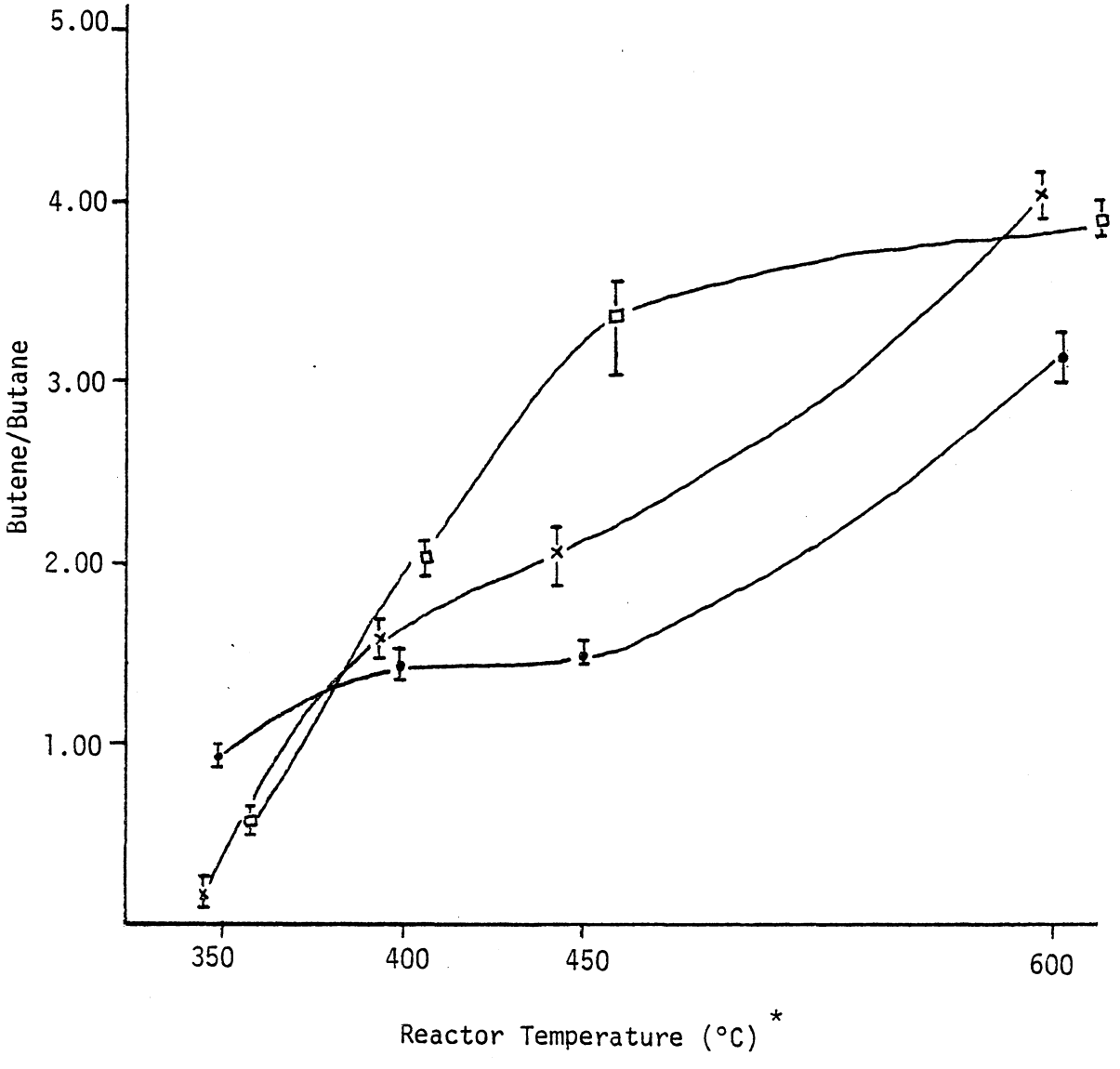

Figure 23. Product Distribution
400°C, 10% H_2S - Sulfiding Conditions

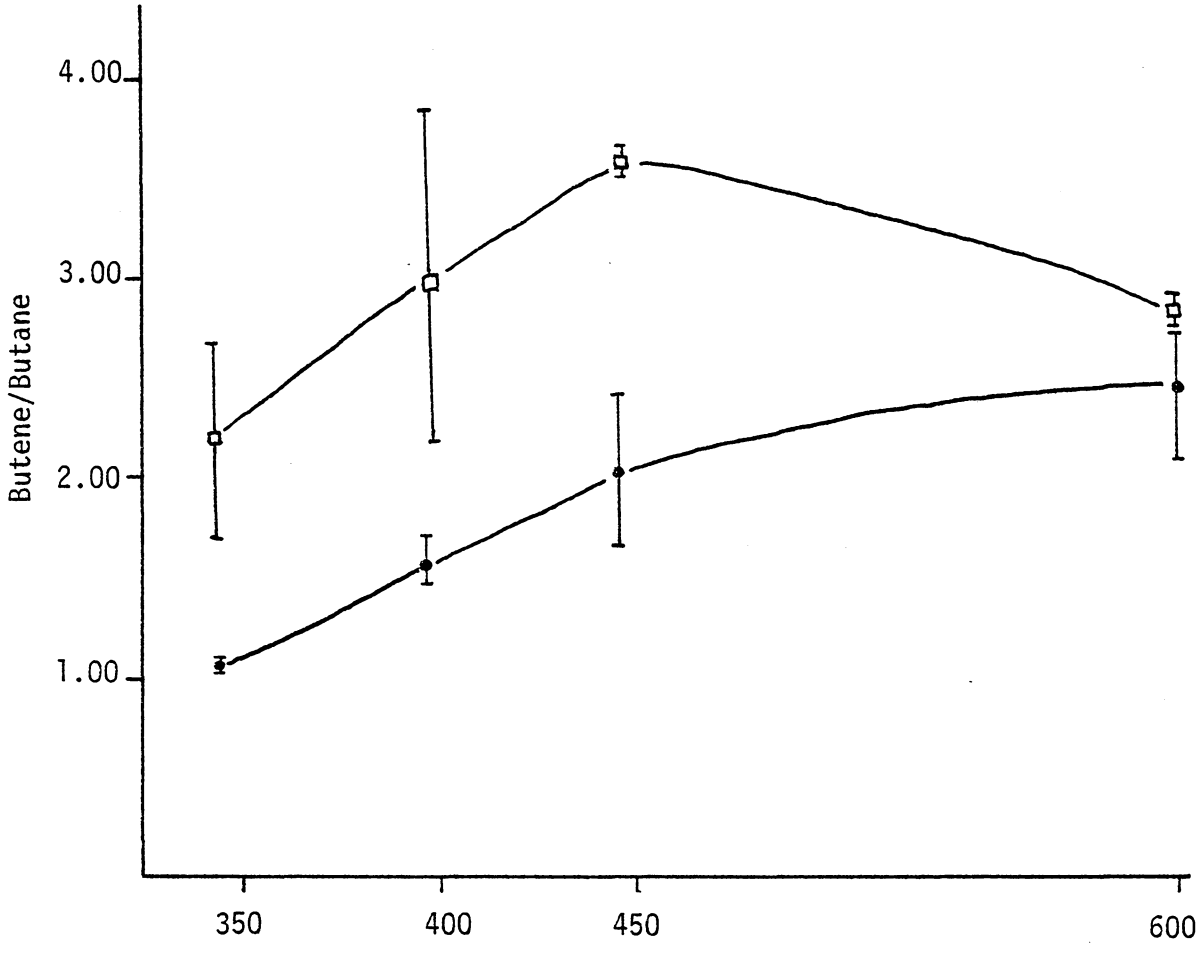

● = $RhCl_3$-ZSM5-G2

□ = $RhCl_3$-13X

Flow Rate = 40 mL/min.

*Data points at T° ± 3°C; Points plotted to allow distinction of error bars.

Figure 24. Product Distribution
100°C, Thiophene-Sulfiding Conditions

F. Catalyst Characterization - After Reactions

After reaction, the surface of the catalysts was characterized by XPS to correlate surface characteristics with thiophene conversion activity and to determine the active rhodium hydrodesulfurization species. However, it was found that definite identification of rhodium oxidation state could not be based on XPS results. Tables 19 and 20 give the XPS results for the H_2S-and thiophene-sulfided $RhCl_3$-13X and $RhCl_3$-ZSM5-G2 zeolites after hydrodesulfurization reactions up to 600°C. The binding energy of the Rh $3d_{5/2}$ peak for each of the sulfided $RhCl_3$-13X zeolites is fairly constant at about 307.1 eV. It cannot be concluded, however, whether this binding energy corresponds to Rh(I) or Rh(0).

The amount of sulfur on the surface of the H_2S-sulfided $RhCl_3$-13X zeolites after reactions decreased about 94% from initial S/(Si + Al) values of 0.25 and 0.33 to values of 0.016 and 0.021 for the 250 and 400°C sulfided samples, respectively. The S/(Si + Al) ratio for the thiophene sulfide $RhCl_3$-13X decreased from 0.10 to a value of 0.037, a decrease of 63%. This result is suggestive of desorption of surface sulfur as H_2S during the reactions. Based on the mole ratio of S/(Si + Al) before and after reactions, and the moles of sulfur in a 0.5 µL injection of thiophene, it was concluded that the amount of surface sulfur which desorbed as H_2S is negligible compared to the amount of H_2S formed from reactions. A calculation to demonstrate this was based on the following equations:

Table 19

XPS Results for Sulfided $RhCl_3$-13X

After Hydrodesulfurization Reactions
(to 600°C)

	Binding Energy (eV)		
	10% H_2S, 250°C (±0.2 eV)	10% H_2S, 400°C (±0.2 eV)	Thiophene, 100°C (±0.2 eV)
Rh $3d_{5/2}$	306.9	307.4	307.0
S 2p	162.2	162.6	162.4
Na 1s	1071.7	1072.2	1072.0
	Atomic Ratios		
S/Rh	0.11	0.21	0.25
S/(Si + Al)	0.016	0.021	0.037
Rh/(Si + Al)	0.14	0.10	0.15
Na/(Si + Al)	0.20	0.13	0.10

Table 20

XPS Results for Sulfided $RhCl_3$-ZSM5-G2

After Hydrodesulfurization Reactions
(to 600°C)

	Binding Energy (eV)		
	10% H_2S, 250°C	10% H_2S, 400°C	Thiophene, 100°C
Rh $3d_{5/2}$	307.6 (±0.3)	307.6 (±0.1)	307.6 (±0.1)
S 2p	162.1 (±0.1)	162.4 (±0.1)	162.1 (±0.2)
	Atomic Ratios		
S/Rh	0.13	0.43	0.074
S/(Si + Al)	0.007	0.043	0.0040
Rh/(Si + Al)	0.056	0.10	0.054

$$\frac{S}{(Si+Al)} \cdot \frac{Si+Al)mole}{mol.wt.zeolite} \cdot \frac{mol.wt.zeol.}{1\ mole\ zeol.} \cdot \frac{moles\ zeol.}{5\ mg\ zeol.} = \text{moles S on catalyst} \qquad (4)$$

$$\text{original moles S on catalyst} - \text{moles S on catalyst after rx.} = \text{moles S desorbed} \qquad (5)$$

$$(\%\ \text{conversion})(\text{moles S in } 0.5\mu L \text{ thiophene}) = \text{moles S converted} \qquad (6)$$

moles S converted >> moles S desorbed

Table 21 shows these results for $RhCl_3$-13X and $RhCl_3$-ZSM5-G2. The amount of desorbed sulfur as H_2S is less than the amount of H_2S produced in the reactions in all cases. Thus, the desorption of surface sulfur as H_2S does not contribute to the total amount of reaction products.

The binding energy of the S 2p photoelectron level on all $RhCl_3$-13X samples suggests the presence of a sulfided species. The binding energy for the S 2p level in Na_2S is 162.0 eV, while the S 2p binding energy for Rh_2S_3 is 162.3 eV. Thus, either or both of these sulfides could be present. It is unlikely, however, the Rh_2S_3 is present on the zeolite due to the lack of a Rh(III) photopeak at 309.6 eV. The rhodium binding energy results suggest that sulfur might be present as the Rh(I) sulfide Rh_2S.

Table 20 presents XPS results on the sulfided $RhCl_3$-ZSM5-G2 zeolites after hydrodesulfurization reactions through 600°C. As in $RhCl_3$-13X, the Rh 3d binding energy for $RhCl_3$-ZSM5-G2 might be suggestive of Rh(I) as the active species in all three samples. The

Table 21

Moles Sulfur Lost During Hydrodesulfurization Reactions

To 600°C Compared to Moles Sulfur Converted

Zeolite	Sulfiding Conditions	Moles Surface Sulfur Lost as H_2S		Moles Thiophene Sulfur Converted to H_2S
$RhCl_3$-13X				
	Thiophene @ 100°C	1.26×10^{-10}	<<	3.21×10^{-7}
	H_2S @ 250°C	4.21×10^{-10}	<<	9.11×10^{-8}
	H_2S @ 400°C	5.56×10^{-10}	<<	1.02×10^{-7}
$RhCl_3$-ZSM5-G2				
	Thiophene @ 100°C	2.52×10^{-11}	<<	7.48×10^{-8}
	H_2S @ 250°C	4.32×10^{-10}	<<	1.13×10^{-7}
	H_2S @ 400°C	8.46 x 10-11	<<	7.93×10^{-8}

S 2p binding energy indicates sulfur is present as sodium sulfide, a rhodium sulfide or both. The amount of sulfur on the surface has decreased, suggestive of desorption as H_2S during reactions.

Since percent thiophene conversion results over thiophene-sulfided $RhCl_3$-13X were a factor of three greater than the other catalysts, XPS studies were carried out after each reaction to determine the source of increased activity. The XPS results were collected after running reactions up to the designated temperature and are given in Table 22. Examination of the results in Table 22 reveals a fairly constant binding energy at 307.2 eV for the Rh $3d_{5/2}$ peak suggesting a reduced rhodium species on the catalyst surface. The binding energy for S 2p corresponds to a sulfide species. As reaction temperature increased, the amount of sulfur decreased, suggesting desorption as H_2S. The Rh/(Si + Al) ratio decreased with increasing temperature which may indicate migration of the rhodium away from the surface to the internal cages of the zeolite. The results on the thiophene-sulfided $RhCl_3$-13X, however, are similar to those results obtained on the H_2S-sulfided systems and unfortunately, do not indicate any reason for the enhanced activity for thiophene-sulfided $RhCl_3$-13X.

Table 23 gives XPS results for the H_2S-sulfided Co-Mo/Al_2O_3 catalyst after hydrodesulfurization reactions up to 600°C. Binding energies of the Mo 3d level have not changed from before reaction results (Table 14). Sulfur 2p binding energies are also unchanged. The S/Mo and S/Al ratios decreased suggesting desorption of sulfur as H_2S. Thus, since the sulfided molybdenum is still present after reactions to

Table 22

XPS Results for Thiophene Sulfided $RhCl_3$-13X after each Temperature

Temperature @ which Catalyst Removed (°C)	Binding Energy (eV) Rh $3d_{5/2}$ (±0.2)	S 2p (±0.1)	Na 1s (±0.2)	Atomic Ratios S/Rh	S/(Si+Al)	Rh/(Si+Al)
350	307.2	162.3	1072.7	0.89	0.16	0.18
400	307.5	162.6	1072.6	0.80	0.12	0.15
450	307.1	162.1	1072.2	0.54	0.070	0.13
600	307.1	161.9	1071.6	0.25	0.030	0.12

Table 23

XPS Results for Sulfided Co-Mo/Al_2O_3

After Hydrodesulfurization Reactions
(to 600°C)

	Binding Energy (eV)	
	10% H_2S/90% H_2, 250°C	10% H_2S/90% H_2, 400°C
Mo $3d_{3/2}$	234.9	234.7
Mo $3d_{3/2}$ + Mo $3d_{5/2}$	232.3	232.2
Mo $3d_{5/2}$	229.0	229.2
S 2p	161.9	161.9
Al 2p	74.7	74.2
	Atomic Ratios	
Mo/Al	0.040	0.043
S/Mo	1.13	2.04
S/Al	0.045	0.088

600°C, it is concluded that MoS_2 is the active species for hydrodesulfurization of thiophene. This conclusion is in agreement with Clausen et al. (33).

For the Rh-zeolites, no definite conclusion as to the oxidation state of rhodium can be drawn from XPS results alone. By comparison with Table 10, binding energies for the rhodium 3 d level indicate that either Rh(0) or Rh(I) is present. However, it is proposed that Rh(I) is present on the zeolite surface and is the active hydrogenation species based on the following results. As explained in a previous section, $RhCl_3$-ZSM5(M) was reduced in flowing H_2 at 600°C for 2 hours. The binding energy for the reduced Rh $3d_{5/2}$ photopeak was 307.5 eV. Under these severe reducing conditions, it is reasonable that this binding energy is indicative of Rh(0). The absence of sulfur on the $RhCl_3$-ZSM5(M) surface after repeated thiophene injections indicates that rhodium (0) was unable to form a sulfide species. Thus, it is concluded that Rh(0) is unable to react with thiophene. Furthermore, it is known (70) that rhodium metal is an excellent catalyst for the hydrogenation of olefins to alkanes. However, in this study, as reaction temperature increased, the butene/butane product ratio increased. This result is opposite from what would be expected if Rh(0) were present on the catalysts. Based on these results, it is concluded that Rh(I) is the predominant species on the catalyst surface. Also, due to the lack of reaction with Rh(0) and thiophene, it is proposed that Rh(I) is the active species for the hydrodesulfurization of thiophene.

CHAPTER V

SUMMARY AND CONCLUSIONS

The adsorption properties of the rhodium complexes $RhCl_3 \cdot 3H_2O$, $Rh_2(CO_2CH_3)_4$, and $Rh(PPh_3)_3Cl$ on 13X, on ZSM5(M) zeolites and on a laboratory synthesized ZSM5-G2 zeolite were investigated. The $RhCl_3$-13X and $RhCl_3$-ZSM5-G2 zeolites were studied for catalytic activity in the hydrodesulfurization of thiophene and the activity results were compared to those of a commercial Co-Mo/Al_2O_3 catalyst. X-ray photoelectron spectroscopy was used to examine the catalyst surfaces both before and after the hydrodesulfurization reactions. It was expected that XPS characterization would give insight into the chemical oxidation state of rhodium and the identification of the active surface species for desulfurization. However, this was not achieved in all cases. The hydrodesulfurization reactions were carried out in a pulse/microreactor gas chromatograph system. Product identification was accomplished using mass spectrometry.

The adsorption of $RhCl_3 \cdot 3H_2O$ on 13X, ZSM5(M), and ZSM5-G2 zeolites yielded a Rh(III) surface species. A near equal amount of rhodium(III) was adsorbed on each zeolite. Calculations based on XPS ratios and the chemical formula of the zeolite indicated approximately 16 wt% Rh was present on the zeolites after adsorption. A small amount of rhodium, Rh/(Si+Al) = 0.030, was adsorbed on 13X from a $Rh_2(CO_2CH_3)_4$ methanol solution. XPS measurements demonstrated the Rh(II) was reduced to a mixture of oxidation states on the zeolite surface during adsorption from solution and x-ray bombardment in the

spectrometer. The amount of rhodium(I) adsorbed on 13X from $Rh(PPh_3)_3Cl$ was equal to that from $RhCl_3 \cdot 3H_2O$, however, the Rh 3d binding energies did not permit a determination of the rhodium oxidation state. A binding energy equal to that of $RhCl_3 \cdot 3H_2O$ was measured. Literature binding energies for Rh(0) and Rh(I) overlap. The binding energy values reported for $Rh(PPh_3)_3Cl$ have a range of 2 eV. Thus, it was not possible to conclude whether Rh(I) adsorbed as Rh(I), or was oxidized to Rh(III) upon adsorption.

To achieve a maximum amount of sulfur on the catalyst surface, two methods of sulfidation were investigated. Thiophene sulfidation of zeolites results in a S/(Si+Al) ratio of approximately 0.10, as measured from XPS photopeak intensities, for all zeolites. Thiophene sulfidation of a Rh(0)-ZSM5(M) catalyst and subsequent XPS measurements resulted in no detectable sulfur on the zeolite surface. It was thus concluded that thiophene is unable to react with Rh(0) on the zeolite surface to produce a rhodium sulfide species. Sulfidation of $RhCl_3$-ZSM5-G2 by a H_2S/H_2 gas mixture resulted in a maximum S/(Si+Al) ratio of 0.25 at a sulfiding temperature of 250°C. The XPS binding energy and peak width of the Rh $3d_{5/2}$ peak suggested a mixture of oxidation states. At a sulfiding temperature of 400°C, sulfur was present as sulfide with a S/(Si+Al) ratio of 0.09. Rhodium binding energy measurements indicated rhodium as a reduced species, either Rh(0) or Rh(I).

Hydrodesulfurization reactions were carried out on sulfided $RhCl_3$-ZSM5-G2 as a function of gas flow rate and reaction temperature.

The percent thiophene conversion increased with increasing temperature and decreasing flow rate.

Thiophene conversion results for the three H_2S-sulfided (250°C) catalysts at a flow rate of 40 mL/min indicated that the commercial Co-Mo/Al_2O_3 catalyst achieved maximum conversion of 5.57% at 600°C. However, for a H_2S-sulfiding temperature of 400°C, the $RhCl_3$-13X exhibited maximum thiophene conversion of 4.28%. The Co-Mo/Al_2O_3 sulfided with H_2S at 400°C was the least active catalyst. When the zeolite catlysts were sulfided with thiophene at 100°C, the most active catalyst was $RhCl_3$-13X. The maximum thiophene conversion was 13.42% at 600°C. Thus, $RhCl_3$-13X is the most active catatlyst for thiophene hydrodesulfurization reactions when presulfided with H_2S at 400°C or with thiophene at 100°C.

The products of the hydrodesulfurization reactions were identified by mass spectrometry. The hydrodesulfurization products were hydrogen sulfide, butene, and butane. It was not possible to distinguish between 1-butene, cis-, or trans-2-butene. In general, over all catalysts and all three sulfiding conditions, the butene to butane product ratio increased with increasing reaction temperature. This distribution result is suggestive of a faster reaction rate for desulfurization of thiophene than hydrogenation of butene. The increase in butene/butane product ratio with increasing temperature also lends support to the absence of Rh(0) as the active site on the zeolite surface. If rhodium (0) were present, butane would be the dominant reaction product.

XPS studies on the catalysts after hydrodesulfurization reactions to 600°C were performed in order to determine the active rhodium surface species. Identification of the oxidation state of rhodium on $RhCl_3$-13X and $RhCl_3$-ZSM5-G2 could not be determined by XPS binding energies alone. The binding energies of the Rh 3d levels indicated rhodium was present either as Rh(0) or Rh(I). The S 2p binding energy revealed that sulfur existed on the catalyst surface as sulfide. The S/(Si+Al) ratio for all three catalysts under all sulfiding conditions decreased throughout the reaction. It was proposed that surface sulfur desorbed as H_2S. Calculations based on mole ratios of sulfur on the catalyst surface and moles of sulfur in a 0.5μL thiophene injection indicated that the surface sulfur which desorbed as H_2S was negligible in comparison to the H_2S formed from hydrodesulfurization reactions. Therefore, the additional H_2S does not contribute significantly to the hydrodesulfurization reaction products.

The binding energy of the 3d levels could not distinguish between Rh(I) and Rh(0), but it was concluded that the active thiophene hydrodesulfurization species was Rh(I) based on the following results. Rh(0)-ZSM5(M) was unable to interact with thiophene and produce a sulfided species or to desulfurize thiophene. Also, the increase in the butene/butane product ratio with increasing temperature argues against the possiblity of Rh(0) on the zeolite surface.

XPS results on the reacted Co-Mo/Al_2O_3 catalyst indicated a reduction in surface sulfur, explained by desorption as H_2S. The Mo 3d binding energies indicated molybdenum was present as both the oxide

and the sulfide species. Since molybdenum sulfide was still present after reactions, it was concluded that MoS_2 was the active species in the hydrodesulfurization of thiophene. This conclusion agrees with the results of others (33).

The results of this study indicate that rhodium incorporated zeolites can be effective catalysts for the hydrodesulfurization of thiophene. XPS can be a useful tool in determining the binding energies of Rh(III) and Rh(II) compounds. However, the similarity in binding energies of Rh(0) and Rh(I) make exact determination of oxidation state impossible. From chemical considerations in this study, it is proposed that Rh(I) is the active species for thiophene hydrodesulfurization on catalysts prepared from rhodium(III)-zeolites.

REFERENCES

1. U. S. News & World Report, 51, January 8, 1982.

2. S. Akhtar, A. G. Sharkey, Jr., J. L. Shultz, and P. M. Yavorsky, paper presented at 167th Nat'l Meeting ACS, Los Angeles, Calif., 3/31-4/5, (1974).

3. D. E. W. Vaughan in The Properties and Applications of Zeolites, The Chemical Society, London, 298 (1980),

4. W. W. Kaeding and S. A. Butter, J. Catal., 61, 155 (1980).

5. E. G. Derouane, J. B. Nagy, P. Dejaifre, J. H. C. vonHooff, B. P. Spekman, J. C. Vedrine, and C. Naccache, J. Catal., 53, 40 (1978).

6. T. A. Pecoraro and R. R. Chianelli, J. Catal., 67, 430 (1981).

7. M. Houalla, N. K. Nag, A. V. Sapre, D. H. Broderick, and B. C. Gates, AIChE J., 24, 1015 (1978).

8. P. J. Owens and C. H. Amberg, Adv. Chem. Ser., 33, 182 (1961).

9. P. J. Owens and C. H. Amberg, Can. J. Chem., 40, 941 (1962).

10. P. J. Owens and C. H. Amberg, Can. J. Chem., 40, 947 (1962).

11. S. Kolboe, and C. H. Amberg, Can. J. Chem., 44, 2623 (1966).

12. S. Kolboe, Can. J. Chem., 47, 352 (1969).

13. D. E. Nicholson, Anal. Chem., 32, 1365 (1960).

14. D. E. Nicholson, Anal. Chem., 34, 370 (1962).

15. L. Meites, and D. E. Nicholson, "Handbook of Analytical Chemistry," Chapter on Infrared Spectroscopy in the Sodium Chloride Region, McGraw-Hill, New York, 6-106 (1963).

16. J.M.J.G. Lipsch and G.C.A. Schuit, J. Catal., 15, 179 (1969).

17. A. E. Hargreaves and J.R.H. Ross, J. Catal., 56, 368 (1979).

18. D. E. Kilanowski, H. Teeuwen, V.H.J. deBeer, B. C. Gates, G.C.A. Achuit, and H. Kwart, J. Catal., 55, 129 (1978).

19. E. N. Givens and P. B. Venuto, Prepr. Amer. Chem. Soc. Div. Petrol. Chem., 15, A183 (1970).

20. C. G. Frye, J. F. Mosby, Chem. Eng. Prog., 63, 66 (1967).

21. H. Kwart, G.C.A. Schuit, and B. C. Gates, J. Catal., 61, 128 (1980).

22. M. Houalla, D. H. Broderick, A. V. Sapre, N. K. Nag, V.H.J. deBeer, B. C. Gates, and H. Kwart, J. Catal., 61, 523 (1980).

23. M. Houalla, D. Broderick. V.H.J. deBeer, B. C. Gates, and H. Kwart, Prepr. Amer. Chem. Soc. Div. Petrol. Chem., 22, 941 (1977).

24. G. H. Singhal, R. L. Espino, and J. E. Sobel, J. Catal., 67, 446 (1981).

25. R. L. Chin and D. M. Hercules, J. Phys. Chem., 86, 360 (1982).

26. M. Breysse, B. A. Bennett, and D. Chadwick, J. Catal., 71, 430 (1981).

27. F. Delannay, E. N. Haeussler, and B. Delmon, J. Catal., 66, 469 (1980).

28. Y. Okamoto, T. Shimokawa, T. Imanaka, and S. Teranishi, J. Catal., 57, 153 (1979).

29. K. S. Chung and F. E. Massoth, J. Catal., 64, 320 (1980).

30. K. S. Chung and F. E. Massoth, J. Catal., 64, 332 (1980).

31. Y. Okamoto, T. Imanaka, and S. Teranishi, J. Phys. Chem., 85, 3798 (1981).

32. F. E. Massoth and C. L. Kibby, J. Catal., 47, 300 (1977).

33. B. S. Clausen, H. Topsoe, R. Candia, J. Villadsen, B. Lengeler, J. Als-Nielsen, and F. Christensen, J. Phys. Chem., 85, 3868 (1981).

34. K. Fukuda, M. Dokiya, T. Kameyama, Y. Kotera, J. Catal., 49, 379 (1977).

35. P. D. Caesar, J. A. Brennan, W. E. Garwood, and J. Ciric, J. Catal., 56, 274 (1979).

36. Y. Ono and T. Mori, J. Chem. Soc., Faraday Trans. I, 77, 2209 (1981).

37. C. D. Chang and A. J. Silvestri, J. Catal., 47, 249 (1977).

38. D. Kagi, J. Catal., 69, 242 (1981).

39. C. D. Chang, J. Catal., 69, 244 (1981).

40. D. A. Dowden, N. Mackenzie, and B.M.W. Trapnell, Proc. Roy. Soc. A237, 245 (1956).

41. D. A. Dowden, Catal. Rev., 5, 1 (1971).

42. D. W. Breck, J. Chem. Educ., 41, 678 (1964).

43. W. M. Meir, Molecular Sieves, Society of Chemical Industry, London, 10 (1968).

44. R. J. Argauer and G. R. Landolt, U. S. Patent # 3,702,886.

45. E. G. Derouane and Z. Gabelica, J. Catal., 65, 486 (1980).

46. W. W. Kaeding, C. Chu, L. B. Young, and S. A. Butter, J. Catal., 69, 392 (1981).

47. N. Y. Chen, W. W. Kaeding, and F. H. Dwyer, J. Amer. Chem. Soc., 101, 6783 (1979).

48. E. G. Derouane and J. C. Vedrine, J. Molec. Catal., 8, 479 (1980).

49. C. S. Brooks, Surface Tech., 10, 379 (1980).

50. B. Christensen and M. S. Scurrell, J. Chem. Soc., Faraday Trans. I, 73, 2030 (1977).

51. S.L.T. Andersson and M. S. Scurrell, J. Catal., 71, 233 (1981).

52. M. S. Scurrell and R. S. Howe, J. Molec. Catal., 7, 535 (1980).

53. J. S. Brinen and A. Melera, J. Phys. Chem., 76, 2525 (1972).

54. S. M. Kuznicki and E. M. Eyring, J. Catal., 65, 227 (1980).

55. D. W. Breck, Zeolite Molecular Sieves, John Wiley & Sons, New York, N.Y., 369-373 (1974).

56. G. A. Rempel, Inorg. Synth., 13, 90 (1972).

57. R. Mason, D.M.P. Mingos, G. Rucci, and J. A. Connor, J. Chem. Soc. (Dalton), 1730 (1972).

58. V. I. Nefedov, Va.V. Salyr, A. G. Mairova, C. A. Nazorova, and I. B. Baronovskii, Zh. Neorg. Khim, 19, 1353 (1974).

59. J. G. Norman, Jr. and H. J. Kolari, J. Amer. Chem. Soc., 100, 791 (1978).

60. V. I. Nefedov and M.A. Porai-Koshits, Mat. Res. Bull., 1, 1543 (1972).

61. T. Iizuka and J. H. Lunsford, J. Molec. Catal., 3, 391 (1980).

62. M. Primet, J. C. Vedrine, and C. Naccache, J. Molec. Catal., 4, 411 (1978).

63. S.L.T. Andersson and M. S. Scurrell, J. Catal., 59, 340 (1979).

64. A. Luchetti, L. F. Wieserman, and D. M. Hercules, J. Phys. Chem., 85, 549 (1981).

65. V. I. Nefedov, E. F. Schubockina, I. S. Kolomnikov, I. B. Baronovski, V. P. Kukolev, M. A. Golubnichaya, L. K. Shubochkia, M. A. Porai-Koshits, and M. E. Vol'pin, Zh. Neorg. Khim., 18, 845 (1973).

66. J. Hedman, M. Klasson, R. Nilssan, c. Nordling, M. F. Sorokina, D. I. Kljushnikov, S. A. Nemnonov, V. A. Trapeznikov, and V. G. Zyryanov, Phys. Scr., 4, 195 (1971).

67. B. J. Lindberg, K. Hamrin, G. Johansson, U. Gelius, A. Fahlmann, C. Nordling, and K. Siegbahn, Phys. Scr., 1, 277 (1970).

68. T. A. Patterson, J. C. Carver, D. E. Leyden, and D. M. Hercules, J. Phys. Chem., 80, 1702 (1976).

69. D. E. Walsh and L. D. Rollmann, J. Catal., 49, 369 (1977).

70. P. N. Rylander, Catalytic Hydrogenation over Platinum Metal," Academic Press, New York, N.Y., 309 (1967).

The vita has been removed from the scanned document

RHODIUM ZEOLITES AS CATALYSTS FOR HYDRODESULFURIZATION REACTIONS

by

Kathryn Elizabeth Givens

(ABSTRACT)

Fuel stocks today contain a large percentage of sulfur, nitrogen, and metals. To meet processing and environmental regulations, these components must be removed. Hydrodesulfurization reactions and the use of catalysts to enhance this process have been under extensive study in recent years. The main hydrodesulfurization catalyst used has been cobalt-molybdenum on an alumina support. This study investigated rhodium incorporated zeolites as catalysts for thiophene hydrodesulfurization reactions.

The compounds $RhCl_3 \cdot 3H_2O$, $Rh_2(CO_2CH_3)_4$, and $Rh(PPh_3)_3Cl$ were adsorbed onto 13X and ZSM5 zeolites. Results of thiophene hydrodesulfurization over $RhCl_3$-13X and $RhCl_3$-ZSM5 were compared to those of commercial Co-Mo/Al_2O_3 to determine the most active catalyst under different experimental conditions.

X-ray photoelectron spectroscopy, infrared spectroscopy, x-ray diffraction and microelectrophoresis were used to characterize the zeolites. Hydrodesulfurization reactions were carried out in a pulse microreactor/gas chromatograph system as a function of gas flow rate and reaction temperature. Reaction products were identified by mass spectrometry.

$RhCl_3$-13X exhibited maximum thiophene conversion when presulfided with thiophene injections at 100°C, or with a 10 vol% H_2S/90 vol% H_2 gas mixture at 400°C. At a H_2S-sulfiding temperature of 250°C, the commercial Co-Mo/Al_2O_3 catalyst was most active. Over all catalysts, the only reaction products were hydrogen sulfide, butene and butane. The butene/butane product ratio increased with increasing temperature. On the basis of these results and XPS measurements, Rh(I) was identified as the active hydrodesulfurization species.